UNIVERSIDADE DE SÃO PAULO

INSTITUTO DE FÍSICA
CAIXA POSTAL 20516
01498 - SÃO PAULO - SP
BRASIL

publicações

IFUSP/P-458

POLARIZATION POTENTIALS IN HEAVY ION SCATTERING

by

M.S. Hussein

Instituto de Física, Universidade de São Paulo

A.J. Baltz

Physics Department, Brookhaven National Laboratory
Upton, New York 11973, U.S.A.

B.V. Carlson

Centro Técnico Aeroespacial, Instituto de Atividades Espaciais, Divisão de Estudos Avançados
12200, São José dos Campos, SP, Brazil

Março/1984

Polarization Potentials in Heavy Ion Scattering

M. S. Hussein*
Instituto de Fisica, Universidade de Sao Paulo
C.P. 20.516, Sao Paulo, Brazil

A. J. Baltz**
Physics Department, Brookhaven National Laboratory
Upton, New York 11973, U.S.A.

B. V. Carlson
Centro Técnico Aeroespacial, Instituto de Atividades
Espaciais, Divisao de Estudos Avançados
122000, Sao José dos Campos, SP., Brazil

March 1984

* Supported in part by the CNPq-Brazil

**U.S. Department of Energy Contract DE-AC02-76CH00016

Contents

1. Introduction

2. Polarization Potentials in Heavy Ion Scattering

   2.1 Introduction
   2.2 Theory of the Dynamic Components of the Generalized Optical Model Potential
   2.3 The Semiclassical Inversion Method

3. The Coulomb Polarization Potential

   3.1 Early Work
   3.2 Quantal Theory of Multiple Coulomb Polarization Potentials
   3.3 The Quantum Mechanical Coupled Channels Equations for Multiple Coulomb Excitation
   3.4 The On-energy-shell Approximation and the Equivalent Local Coulomb Polarization Potential
   3.5 Considerations of Off-shell Effects
   3.6 The Adiabatic Polarization Potential
   3.7 Relativistic Potential

4. Evaluation of the Elastic Scattering Cross Section

   4.1 The Cross Section Formula
   4.2 Applications
      4.2a The Coulomb Polarization Potential
      4.2b The Adiabatic Coulomb Polarization and Relativistic Potentials
   4.3 Comparison with Coupled Channels Calculation and Trivially Equivalent Local Potentials

5. The Volume Heavy Ion Optical Potential

6. The Nuclear Polarization Potential

   6.1 A Review
   6.2 Polarization Potentials and the DWBA

7. Conclusions

   References
   Appendix A The total Reaction Cross Section
   Appendix B Large ℓ 3-j and 6-j Coefficients
   Appendix C Angular Deviation for Virtual Dipole, Quadrupole and Octupole Excitation

Abstract

A polarization potential is defined in terms of the Feshbach projection operator formalism to represent the effect upon the elastic channel of the coupling to non-elastic channels in heavy ion scattering. The polarization potential represents coupling to specific surface degrees of freedom of the particular reaction considered and it is contrasted to the complementary global approaches for the volume potential such as the folding model and the proximity potential. The coupled channels method is used both as a source of exact model solutions for comparison with the various approximate potential forms and also as a numerical means of constructing trivially equivalent local potentials. The imaginary Coulomb polarization potential is due in lowest order to quadrupole coupling to the lowest collective 2^+ state of a nucleus. It is considered in detail since it provides the insight of closed analytical forms in various approximations. Multistep coupling to higher states, energy loss and off-energy shell effects are also considered analytically. The real Coulomb polarization potential due to the virtual excitation of multipole giant resonances, and the polarization potential arising from relativistic corrections, are investigated in detail. Polarization potential components due to nuclear coupling are investigated numerically for inelastic scattering and particle transfer. Approximate analytical expressions for the nuclear polarization potential are surveyed and tested numerically. Analytical cross section approaches are contrasted with the polarization potential approach and with coupled channels.

I. Introduction

In heavy ion reactions, strong direct channel coupling effects are quite commonplace. A well known example is multiple Coulomb excitation of deformed nuclei. There are many instances where a simple one-channel description of the elastic scattering requires ion-ion interactions that are not reproducible by microscopic or semimicroscopic (e.g. double- or single-folding) calculation. This indicates that strong channel coupling is coming into play and is generating dynamical polarization components to be added to the bare potential.

In recent years there have been several papers published which dealt with the calculation of these polarization potentials. In particular the Coulomb polarization potential that arises from the Coulomb coupling of the entrance channel to the inelastic collective channels, has been derived and discussed in great detail. Short-ranged nuclear polarization potentials arising from the nuclear coupling to inelastic and transfer chennels, have also been considered.

The great advantage in obtaining closed form, albeit approximate, expressions for these polarization potentials, is obvious. Coupled channel calculations can be rendered doable with usual DWBA codes with the use of the appropriate distorting potentials. Furthermore, closed expressions for the elastic scattering amplitudes can be achieved, which provides insight into the direct reaction mechanism.

The purpose of this Report is to review the topic of heavy ion polarization potentials. We do not attempt to start from the fundamental microscopic level of the nucleon-nucleon interaction. Rather, our purpose, given a nuclear model, is to supply potentials that should be added to the bare ion-ion potential which are assumed to be given a priori. Our study should, therefore, go hand in hand with coupled channel calculations which we purport to simplify and illuminate.

The Report is organized as follows. In Section 2, the formal structure of the polarization potential is discussed within Feshbach's projection operator method. We also discuss the semiclassical inversion method. In Section 3, we discuss in detail the Coulomb polarization potential. This chapter constitutes the bulk of our review, since these potentials can be obtained in simple closed form. The on-energy shell approximation used in the derivation is assessed by considering approximately the effects of the off-shell terms. The adiabatic Coulomb polarization potential arising from the virtual excitation of giant multipole resonance is then considered. We also derive and discuss the relativistic polarization potentials that comes about as a consequence of the relativistic corrections to Rutherford scattering. In Chapter 4, closed expressions for the sub-barrier elastic scattering cross section ratio to Rutherford are derived. These expressions contain the effect of the polarization potentials derived in Chapter 3. In Section 5 we discuss the background volume or bare potential in the context of a simple geometrical model, the proximity potential. In Chapter 6, the short range nuclear polarization potentials are briefly discussed, and finally, in Chapter 7, concluding remarks are made.

2. Polarization Potentials in Heavy-ion Scattering

2.1 Introduction

In this section we give a detailed discussion of the dynamic polarization component of the generalized optical potential appropriate for heavy-ion collision phenomena.

The term polarization potential might suggest some temporary macroscopic shape or orientation change induced in one or both of the heavy

nuclei involved in a heavy-ion elastic scattering experiment. This is a good physical description, for example, of the strong coupling of the lowest collective quadrupole (2^+) state to the ground state in a heavy-ion reaction on an even-even nucleus. However, we would like to generalize the concept of a polarization potential to the representation of any particular direct couplings to the elastic channel in a heavy-ion reaction by an optical potential component. Thus we are not specifically interested in the volume part of the heavy-ion optical potential, such as might be generated theoretically by a density folding procedure, but in surface components and, in the case of Coulomb excitation, long range components.

A basic framework for discussing the polarization potential is found in the Feshbach projection operator formalism [1]. The P space which is treated explicitly is the elastic channel while all other channels are grouped into the Q space. One then has for the elastic channel optical potential

$$U(\vec{r},\vec{r}') = (\psi_o\phi_o|V|\psi_o\phi_o) + (\psi_o\phi_o|PVQ\frac{1}{E-QHQ+i\varepsilon}QVP|\psi_o\phi_o) \qquad (2.1)$$

where round brackets indicate integration over intrinsic coordinates of the two nuclei and P and Q are projection operators onto the P or Q space. The first term of Eq. (2.1) is the volume potential, which might be generated by some density folding or nuclear matter approach as we will indicate in Section 5. We will treat this term only relatively briefly so as to provide a background for the treatment of polarization potential components which fall naturally within the second term.

We would like to make some connection also with the reasonably successful theory of microscopic optical potentials for the nucleon-nucleus

interaction. One certainly cannot expect to be as successful in a fundamental sense in constructing the entire generalized optical potential from the nucleon-nucleon interaction. One must point out the difference emphasized by Mahaux [2] between the phenomenological optical potential which has a simple radial shape and depends smoothly on target mass number on the one hand and the generalized optical model arising from computational models which may have a complicated non-locality, wild energy dependence and strong ℓ-dependence. In the nucleon-nucleus case some success was had in obtaining computed optical potentials which have desirable smooth properties of a phenomenological optical potential.

In our heavy ion case there is a natural break between the volume part of the optical potential and the surface parts arising from coupling of low lying states. For the most part the volume optical potential will be treated completely phenomenologically by a fit to data, perhaps in terms of global potentials.

With distorted waves thus assumed for the background we come naturally to the consideration of coupled channels. As an extension of the DWBA, coupled channels has been very successful in representing cross sections for low lying inelastic excitations. We will extensively use coupled channels as a model of an exact theory with all the couplings put in fully to which we can compare results of polarization potentials calculated for the same physical systems. In such comparisons, also, one realizes a prime motivation for considering polarization potential representations of coupled channels. Results of a coupled channels code can at times seem like the output of a "black box." A real or imaginary potential on the other hand is something a physicist thinks he understands something about.

It is just this insight into the nature of the scattering through the potential that stands out most clearly in the analytical results for the long range polarization potentials due to the effects of Coulomb excitation. The striking success of this approach for the Coulomb excitation problem will provide a substantial part of this review.

2.2 Theory of the Dynamic Components of the Generalized Optical Model Potential

The dynamic component of the optical model potential as was mentioned already in the introduction to this section is given by

$$U_D(\vec{r},\vec{r}') = (\psi_o\phi_o|VQ\,\frac{1}{E-QHQ-i\varepsilon}\,QV|\psi_o\phi_o) \tag{2.2}$$

where ψ_o,ϕ_o refer to the ground state wave function of the target and projectile nuclei respectively, V is the interaction that couples the elastic channel to the channels contained in Q. The same V couples among the different channels in Q, since $QHQ = QH_oQ + QVQ$, where H_o is the piece of H which is diagonal in channel space.

A particularly transparent form of U_D may be obtained by using the spectral expansion of the Q-space Green's function,

$$U_D = (\psi_o\phi_o|VQ\sum_{Q_i}\frac{|\psi^{(+)}_{Q_i}\rangle\langle\psi^{(+)}_{Q_i}|}{E-E_{Q_i}+i\varepsilon}\,QV|\psi_o\phi_o) \tag{2.3}$$

where $\{|\psi^{(+)}_{Q_i}\rangle|$ are the exact solutions of the coupled channels equations pertaining to the Q-subspace. The above equation, Eq. (2.3), shows clearly that

U_D may be written as a sum involving contributions from the different channels in Q,

$$U_D = \sum_{i=1}^{N_Q} U_D^i \tag{2.4}$$

Owing to the presence of the factor $i\varepsilon$ in the Q-space Green's function, the potential U_D is non-Hermitian. The imaginary part of U_D is responsible for the removal of flux from the elastic channel. The form (2.4) of U_D indicates that the absorption which arise from $\mathrm{Im}U_D$ may be considered as a sum of absorptions due to the populations of the different channels in Q. This has an immediate consequence on the total reaction cross section extracted from elastic scattering. From unitarity we have (see Appendix 1)

$$\sigma_R(Q) = \frac{k}{E} \langle \psi_{e\ell}^{(+)} | -\mathrm{Im}\, U_D | \psi_{e\ell}^{(+)} \rangle \tag{2.5}$$

where $|\psi_{e\ell}^{(+)}\rangle$ is the exact, elastic channel wave function k and E are the asymptotic wave number and the c.m. energy respectively. Equation (2.5) may be rewritten as a sum, with the help of Eq. (2.4)

$$\sigma_R(Q) = \sum_{i=1}^{N_Q} \sigma_R^i \tag{2.6}$$

which is certainly the expected result. The argument Q in σ_R is used to remind the reader that other processes, e.g. fusion, which are not contained in Q, also contribute to σ_R. Thus $\sigma_R(Q)$ is that part of σ_R which is directly connected with the Q-channels. Incidentally, all other absorption processes not described by Q, are usually accounted for by using a "volume" imaginary part whose geometry is closely connected to that of the static, real, component of the optical potential. In contrast, all the terms contributing to U_D, Eq. (2.4), are surface peaked (see discussion below).

Equation (2.3) is not very useful from the practical point of view. For the purpose of developing approximate analytic expressions for U_D, it is more convenient to develop an appropriate expansion for the Q-space Green's function. We accomplish this by studying in detail the structure of $G_Q^{(+)}$. For this purpose we write for the projection operator Q, the following

$$Q = q + Q' \tag{2.7}$$

where q is the projection operator for a particular channel in Q and $qQ'=Q'q=0$. The significance of q will become clear later.

Simple operator algebra would then permit us to write the following expression for U_D

$$\begin{aligned} U_D = {} & (\psi_o\phi_o | V G_q^{(+)} V | \psi_o\phi_o) \\ & + (\psi_o\phi_o | (V + V G_q^{(+)} V) Q' G_Q^{(+)} Q' (V G_q^{(+)} V + V) | \gamma_o\phi_o) \end{aligned} \tag{2.8}$$

where we have introduced the bare q-channel Green's function $G_q^{(+)}$ defined through

$$G_q^{(+)} = (E - H_{qq}^{(o)} - V_{qq} + i\varepsilon)^{-1} \tag{2.9}$$

The quantity $V_{qq} = qVq$ refers to the reorientation matrix element in channel q.

The second term on the RHS of Eq. (2.8) exhibits clearly the multistep nature of absorption in coupled channels phenomena. The first term on the other hand represents the effect of a <u>particular</u> channel on the elastic potential. The long-range absorption potentials of Love et al. [3] and Baltz et al. [4] are based on this first term with the further neglect of V_{qq} in $G_q^{(+)}$ (Eq. (2.9)). This last restriction was removed in Ref. [5]. The multistep term in U_D was

also considered recently in connection with multiple Coulomb excitation [6],[7] Several approximations were utilized in all these attempts. A full account of the matter is given in the next section.

In Eq. (2.8) the channel q was unspecified. However, the decomposition above is quite convenient in cases where one particular channel is strongly coupled to the elastic channel and thus has to be considered explicitly. Then the Q'-part of the full Q-subspace may be treated on the average in the form of an optical potential in channel q. In certain instances the nature of the coupling may force the channel q to act as a pure "doorway" connecting the elastic channel to the Q'-subspace. In such a case the potential U_D acquires the form

$$U_D = (\psi_o\phi_o\Big|[VG_q^{(+)}V + VG_q^{(+)}VQ'\ G_Q^{(+)}Q'VG_q^{(+)}V]\Big|\psi_o\phi_o) \qquad (2.10)$$

The above form of U_D', considered in great detail in Section 3, would arise in the case of pure quadrupole Coulomb excitation of a quadrupole deformed even-even nucleus. The channel q would then correspond to the first excited 2^+ and Q' to the other members of the ground rotational band (4^+, 6^+, ...). Coupling higher than the quadrupole (e.g. hexadecapole) may be included through the direct coupling term V that appears in the second term of Eq. (2.8).

Clearly an exact evaluation of U_D is possible only numerically. In order to exhibit the salient features of the physics involved in multistep absorption, analytic calculation of U_D is called for. This is generally not possible exactly. Several approximations are required. One possible starting point is to use an on-energy-shell approximation for the bare channel Green's function $G_q^{(+)}$. This amounts to taking the system to infinity after each transition and bringing it back for the next. Though such an approximation

considers only part of the physics involved, it does supply a simple algebraic solution to U_D, as will be shown in the next section.

Once the on-shell calculations are carried out exactly one may then consider off-shell effects in an approximate way. This is the method which we follow in our treatment of sub-barrier multiple Coulomb excitation effects on heavy-ion elastic scattering.

As a result of the multistep nature of U_D, one would necessarily end up dealing with energy- and angular momentum-dependent complex non-local interaction. The dependence on angular-momentum and energy does not lead to major complications. However, the non-locality of U_D would render the optical model analysis of elastic scattering rather cumbersome.

One possible way of removing the non-locality, is to define, and eventually calculate, an equivalent local potential U_D^L. This is accomplished via

$$U_D^L(\vec{r})\psi(\vec{r}) = \int d\vec{r}'\ U_D(\vec{r},\vec{r}')\psi(\vec{r}') \qquad (2.11)$$

where $\psi(\vec{r}')$ is the exact elastic channel wave function. As such, Eq. (2.11), as it stands, is not very useful since it requires, for the solution of $U_D^L(\vec{r})$, the <u>a priori</u> knowledge of the wave function which contains the effect of U_D itself. Nevertheless Eq. (2.11) could be used to construct $U_D^L(\vec{r})$ numerically using a coupled channel description of $\psi(\vec{r})$. In our discussion of the Coulomb polarization potential in Section 3, we shall use Eq. (2.11) to obtain the equivalent local potential by using lowest order approximation for $\psi(\vec{r})$ by treating U_D as a small perturbation. In the cases studied we find this approximation (replacing $\psi(\vec{r})$ by the Coulomb wave function) to be valid to lowest order in the small quantity η^{-1} where η is the Sommerfeld parameter.

Eq. (2.11) may also be written in the following simple forms

$$U_D^L(\vec{r}) = E - U_o(\vec{r}) + \frac{\hbar^2}{2\mu}\frac{1}{\psi(\vec{r})}\vec{\nabla}^2\psi(\vec{r}) \tag{2.12}$$

or

$$U_D^L(\vec{r}) = \frac{\hbar^2}{2\mu}\left[\frac{1}{\psi(\vec{r})}\nabla^2\psi(\vec{r}) - \frac{1}{\phi(\vec{r})}\nabla^2\phi(\vec{r})\right] \tag{2.13}$$

where $U_D(\vec{r})$ is the static, folding, component of the ion-ion potential and $\phi(\vec{r})$ is the solution of the optical Schrödinger equation in the absence of U_D. For a given partial wave, ℓ, we may write, from Eq. (2.13)

$$U_{D,\ell}^L(r) = \frac{\hbar^2}{2\mu}\left[\frac{1}{\psi_\ell(r)}\frac{d^2}{dr^2}\psi_\ell(r) - \frac{1}{\phi_\ell(r)}\frac{d^2}{dr^2}\phi_\ell(r)\right] \tag{2.14}$$

where $\psi_\ell(r)$ and $\phi_\ell(r)$ are radial wave functions. Since heavy-ion reactions at above-barrier energies are characterized by strong absorption in the interior region, the potential $U_{D,\ell}^L(r)$ given in Eq. (2.14), in the case of short-range nuclear couplings (inelastic, transfer, etc.), peaks around the grazing angular momentum, ℓ_g. This is so since for low partial waves both terms on the RHS of Eq.(2.14) are small, whereas for $\ell > \ell_g$, ψ_ℓ tends towards ϕ_ℓ at $r > r_t^\ell$, the classical turning point. The only region in ℓ-space where one finds an appreciable contribution to $U_{D,\ell}^L$ is centered around ℓ_g. This clearly indicates that $U_{D,\ell}^L(r)$ has a window-like form in ℓ-space. Similar arguments can be made to show that $U_{D,\ell}^L(r)$ is surface peaked in r-space (see Chapter 6).

In the particular case of long-range Coulomb coupling, the above arguments do not hold. Considering the case of sub-barrier elastic scattering, one expects $U_{D,\ell}^L(r)$ to exhibit long-ranged ℓ and r dependences. Thus $\psi_\ell(r)$ would be basically the function $\phi_\ell(r)$ multiplied by a damping factor which attains maximum effect at backward angles (smallest distance of closest approach). This case will be fully discussed in the next section.

2.3 The Semiclassical Inversion Method

Another way of constructing U_D is based on Feynman's path integral method. The version of this method developed by Pechukas [8] seems to be particularly appropriate for treating many-body collision phenomena. In heavy-ion processes, one expects a semiclassical description to be appropriate. This entails the definition of an average classical trajectory that describes the relative motion. In such a case the path integral may be evaluated using stationary phase approximations. The resulting amplitude may then be used to obtain the optical potential as we demonstrate below.

We first recall Feynman's expression for the elastic transition amplitude describing the scattering by an optical potential $U_o + U_D$

$$K_{oo}(t_1,t_o) = \int_{t_o}^{t_1} D(\vec{r})\exp\left[\frac{i}{\hbar}S[\vec{r}(t)]\right] \tag{2.15}$$

where $\vec{r}(t)$ is a path for the relative coordinate satisfying end point (boundary) conditions appropriate for a scattering problem and the path integral extends over all possible paths satisfying these conditions. The classical action integral, $S[\vec{r}(t)]$ is given by

$$S[\vec{r}(t)] = \int dt\left[\frac{1}{2}\mu\dot{\vec{r}}^2 - U_o(\vec{r}) - U_D(\vec{r})\right] \tag{2.16}$$

where $U_o(\vec{r})$ is a known piece of the optical potential (e.g. folding model

component). For $U_D(\vec{r})$ to represent correctly the effects on the elastic channel due to its coupling to other channels, it must be such as to give for K_{oo} at any time t_1 identical results as those obtained from a microscopic description of the reaction.

Let us assume now that the intrinsic motion of the two heavy ions are described by a Hamiltonian H_o with eigenstates $\{|i\rangle\}$ and energies $\{\varepsilon_i\}$. The time evolution operator, of the interacting system obeys the equation

$$ih \frac{\partial}{\partial t} U = [H_o + V(\vec{r}(t),\xi)]U \tag{2.17}$$

where $V(\vec{r}(t),\xi)$ is a potential which represents the coupling between relative motion, described by $\vec{r}(t)$, and the internal (intrinsic) coordinates $\{\xi\}$. Equation (2.17) is to be solved with the boundary condition U=1 at $t=t_o$ for a given path $\vec{r}(t)$. The amplitude K_{oo} for the system to remain in the ground state at time t, is given by

$$K_{oo}(t_1,t_o) = \int_{t_o}^{t_1} D(\vec{r}(t))\exp\left[\frac{i}{h} S_o[\vec{r}(t)]\right] \langle o|U(\vec{r},t_1,t_o)|o\rangle \tag{2.18}$$

where the "free" action $S_o[\vec{r}(t)]$ is given by

$$S_o[\vec{r}(t)] = \int_{t_o}^{t_1} dt\left[\frac{1}{2}\mu\dot{\vec{r}}^2 - U_o(\vec{r})\right] \tag{2.19}$$

Assuming the validity of the semiclassical description of the collision process, we may then evaluate $K_{oo}(t_1,t_0)$ of Eq. (2.15) and Eq. (2.18) using the stationary phase approximation. We then obtain the following identification

$$\exp\left[\frac{-i}{h}\int_{t_o}^{t_1} dt\ U_D(\vec{r}_{c\ell}(t))\right] = \langle o|U(\vec{r}_{c\ell},t_1,t_o)|o\rangle \tag{2.20}$$

where $\vec{r}_{c\ell}(t)$ is the real classical trajectory that obeys the Newtonian equations of motion

$$\mu\ddot{\vec{r}}_{c\ell} + \vec{\nabla}\ \mathrm{Re}\ U_D(\vec{r}_{c\ell}) + \vec{\nabla}\ \mathrm{Re}\ U_D(\vec{r}_{c\ell}) = 0 \tag{2.21}$$

or

$$\mu\ddot{\vec{r}}_{c\ell} - h\ \vec{\nabla}\ \mathrm{Im}\ell n\ \langle\left|U(\vec{r}_{c\ell},t_1,t_o)\right|o\rangle + \vec{\nabla}\ \mathrm{Re}\ U_D(\vec{r}_{c\ell}) = 0 \tag{2.22}$$

In most cases of practical interest in heavy-ion collision phenomena, the effect of U_D on the trajectory is small. Therefore a very good approximation for $\vec{r}_{c\ell}$ would be

$$\mu\ddot{\vec{r}}_{c\ell} + \vec{\nabla}\ \mathrm{Re}\ U_o(\vec{r}_{c\ell}) = 0 \tag{2.23}$$

which can be solved once $U_o(\vec{r})$ is given. For the application of the semiclassical formalism to the case of sub-barrier absorption due to Coulomb excitation, one usually assumes that U_o is given by the Coulomb monopole-monopole interaction which would then lead to a pure Rutherford trajectory for $\vec{r}_{c\ell}$. Corrections due to nuclear effects, may be made through classical perturbation theory.

Since the dynamic potential defined in Eq. (2.11) represents the <u>average</u> effect of channel coupling on the elastic channel wave function, which is composed to ingoing and outgoing components, one expects to obtain equivalent results for U_D^L within the semiclassical theory described above, through the evaluation of what we might call the algebraic average of two components of U_D^L; one defined on the outgoing and the other on the ingoing branches of the classical trajectory $\vec{r}_{c\ell}$. These two components of U_D^L are given by (see Eq. (2.20)).

$$\frac{U_D^{L(\pm)}(r)}{|v(r)|} = \pm \frac{h}{i}\frac{d}{dr}\,\ell n\langle 0|V(r,t^{\pm},t_o)\,0\rangle \qquad (2.24)$$

where v(r) is the local relative velocity. The semiclassical equivalent local potential U_D^L is then given by (for a given impact parameter)

$$U^L_{D,\ell}(r) = \frac{1}{2}\left(U_D^{L(+)}(r) + U_D^{L(-)}(r)\right) \qquad (2.25)$$

3. The Coulomb Polarization Potential

3.1 Early Work

The original comprehensive treatment of the semiclassical theory of Coulomb excitation did not treat the loss of particle flux into excited channels in terms of an absorptive optical potential. However, in the adiabatic limit, where the frequencies of the virtual excitations are large compared to the inverse collision time, several authors obtained from a perturbation calculation a real polarization potential to represent the effects of such virtual excitations in the form [9]

$$V_{pol}(r) = 4\pi\, Z_1^2 e^2 \sum_{\lambda=1}^{\infty} \frac{1}{(2\lambda+1)^2}\frac{1}{r^{2\lambda+2}} \sum_{Z\neq 1} \frac{B(E\lambda, i\to Z)}{E_1 - E_Z} \quad . \qquad (3.1)$$

We note that for quadrupole excitation, which is of major interest for us in this work, the real adiabatic polarization potential falls off as r^{-6}, although the adiabatic approximation is inappropriate for our cases of heavy ions incident on rotational nuclei. We shall discuss the adiabatic polarization potential in some detail in Section 3.6.

The interest in an imaginary optical potential to represent the effects of flux loss due to Coulomb excitation was given impetus by experimental

results of heavy ion induced elastic scattering on rotational nuclei above the Coulomb barrier. Figure 3.1 shows Brookhaven data for 90 MeV $^{18}O + ^{184}W$ [10] elastic scattering with the damping of the characteristic Fresnel pattern brought about by Coulomb excitation. Weber et al. fitted their similar MeV ^{16}O data with an imaginary potential component with a $r^{-6.3}$ dependence [11]. The Brookhaven analysis was in terms of a coupled channels calculation which included Coulomb excitation.

While the coupled channels analysis was a completely adequate treatment of the Brookhaven data, producing an excellent fit to the elastic scattering cross section, there was still a considerable interest in the theoretical construction of a potential to produce the experimental effect. Love, Terasawa and Satchler [3] produced a negative imaginary potential which, apart from finite size corrections, has a radial dependence of $r^{-5}(1-Z_1Z_2e^2/E_{c.m.}r)^{-1/2}$. This potential was very successful in reproducing the Brookhaven data. Furthermore, illustrative calculations done by these authors indicated the importance of Coulomb absorption in above Coulomb elastic scattering with heavier projectiles (Fig. 3.2).

In deriving their potential, Love, Terasawa and Satchler made several approximations. The first was to use plane waves forms for both the wave functions and the Green function used in constructing the trivially equivalent local potential. If this was the only approximation then this potential would be the plane wave limit of the ℓ-dependent potential of Baltz et al. (see below) which it is not. In their derivation Love, Terasawa and Satchler made a further approximation whose validity is impossible to estimate. From their product of the $1/\dot{x}(R)$ and $\dot{x}(R')$ in the trivially equivalent local potential they obtain

$e^{-i\vec{k}\cdot\vec{x}}$ where $\vec{x} = \vec{R}-\vec{R}'$ is the non-locality coordinate and $\vec{k}$ is the scattering wave number. This plane wave is approximated by its spherical part $j_0(kx)$. Since neither $\vec{k}$ nor $\vec{x}$ should in general be small this approximation is without foundation. LTS also make a similar approximation for $e^{i\vec{q}\cdot\vec{r}}$ which arises in the Fourier transform used to evaluate the potential. Love, Terasawa, and Satchler were able to compensate for the plane wave aspect of their derivation by an ad hoc use of the local (r-dependent) momentum instead of the asymptotic momentum in the derived formula. Thus the good agreement with the data and coupled channels of the LTS potential is fortuitous and the LTS potential finds its only real justification in the universal comparison between its result and that of the more exact potential of the Baltz et al. [4] which we will discuss below.

The ℓ-dependent BKGP potential [4] was derived by using Coulomb wave functions for both the Green functions and the elastic wave function. The non-local potential equivalent of the effect of channel coupling on the elastic channel may then be given

$$U_\ell(r,r') = \frac{-2\mu}{\hbar^2 k}\frac{4\pi}{25}Z_p e^2 B(E2)\uparrow \frac{1}{r^3}\frac{1}{r'^3} \times \sum_{\ell'} \langle \ell 020 | \ell' 0\rangle^2 F_{\ell'}(r_<)H_{\ell'}(r_>) \tag{3.2}$$

where F_ℓ and H_ℓ are the regular and outgoing Coulomb wave functions. The outgoing wave function can be expressed in terms of the irregular and regular wave functions

$$H_\ell = G_L + iF_\ell \tag{3.3}$$

and an on energy shell approximation is made by setting H_ℓ equal to F_ℓ. To lowest order this is a good approximation in the semiclassical limit since one is only ignoring the effect of integrals over $G_\ell r^{-3} F_\ell$ which oscillate rapidly.

It is interesting to observe at this point that in the case of giant resonance polarization effects on elastic scattering, the situation is completely reversed from the one above, as the principal part of the intermediate channel Green function gives the dominant contribution. For details see Section 3.6.

Using Coulomb wave functions also to localize the nonlocality to lowest order one obtains

$$U_\ell(r) = -i\frac{2\mu}{\hbar^2 k}\frac{4\pi}{25}Z_p^2 e^2 B(E2)\uparrow \times \frac{1}{r^3}\sum_{\ell'} \langle \ell 020 | \ell' 0\rangle^2 \frac{F_{\ell'}(r)}{F_\ell(r)}\int_0^\infty dr' F_{\ell'}(r')\frac{1}{r'^3}F_\ell(r') \tag{3.4}$$

In the limit of no energy loss there are closed forms for the Coulomb wave function integrals which are taken in their semiclassical form with $\hat{\ell}=\ell+1/2$

$$\int_0^\infty dr' F_{\ell\pm2}(r')\frac{1}{r'^3}F_\ell(r') = \frac{1}{6}k^2\frac{1}{\hat{\ell}^2+\eta^2} \tag{3.5}$$

$$\int_0^\infty dr' F_\ell(r')\frac{1}{r'^3}F_\ell(r') = \frac{1}{2}\frac{k^2}{\hat{\ell}^2}\left(1-\frac{\eta}{\hat{\ell}}\arctan\frac{\hat{\ell}}{\eta}\right) \tag{3.6}$$

Likewise use is made of the semiclassical form for the Clebsch-Gordan coefficients and from Coulomb wave function recursion relations the ratios of wave functions may be eliminated

$$\frac{F_{\ell+2}}{F_\ell} + \frac{F_{\ell-2}}{F_\ell} = -2 + \frac{4}{\hat{\ell}^2+\eta^2}\left[\eta + \frac{\hat{\ell}^2}{kr}\right]^2 \tag{3.7}$$

The ℓ-dependent BKGP potential is then obtained

$$U_\ell(r) = i\frac{2\mu}{\hbar^2 k}\frac{\pi}{50}Z_p^2 e^2 B(E2)\uparrow \times \left[\left(\frac{\eta^2 k^2(3\hat{\ell}^2+\eta^2)}{\hat{\ell}^2(\hat{\ell}^2+\eta^2)^2} - \frac{\eta k^2}{\hat{\ell}^3}\arctan\frac{\hat{\ell}}{\eta}\right)\frac{1}{r^3} + \frac{4\eta k\hat{\ell}^2}{(\hat{\ell}^2+\eta^2)^2}\frac{1}{r^4} + \frac{2\hat{\ell}^4}{(\hat{\ell}^2+\eta^2)^2}\frac{1}{r^5}\right. \tag{3.8}$$

One can come back to the comparison with the LTS potential by noting that the plane wave limit is reached in the BKGP potential by setting η to zero leaving only the r^{-5} term and no ℓ dependence. It is thus identical to the LTS potential in this limit except that the LTS is 4/3 larger. Since the only approximation made by BKGP and not by LTS is the on-energy-shell prescription for the Green function and that approximation is valid in the semiclassical limit to first order, we must conclude that the LTS potential is wrong by a factor of 4/3 in this limit.

A more universal comparison between the LTS and BKGP potential was made using an analytical JWKB evaluation of scattering amplitudes along a Coulomb trajectory. The sub-Coulomb ratio to Rutherford cross section is then given by

$$\frac{\sigma(\theta)}{\sigma_R(\theta)} = \exp(-Kf(\theta)) \tag{3.9}$$

for the BKGP potential where

$$K = \frac{16\pi}{225}\frac{K^4}{\eta^2}\frac{B(E2)\uparrow}{Z_r^2 e^2} \tag{3.10}$$

is a function of the constants of the reaction and $f(\theta)$ is a universal function of angle.

$$f(\theta) = \frac{9}{4}\left[(\cos\tfrac{1}{2}\theta)^4\left(\tfrac{4}{3}D^4 + \tfrac{104}{105}D^5\right) + (\sin\theta)^2\left(\tfrac{\pi}{4}D^3 + \tfrac{1}{30}(64-15\pi)D^4\right)\right.$$
$$\left. + \left[(3 + (\tan\tfrac{1}{2}\theta)^2)(\sin\tfrac{1}{2}\theta)^4 - ((\tan\tfrac{1}{2}\theta)^3\tfrac{1}{2}(\pi-\theta))\right](D^2 + \tfrac{2}{3}D^3)\right] \tag{3.11}$$

with

$$D = (1 + \csc\tfrac{1}{2}\theta)^{-1}$$

The exponential form is just an S-matrix form for the flux lost to the 2^+ cross section. Thus to lowest order

$$\frac{\sigma^{0^+}(\theta)}{\sigma_R(\theta)} = 1 - Kf(\theta) \tag{3.12}$$

and one would expect $Kf(\theta)$ to correspond to the semiclassical excitation probability for Coulomb excitation of the 2^+ state. Curiously enough while this correspondence is true at 180° the particular approximations used in evaluating $f(\theta)$ lead to small deviations in the angular function $f(\theta)$ from the standard semiclassical result $g(\theta)$ at other angles. And there is no manifest similarity in form between $f(\theta)$ and the semiclassical analogue

$$g(\theta) = \frac{9}{4}\left[\tfrac{1}{3}(\sin\tfrac{1}{2}\theta)^4 + (\tan\tfrac{1}{2}\theta)^4\left[1 - (\tan\tfrac{1}{2}\theta)\tfrac{1}{2}(\pi-\theta)\right]^2\right] \tag{3.13}$$

even though their maximum deviation at any angle is 2%.

One may also derive a JWKB representation of the LTS potential in which one obtains a function $\bar{f}(\theta)$ instead of $f(\theta)$ to be used in the exponential

$$\bar{f}(\theta) = D^4\left[4 + 6\ln\left[1 + \frac{8e^{-5/2}}{\csc\frac{1}{2}\theta - 1}\right]\right] \tag{3.14}$$

The universal ratio of these functions for the LTS potential and the BGKP potential is plotted in Figure 3.3. As we have observed, the LTS potential gives 33% too much flux loss in the forward direction corresponding to the plane wave (or large ℓ_p) limit. At intermediate angles of about 40° to 110° the ratio deviates little from unity, which explains the success of the LTS potential in this angular region. Thus the universal comparison with the BKGP potential, which potential has been shown to be correct in its proper limits, provides the only solid justification for use of the LTS potential, and then only in the prescribed angular range.

In the following, we discuss the extension of the work originated by BKGP to the more general case of multiple Coulomb polarization effects where reorientation of the 2^+ as well as coupling to higher excited states (4^+, 6^+, etc.) come into play.

3.2 Quantal Theory of Multipole Coulomb Polarization Potentials

Whenever the coupling strength is large, multistep contributions to the elastic scattering become important. Therefore in cases involving strongly deformed nuclei, the two-step Coulomb polarization potential of BKGP or LTS is inadequate, and one has to construct corrections that carry with them the multistep nature of the elastic to inelastic feedback coupling.

Attempts have been made previously to use the semiclassical theory of multiple Coulomb excitation of Alder and Winther [12] as a starting point for ar inversion procedure aimed at constructing the wave function equivalent polarization potential, using Eq. (2.24) and (2.25).

These equations have been used in Ref. [6] to obtain U_D^L for sub-barrier multiple Coulomb absorption using the sudden-limit closed expressions for $\langle 0|U(r,t^{\pm},t_o)|0\rangle$ obtained by Alder and Winther. In the weak coupling case, which corresponds to the inclusion of only the 2^+ channel, it wa found that the semiclassically derived U_D^L coincides exactly with the quantum mechanical expression obtained using the first term on the RHS of Eq. (2.10), namely the BKGP potential Eq. (3.8). The trajectory unsymmetrized inversion formula of Eq. (2.25) (without the factor 1/2 and the second term) was used by Broglia and Winther [13] to derive the polarization potential which is ℓ-independent.

For large values of the coupling strength, however, the semiclassical theory supplies basically a numerical algorithm for the obtaining of U_D^L once

the amplitudes $\langle 0|U^{\pm}|0\rangle$ are given. This, in a way, is analogous to the numerical obtaining of U_D^L from the exact elastic wave function (see Eq. (2.12)).

A major disadvantage of the semiclassical method is the necessity for dealing with complex "classical" trajectories when volume absorption becomes effective at above-barrier-energies (of course complex trajectories are required even in the absence of absorption, when considering contributions from classically forbidden regions). This, though in principle tractable, makes the semiclassical method less convenient. Another, quantal, inversion calculation was performed by Frobrich et al. [14].

A more convenient starting point for the derivations of the Coulomb polarization potential is the set of coupled radial equations for multipole Coulomb excitation. These equations were employed by Hussein [5] to derive the polarization potential for the process $0^+ \to 2^+ \to 0^+$ with reorientation of the 2^+ exactly. The procedure suggested in [5] was further extended by Carlson, Hussein and Baltz [7] to the calculation of the potential for the process $0^+ \to 2^+ \to 4^+ \to 2^+ \to 0^+$, with reorientation in the 2^+ considered exactly. The essential approximation used in the above procedure was the replacement of the intermediate channel Green's function by its on-energy shell (delta function) part. The potential for higher order processes can be straightforwardly derived following the lines of [5] and [7].

In the following subsections, we present in some detail the method of Ref. [5] and [7]. We also develop a procedure that would enable one to take into account the effects arising from the previously neglected principal part of the intermediate channel Green function.

3.3 The Quantum Mechanical Coupled Channel Equations for Multiple Coulomb Excitation

We investigate the collision of a spherical nucleus 1 (considered as a point charge, Z,e) on a deformed target nucleus 2, at sub-barrier energies. We study the Coulomb excitation of low-lying states IM of spin I and magnetic quantum number M with excitation energy E_I. For the total wave function in the center of mass system we use the expansion [12]

$$|\psi\rangle = \sum_{\substack{\ell_o \ell \\ IJN}} \frac{\sqrt{\pi}(2\ell_o+1)}{k_{I_o} r} i^{\ell_o+1} e^{i\sigma_{\ell_o}(\eta_{I_o})} \langle \ell_o\, 0\, I_o M_o | JN\rangle \tag{3.15}$$

$$\times \psi^{\ell_o I_o}_{(\ell I)J}(r) |(\ell I)JN\rangle$$

where the channel wave functions are given by

$$|(\ell I)JN\rangle = \sum_{Mm} \langle \ell m\ IM | JN\rangle\, |IM\rangle\, Y_{\ell m}(\hat{r}). \tag{3.16}$$

Here J is the total conserved channel angular momentum and N its projection on the z-axis. The relative position of the centers of mass of 1 and 2 is denoted by r while the superindices $\ell_o I_o$ indicate the initial projectile orbital angular momentum and target spin respectively. Inserting the wave function (3.15) into the time-independent Schrödinger equation

$$(H-E)|\psi\rangle = 0\ . \tag{3.17}$$

We obtain a system of coupled equations for the radial wave functions for each channel angular momentum J

$$\left(\frac{d^2}{dr^2} + k_I^2 - \frac{2\mu}{\hbar^2}\frac{\ell(\ell+1)}{2\mu r^2} - \frac{2\mu}{\hbar^2}\frac{Z_1 Z_2 e^2}{r} \right) \psi^{\ell_o I_o}_{(\ell I)J}(r) = \sum_{\ell' I'} V^J_{\ell I, \ell' I'}(r)\, \psi^{\ell_o I_o}_{(\ell' I')J}(r) \tag{3.18}$$

The coupling potential $V^J_{\ell I, \ell' I'}$ is given by

$$V^J_{\ell I, \ell' I'}(r) = \frac{4\sqrt{\pi} Z_1 e\mu}{\hbar^2} \sum_\lambda \left[\frac{(2\ell+1)(2\ell'+1)}{(2\lambda+1)}\right]^{1/2} (-1)^{J+I'+\lambda} \tag{3.19}$$

$$\times \langle I' \| M(E\lambda) \| I\rangle \begin{pmatrix} \ell & \ell' & \lambda \\ 0 & 0 & 0 \end{pmatrix} \begin{Bmatrix} J & \ell' & I' \\ \lambda & I & \ell \end{Bmatrix} \frac{1}{r^{\lambda+1}} \equiv \sum_\lambda a^\lambda_{\ell I \ell' I'} \frac{1}{r^{\lambda+1}}$$

where $\langle I' \| M(E\lambda) \| I\rangle$ is the reduced matrix element of the electric λ-pole moment of the target. We shall, in the following, consider the specific case of a quadrupole-deformed even-even target nucleus 2.

For a simple rotor

$$|\langle 0 \| M(E2) \| 2\rangle|^2 = B(E2)\uparrow \tag{3.20}$$

and all other reduced matrix elements in the ground state (K=0) band can be related to the matrix element between the ground state and first excited state

$$\langle I \| M(E2) \| I'\rangle = \sqrt{(2I+1)(2I'+1)} \begin{pmatrix} I' & I & 2 \\ 0 & 0 & 0 \end{pmatrix} \tag{3.21}$$

$$\times \langle 0 \| M(E2) \| 2\rangle\ .$$

Likewise, a symmetrized dimensionless quadrupole strength parameter may also be defined to include dynamic effects

$$q_{I\to I'} = (-1)^{\frac{I+I'+2}{2}} q_{0\to 2} = (-1)^{\frac{I+I'+2}{2}} \sqrt{\frac{\pi}{5}} \sqrt{\frac{\eta_I \eta_{I'}}{a_I a'_I}} \frac{\langle 0 \| M(E2) \| 2\rangle}{Z_2 e}\ . \tag{3.22}$$

a_I is half the distance of closest approach for a head on collision in channel I, $a_I = \frac{Z_1 Z_2 e^2}{2(E-E_I)}$, and $\eta_I = \frac{Z_1 Z_2 e^2}{\hbar v_I} = k_I a_I$ is the Sommerfeld parameter in channel I. Once the $\psi^{\ell_o I_o}_{(\ell I)J}(r)$ are obtained from Eq. (3.18) the corresponding T-matrices $T^J_{\ell I, \ell_o I_o}$ are extracted from their asymptotic forms, i.e.,

$$\psi^{\ell_o I_o}_{(\ell I)J}(r) \overset{r\to\infty}{=} \delta_{II_o} e^{-i\phi_{\ell I}(r)} - \sqrt{\frac{k_{I_o}}{k_I}}\, e^{i\phi_{\ell I}(r)}\, T^J_{\ell I,\ell_o I_o} \tag{3.23}$$

where $\phi_{\ell I}(r) = k_I r - \eta_I \ell n(2k_I r) - \frac{\pi}{2}\ell + \sigma_\ell(\eta_I)$, σ_ℓ being the Coulomb phase shift. With the $T^J_{\ell I,\ell_o I_o}$ one can then calculate the amplitudes $f_{I_o M_o \to IM}(\theta,\phi)$ for Coulomb excitation from the ground state $|I_o M_o\rangle$ to the final state $|IM\rangle$

$$f_{I_o M_o \to IM}(\theta,\phi) = \frac{i\sqrt{\pi}}{\sqrt{k_I k_{I_o}}} \sum_{\ell\ell_o J} \sqrt{(2\ell_o+1)}\langle \ell_o 0\ I_o M_o | JM_o\rangle$$

$$i^{\ell_o-\ell}\langle \ell m\ IM | JM_o\rangle \{\delta_{II_o}\delta_{\ell\ell_o} - e^{i(\sigma_\ell(\eta_I)+\sigma_{\ell_o}(\eta_{I_o}))} \times T^J_{\ell I,\ell_o I_o}\}\, Y_{\ell m}(\theta,\phi) \tag{3.24}$$

The differential cross sections are then calculated as usual.

3.4 The On-Energy-Shell Approximation and the Equivalent Local Coulomb Polarization Potential

In order to calculate the cross section for inelastic Coulomb scattering one has to solve Eq. (3.18) with the appropriate boundary condition of an incoming wave present only in the elastic channel [12]. It is important to recognize that with an increasing number of coupled channels the solution to Eq. (3.18) becomes more and more complicated. However, much progress has been made recently in solving these equations, even fully quantum mechanically, rapidly on a computer [15,16,17]. For the case of low lying rotational states we adopt the on-energy-shell approximation for the channel Coulomb Green's function [4,7]

$$G^{(+)}_{(\ell I)}(r,r') = -\frac{i}{k_I} F_\ell(k_I r_<) H^{(+)}_\ell(k_I r_>) \approx -\frac{i}{k_I} F_\ell(k_I r) F_\ell(k_I r') \ . \tag{3.25}$$

We shall assess the accuracy of this approximation later. In the above, $F_\ell(kr)_I(H^{(+)}(k\,r))$ is the regular (outgoing) Coulomb function and $r_<(r_>)$ ℓ corresponds to the smaller (larger) of r and r'.

The solution of Eq. (3.18) may be written as an integral equation

$$\psi_{(\ell I)\ell_0}(r) = F_{\ell_0}(k_0 r)\,\delta_{II_0}\,\delta_{\ell\ell_0} + \sum_{\ell' I'} \int G_{\ell I}(r,r')\, a_{\ell I \ell' I'}\, \frac{1}{r'^3}\, \psi_{(\ell' I')\ell_0}(r')dr' \tag{3.26}$$

We now use the approximation (3.26) in (3.27) and obtain

$$\psi_{(\ell I)\ell_0}(r) = F_{\ell_0}(k_0 r)\,\delta_{II_0}\,\delta_{\ell\ell_0} + \left(\frac{-i}{k_I}\right) F_\ell(k_I r) \sum_{\ell' I'} \int_0^\infty dr' \times F_\ell(k_I r')\, a_{\ell I \ell' I'}\, \frac{1}{r'^3}\, \psi_{(\ell' I')\ell_0}(r') \tag{3.27}$$

Note the separable form of the integral equation. Matrix techniques may now be used to obtain the solution (details are in reference [7]). The result is

$$\psi_{(\ell I)\ell_0}(r) = F_{\ell_0}(k_0 r)\,\delta_{I0}\,\delta_{\ell\ell_0} + (-1)\, F_\ell(k_I r)\, [\underline{1} + i\,\underline{C}]^{-1}_{12}\,\underline{C}_{20} \tag{3.28}$$

where we have introduced the coupling matrix $\underline{C}$ whose matrix elements are given by

$$C_{\ell'' I'',\ell I} = \frac{1}{k_{I''}}\, a_{\ell'' I'' \ell I} \int dr\, F_{\ell''}(k_{I''},r)\, \frac{1}{r^3}\, F_\ell(k_I r) \ . \tag{3.29}$$

Equation (3.28) can be used to calculate the trivially equivalent local Coulomb polarization potential in the elastic channel as was done in Refs. [4] and [5]. Inserting the second term of Eq. (3.28) in the r.h.s. of Eq. (3.18) for $\psi_{(\ell_0 0)\ell_0}(r)$ we immediately obtain for the sum

$$\sum_{\ell' I'} V^{\ell_0}_{\ell_0 0 \ell' I'}(r)\, \psi^{\ell_0 0}_{(\ell' I')\ell_0}(r) \tag{3.30}$$

$$= a_{\ell_0 0 \ell 2} \frac{1}{r^3} (-i)\, F_{\ell}(k_2 r)[\underline{1} + i\underline{C}(\ell)]^{-1}_{22}\, C_{20}(\ell)$$

$$\equiv \frac{2\mu}{k^2} V_{opt}(r)\, \psi_{(\ell_0 0)\ell_0}(r) = \frac{2N}{h^2} V_{opt}(r)\, F_{\ell_0}(k_0 r)$$

$$\text{or} \quad \frac{2\mu}{h^2} V_{opt}(r) = -\, i(F(\ell;r))_{02}\, [\underline{1} + i\, \underline{C}(\ell)]^{-1}_{22}\, C_{20}(\ell) \tag{3.31}$$

where $F(\ell;r)$ is a 3-component vector given by

$$(F(\ell;r))_{02} = \left(\frac{F_{\ell_0+2}(k_2 r)}{F_{\ell_0}(k_0 r) r^3}\, a_{\ell_0 0, \ell_0+2, 2}\, , \frac{F_{\ell_0}(k_2 r)}{F_{\ell_0}(k_2 r) r^3}\, a_{\ell_0 0, \ell_0 2} \right. \tag{3.32}$$

$$\left. \frac{F_{\ell_0-2}(k_2 r)}{F_{\ell_0}(k_0 r) r^3}\, a_{\ell_0 0, \ell_0-2, 2} \right) .$$

Equation (3.31) describes the effect of the coupling of the elastic channel to all other inelastic channels. It is a simple realization of the Feshbach theory for the optical potential [1]. Denoting the projection operator that projects out the elastic channel of the full wave function by P and the complementary operator $Q \equiv 1-P$ which projects out all inelastic channels, we can write Eq. (3.31) as

$$V_{opt} = V_{PQ}[\underline{1} + i\, \underline{C}_{QQ}]^{-1} V_{QP} \quad . \tag{3.33}$$

Therefore, the matrix $[\underline{1} + i\, \underline{C}_{QQ}]^{-1}$ is effectively the Q-space propagator.

In our particular case of multiple Coulomb excitation through the quadrupole coupling, V_{QP} is just V_{20} as only the 2^+ channel is coupled directly to the elastic, 0^+, channel. Within the Q-space the 2^+ channel couples directly only to the 4^+. The 4^+ then couples to the 6^+ state and so on. This suggests that the structure of the matrix $[\underline{1} + iC_{QQ}]^{-1}$ is

$$[\underline{1} + i\, \underline{C}_{QQ}]^{-1}_{22} = [\underline{1} + i\, \underline{C}_{22} + \underline{C}_{24}\ \ [\underline{1} + i\, \underline{C}_{Q-2\ Q-2}]^{-1}_{44}\, \underline{C}_{42}]^{-1} \tag{3.34}$$

where the symbol Q-2 refers to the subspace spanned by states in the Q-space except the 2^+. Eq. (3.34) can easily be derived by expanding the matrix propagator in $\underline{C}$ and inserting Q whenever calculating products of $\underline{C}$'s [7]. It should be emphasized that once the matrix propagator is decomposed into propagation in smaller subspaces as given in (3.34) the calculation of V_{opt} becomes quite simple. Realizing that C_{ij} is an $(i+1) \times (j+1)$ matrix (in magnetic quantum number space) such a calculation can then be easily made by inverting the matrix propagator.

In the following we assume zero energy loss in the different excitation processes ($k_I = k_0$). We can correct for this approximation by inserting the semiclassical energy loss factor $q_{I \to I'}(\varepsilon_{I \to I'})$ for each coupling. We also utilize the simple relations, valid for large ℓ, among $F_\ell(kr)$, $F_{\ell+2}(kr)$ and $F_{\ell-2}(kr)$ obtained in Ref. [4] and given in Eq. (3.7). Finally, we shall use the large ℓ values of the 3-j and 6-j symbols needed in the calculation and given in Appendix B. With the above approximations and assumptions the expressions for $V_{opt}^{(2)}(r)$ given in (3.31) reduces to the BKGP potential considered Section 3.1 if all coupling except C_{20} is set to zero.

It is easily seen that the simple r-dependence of the potential given in the BKGP potential also holds for the more exact potential of Eq. (3.31) if the same assumptions and approximations are made [5], i.e.,

$$iV_{opt}(r) = \frac{a_\ell}{r^3} + \frac{b_\ell}{r^4} + \frac{c_\ell}{r^5} \quad . \tag{3.35}$$

This is clear since the r-dependence of $V_{opt}(r)$ is contained only in the vector $F(r;\ell)$. The propagator $[\underline{1} + i\,\underline{C}(\ell)]^{-1}$, which is the quantity used to get approximate forms for $V_{opt}(r)$, does not depend on r. In Eq. (3.35) the complex coefficients, a_ℓ, b_ℓ and c_ℓ depend on the orbital angular momentum, ℓ, the Sommerfeld parameter, η, the center of mass energy, E, and the quadrupole coupling strength q_{ij}. In Ref. [6] the potential $V_{opt}(r)$ was derived using the semiclassical theory of Coulomb excitation developed by Alder and Winther [12]. The ℓ- and r-dependence of $V_{opt}(r)$ of Eq. (3.35) and that of Frobrich et al [14] are quite different. One advantage of $V_{opt}(r)$ of Eq. (3.35) is its simple r-dependence as well as the explicit ℓ-dependence which can be obtained by inverting the matrix $(\underline{1} + i\,\underline{C}(\ell))$ in Eq. (3.31). We shall give below the result for the case of the coupling of the 0^+ channel to the 2+ channel including the reorientation of the 2+ to all orders. We shall also present the result when including the coupling to the 4+ channel. In order to perform these calculations we first rewrite Eq. (3.34) in the equivalent, but more transparent form

$$[\underline{1} + i\,\underline{C}(\ell)]^{-1}_{22} = [1 + i\,\underline{C}_{22}(\ell) + \underline{C}_{24}(\ell)[1 + i\,\underline{C}_{44}(\ell) + \underline{C}_{46}(\ell)[\cdots]]^{-1}\underline{C}_{42}(\ell)]^{-1} \tag{3.36}$$

in the above each coupling matrix $\underline{C}_{ij\neq i}(\ell)$ contains an appropriate energy loss factor $\sqrt{g_{ij}(E_{ij})}$ whereas the reorientation matrices $\underline{C}_{ii}(\ell)$ do not. Therefore, the Coulomb polarization potential for the two channel case with reorientation is given by

$$V^{(2)Reor.}_{opt}(r) = -\frac{i}{\gamma^3}\left(\frac{\hbar^2}{2\mu}\right)(F(r;\ell))_{02}\,[\underline{1} + i\,\underline{C}_{22}(\ell)]^{-1}\,\underline{C}_{20}(\ell) \tag{3.37}$$

Explicitly inverting the matrix [7] we obtain expressions for the real and imaginary part of $V^{(2)Reor}_{opt}$.

$$\begin{aligned}
\mathrm{Re}\,V^{(2)Reor.}_{opt}(r) = &-\frac{4}{35}\left(\frac{E}{\eta}\right) q^2_{0\to2}\, q^2_{2\to2}\left(\frac{a}{r}\right)^3 g_{02}(\varepsilon_{0\to2}) \\
&\times \Big[1 + \frac{4}{49} q^2_{2\to2}\Big(\frac{1}{\bar{\ell}^4}\Big(1 - \frac{\arctan\bar{\ell}}{\bar{\ell}}\Big)^2 + \frac{1}{3}\frac{1}{(1+\bar{\ell}^{-2})^2}\Big)\Big]^{-1} \\
&\times \Big[\frac{(1-\arctan\bar{\ell}/\bar{\ell})^2}{\bar{\ell}^4} + 2\frac{(1-\arctan\bar{\ell}/\bar{\ell})}{\bar{\ell}^2}\Big(\frac{\bar{\ell}^{-2}-1}{(\bar{\ell}^{-2}+1)^2}\Big) \\
&- \frac{1}{3(\bar{\ell}^{-2}+1)^2} - 8\frac{(1-\arctan\bar{\ell}/\bar{\ell})}{(\bar{\ell}^{-2}+1)^2}\left(\frac{a}{r}\right) \\
&- 4\frac{\bar{\ell}^{-2}(1-\arctan\bar{\ell}/\bar{\ell})}{(\bar{\ell}^{-2}+1)^2}\left(\frac{a}{r}\right)^2\Big]
\end{aligned} \tag{3.38}$$

and

$$\mathrm{Im}\,V^{(2)Reor}_{opt}(r) = \Big[1 + \frac{4}{49} q^2_{2\to2}\Big(\frac{1}{\bar{\ell}^4}(1-\arctan\bar{\ell}/\bar{\ell})^2 + \frac{1}{3}\frac{1}{(\bar{\ell}^{-2}+\ell)^2}\Big)\Big]^{-1} V^{(2)}_\ell(r) \tag{3.39}$$

where $V^{(2)}_\ell(r)$ is the BKGP potential Eq. (3.8). Eq. (3.39) is the potential obtained by Hussein [5]. It is interesting to notice that Re $V^{(2)Reor}_{opt}(r)$ becomes identically zero when $q_{2\to2} = 0$, i.e., no reorientation effect. As a matter of fact this result is more general, Re $V_{opt}(r) = 0$ when all reorientation couplings vanish, $q_{ii} = 0$, as can be seen from Eq. (3.36) and (3.31). The above observation sheds some light on the results of Ref. [6] where $V_{opt}(r)$ was calculated assuming a harmonic vibrational spectrum for the target nucleus (all $q_{ii} = 0$) and it was found that $V_{opt}(r)$ is purely imaginary.

Including the coupling to the 4^+ state to all orders results in a potential $V^{(4)}_\ell(r)$ which has the form [7]

$$V_{\ell}^{(4)}(r) = -i\,\underline{F}(r,\ell)\,\frac{1}{1 + i\,\underline{C}_{22}(\ell) + \underline{C}_{24}(\ell)\underline{C}_{42}(\ell)}\,\underline{C}_{20}(\ell)$$

$$= -i\,\frac{2}{5}\,\frac{E}{\eta}\,q_{0\to 2}^2\,\left(\frac{a}{r}\right)^3\,g_{02}(\xi_{02})\,\{(-1 + f(r))\,[1 + \frac{3}{49}\,q_{2\to 4}^2\,g_{24}(\xi_{24})\,(\alpha^2 + \frac{\gamma^2}{3})$$

$$- i\,\frac{4}{7}\,q_{2\to 2}\alpha]\,\gamma$$

$$- (1 + \frac{6}{49}\,q_{2\to 4}^2\,g_{24}(\xi_{24})(\alpha^2 + \frac{\gamma^2}{3}))\,\alpha$$

$$+ i\,\frac{2}{7}\,q_{2\to 2}\,(\frac{\gamma^2}{3} - \alpha^2)\}$$

$$\times\,\{(1 + \frac{3}{49}\,q_{2\to 4}^2\,g_{24}(\xi_{24})(\alpha^2 + \frac{\gamma^2}{3}))(1 + \frac{36}{245}\,q_{2\to 4}^2\,g_{24}(\xi_{24})(\alpha^2 + \frac{\gamma^2}{3}))$$

$$+ \frac{4}{49}\,q_{2\to 2}^2\,(\alpha^2 + \frac{\gamma^2}{3}) - i\,\frac{18}{15 \times 49}\,q_{2\to 4}^2\,g_{2\to 4}(\xi_{24})\,q_{2\to 2}(\gamma^2 - \alpha^2)\alpha\}^{-1} \qquad (3.40)$$

where f(r) is given by

$$f(r) = \frac{2}{1 + \bar{\ell}^{-2}}\,[1 + 2\bar{\ell}^{-2}\,(\frac{a}{r}) + \bar{\ell}^{-4}\,(\frac{a}{r})^2] \qquad (3.41)$$

$\alpha \equiv -(1 - \bar{\ell}^{-1}\tan^{-1}\bar{\ell})/\bar{\ell}^2$; $\beta \equiv \frac{1}{\sqrt{6}}(1 + \bar{\ell}^2)^{-1}$

and $\gamma = 8\sqrt{6}$. Eq. (3.40) reduces to (3.38) and (3.39) in the limit $q_{2\to 4} = 0$. It is clear that one could calculate explicitly $V_{opt}(r)$ to whatever order desired. However, such expressions become more and more complicated as already indicated in Eq. (3.40). Instead one could simply invert the matrix propagator numerically in conjunction with optical model calculations. In Fig. 3.4 we show the coefficients a_{ℓ}, b_{ℓ} and c_{ℓ} as function of $\bar{\ell}$ for the different cases studied above as well as for that including the excitation of up to the $I = 16^+$ state. It is clear from Fig. 3.4 that the imaginary part of $V_{opt}(r)$, determined by Re a_{ℓ}, Re b_{ℓ} and Re c_{ℓ}, behaves basically like r^{-3} for small values of $\bar{\ell}$ whereas for large values of $\bar{\ell}$ it goes as r^{-5}. This fact seems to hold irrespective of the value of the quadrupole coupling strengh q. The above

result continues to hold when the energy loss is properly included by use of the semiclassical energy loss factors as discussed before. The real part of $V_{opt}(r)$ shows a similar behavior to Im $V_{opt}(r)$ namely it goes as r^{-3} for small $\bar{\ell}$ and as r^{-5} for large $\bar{\ell}$. For intermediate values of ℓ both the real and the imaginary parts of $V_{opt}(r)$ show the general r-dependence of Eq. (3.35). The q-dependence of V_{opt} is shown in Fig. 3.5 The coefficient q_{ℓ}, b_{ℓ} and c_{ℓ} have a rather smooth dependence on q. Notice that for $\ell = \bar{0}$ the coefficients $b_{\ell=0}$ and $c_{\ell=0}$ are identically zero for all q. This corroborates the discussion above about the r-dependence of $V_{opt}(r)$.

3.5 Considerations of Off-Shell Effects

The optical potential formalism discussed up to now is basically an on-energy-shell approach. In this section, we will investigate the effects of off-shell contributions to polarization potential.

In order to begin the study of off-shell effects, let us temporarily abandon the search for an optical potential. Instead, let us directly sum the Born series for the T-matrix. We look at the case of elastic scattering with coupling to a 2^+ state but with no reorientation. In the on-energy-shell approximation, the series may be summed to yield the following expression for the elastic T-matrix

$$T_{\ell 0^+} = i\,D_{\ell}^{020}\,\sum_{n=0}^{\infty}\,(D_{\ell}^{020})^n \qquad (3.42)$$

The factor D_{ℓ}^{020} is of the form

$$D_{\ell}^{020} = \sum_{\ell'}\,C_{\ell\ell'}\,\left[\int_0^{\infty} F_{\ell}(r)\,\frac{1}{r^3}\,F_{\ell'}(r)\,dr\right]^2 \qquad (3.43)$$

In scattering through intermediate states in the series there will be off-shell terms as well. The lowest order of these are contributions to the term which led to the $(D_\ell^{020})^2$ term in the on-shell series. The off-shell parts of this term contain two integrands of the form $F_\ell(r)\ 1/r^3\ G_{\ell'}(r)$ or one integrand of the from $G_\ell(r)\ 1/r^3\ G_{\ell'}(r)$. As the form are oscillatory, we assume their contribution negligible and approximate the lowest order off-shell contributrion as

$$(D_\ell^{020})^2_{G1} \sim - \sum_{\ell'\ell''} C_{\ell\ell'}C_{\ell\ell''} \int_0^\infty F_\ell(r)\ \frac{1}{r^3}\ F_{\ell'}(r)\ dr$$
$$\cdot \int_0^\infty G_{\ell'}(r')\ \frac{1}{r'^3}\ G_\ell(r')\ dr' \int_0^{r'} F_\ell(r'')\ \frac{1}{r''^3}\ F_{\ell''}(r'')\ dr''$$
$$\cdot \int_0^\infty F_{\ell''}(r''')\ \frac{1}{r'''^3}\ F_\ell(r''')\ dr''' \qquad (3.44)$$

If we ignore the contribution at the turning point and inside (which is relatively small because of the limits of the integrals), then we may approximate in the semiclassical limit

$$\int_r^\infty G_{\ell'}(r')\ \frac{1}{r'^3}\ G_\ell(r')\ dr' \approx \int_r^\infty F_{\ell'}(r')\ \frac{1}{r'^3}\ F_\ell(r')\ dr' \ . \qquad (3.45)$$

We thus may consider terms of the form

$$(D_\ell^{020})_{G1} = - \sum_{\ell'\ell''} C_{\ell\ell'}C_{\ell\ell''} \int_0^\infty F_\ell(r)\ \frac{1}{r^3}\ F_{\ell'}(r)\ dr$$
$$\cdot \int_r^\infty F_{\ell'}(r')\ \frac{1}{r'^3}\ F_\ell(r')\ dr' \int_0^{r'} F_\ell(r'')\ \frac{1}{r''^3}\ F_{\ell''}(r'')\ dr''$$
$$\cdot \int_0^\infty F_{\ell''}(r''')\ \frac{1}{r'''^3}\ F_\ell(r''')\ dr''' \qquad (3.46)$$

Now, we write

$$\int_0^\infty F_\ell(r)\ \frac{1}{r^3}\ F_{\ell'}(r)\ dr = U^\infty_{\ell\ell'} = \int_0^\infty dU_{\ell\ell'} \qquad (3.47)$$

so that

$$(D_\ell^{020})^2_{G1} = - \sum_{\ell'\ell''} C_{\ell\ell'}C_{\ell\ell''} \int_0^{U^\infty_{\ell\ell'}} dU^{(1)}_{\ell\ell'} \int_{U^{(1)}_{\ell\ell'}}^{U^\infty_{\ell\ell'}} dU^{(2)}_{\ell\ell''} \int_0^{U^{(2)}_{\ell\ell''}} dU^{(3)}_{\ell\ell''} \quad [U^\infty_{\ell''\ell}] \qquad (3.48)$$

When the orbital angular momentum is zero (corresponding semi-classically to $\theta = 180°$), we have

$$(D_\ell^{020})^2_{G1} = - C_{02}\ C_{02} \int_0^{U^\infty_{02}} dU^{(1)}_{02} \int_{U^{(1)}_{02}}^{U^\infty_{02'}} dU^{(2)}_{02} \int_0^{U^{(2)}_{02}} dU^{(3)}_{02} \quad [U^\infty_{02}\ ]$$
$$= - C_{02}^2\ \frac{(U^\infty_{02})^4}{3} = - \frac{1}{3}\ (D_0^{020})^2 \qquad (3.49)$$

As there are two terms of the type $(D_0^{020})_{G1}{}^2$, we find that for $\ell = 0$, the lowest order off-shell contribution is - 2/3 of the corresponding on-shell term. If we look now at higher order terms in the Coulomb Born series, we see that the term whose on-shell contribution is $(D_0^{020})^{n+1}$ contains 2n terms with one integrand of the form $G_\ell(r)\ 1/r^3\ G_{\ell'}(r)$. Each of these terms contributes - 1/3 $(D_0^{020})^{n+1}$. Summing over all terms, we find for the T-matrix element

$$\pi T_{00+} = i\ [D_0^{020} \sum_{n=0}^\infty (D_0^{020})^n - \frac{2}{3}\ D_0^{020} \sum_{n=1}^\infty n(D_0^{020})^n]$$
$$= i\ [\frac{D_0^{020}}{1 - D_0^{020}} - \frac{2}{3}\ \frac{(D_0^{020})^2}{(1 - D_0^{020})^2}\ ]. \qquad (3.50)$$

Following the method of Ref. [4], the back angle ratio to Rutherford cross section is then

$$\frac{\sigma(180°)}{\sigma_R(180°)} = \frac{(1 - \frac{7}{43} K^2)^2}{(1 + \frac{1}{4} K)^4} \tag{3.51}$$

where

$$K = \frac{\sigma^{2^+}_{(1)}(180°)}{\sigma_R(180°)} = \frac{16}{45} q^2_{0\to 2} \tag{3.52}$$

is the first order cross section for excitation of the 2^+ state (see Eq. 3.10). We can compare this cross section with the on-energy-shell result of Ref. [4]

$$\frac{\sigma(180°)}{\sigma_R(180°)} = \frac{(1 - \frac{1}{4} K)^2}{(1 + \frac{1}{4} K)^2} \tag{3.53}$$

Through first order in K, the two results are identical. Numerical comparisons show the cross section including off-shell contributions agreeing better with coupled channel calculation.

It is possible to extend the approach we have used here to include higher order off-shell effects by including contributions to the Born series containing two or more integrands of the form $G_\ell(r)\ 1/r^3\ G_{\ell'}(r)$. To do this systematically, one first rearranges the Born summation to write it in terms of the distorted-wave K-matrix. The terms in the series expansion of the latter contain only the off-shell part of the intermediate propagators. The first term in the series is the DWBA matrix element. Truncating the series at this point yields the on-energy-shell expressions. All even order terms in the series vanish with the potential and approximations considered here. They contain two integrands of the form $F_\ell(r)\ 1/r^3\ G_{\ell'}(r)$. The third order term contains a contribution with one integrand of the form $G_\ell(r)\ 1/r^3\ G_\ell(r)$. It is this term that was incorporated into the T-matrix in the preceding calculation. The

advantage of the distorted-wave K-matrix is that each off-shell term appears only once in its expansion. In the Born summation, each off-shell term contributes to all higher order Born terms.

Calculating the higher order terms in the expansion of the distorted-wave K-matrix is a straightforward but tedious means of including the off-shell contributions. An alternative approach is to derive a set of coupled equations for the principal-part wave function (relative to the distorted waves) analogous to the inward-outward equations for the full wave-function. Applying the approximations used here to this set of equations and solving them yields a distorted-wave K-matrix containing the desired off-shell contributions to all orders. Comparison of its expansion with the term by term calculation bears out this statement.

The coupled equations for the principal-part wave-function are however, equivalent to a large number of such sets of coupled equations. Applying our approximations to any of these sets of equations yields the same results. As the inward-outward equations [18] are no doubt the most familiar of these, we will use them to show how all off-shell contributions can be included in the scattering quantities.

In the inward-outward approach, we take as an ansatz for the wave-function for a given value of the total angular moment, ℓ_0,

$$\psi^{\ell_0}_{(\ell I)(\ell' I')} \frac{1}{\sqrt{k_{I'}}} = F_\ell(k_I r) \frac{1}{\sqrt{k_I}} e^{i\sigma_{\ell I}} A^{\ell_0}_{(\ell I)(\ell' I')}(r) - H^+_\ell(k_I r) \frac{1}{\sqrt{k_I}} e^{-i\sigma_{\ell I}} B^{\ell_0}_{(\ell I)(\ell' I')}(r) \tag{3.54}$$

In labelling the states by spin and orbital angular momentum alone, we assume that we continue to treat the problem of Coulomb excitation of the rotational

band. In the general case, additional internal quantum numbers could be necessary in labelling the states.

We rewrite the wave function using matrix notation as

$$\psi^{\ell 0+}(r)\,\frac{1}{\sqrt{k}} = F^{\ell 0}(r)\,\frac{1}{\sqrt{k}}\,e^{i\sigma^{\ell 0}}\,A^{\ell 0}(r) - H^{\ell 0+}(r)\,\frac{1}{\sqrt{k}}\,e^{-i\sigma^{\ell 0}}\,B^{\ell 0}(r) \tag{3.55}$$

The regular and outgoing Coulomb wave-functions, $F_\ell(k_I r)$ and $H_\ell^+(k_I r)$. the Coulomb phase shifts, $\sigma_{\ell I}$, and the asymptotic wave numbers, k_I, form diagonal matrices $F^{\ell 0}(r)$, $H^{\ell 0}(r)$, $\sigma^{\ell 0}$ and k respectively. For the moment, we are interested in a complete set of solutions to the problem. Thus, we take the wave-function, $\psi^{\ell 0}(r)$ and the coefficients, $A^{\ell 0}(r)$ and $B^{\ell 0}(r)$ to be matrices rather than vectors.

To satisfy the incoming-wave boundary condition, we must have

$$A^{\ell 0}(\infty) = 1\ . \tag{3.56}$$

To ensure regularity of the wave-function at the origin, we must have

$$B^{\ell 0}(0) = 0\ . \tag{3.57}$$

Substituting the ansatz for the wave-function and the Coulomb Green's function

$$G^{\ell 0+}(r,r') = -\,F^{\ell 0}(r)\,\frac{1}{k}\,H^{\ell 0+}(r')\,\theta(r'-r) - H^{\ell 0+}(r)\,\frac{1}{k}\,F^{\ell 0}(r')\,\theta(r-r') \tag{3.58}$$

into the appropriate Lippmann-Schwinger equation, we can extract the inward-outward equations for the coefficients $A^{\ell 0}(r)$ and $B^{\ell 0}(r)$.

$$\frac{d}{dr}\,(e^{i\sigma^{\ell 0}}A^{\ell 0}(r)) = \frac{1}{\sqrt{k}}\,H^{\ell 0+}(r)\,V^{\ell 0}(r)\,F^{\ell 0}(r)\,\frac{1}{\sqrt{k}}\,(e^{i\sigma^{\ell 0}}A^{\ell 0}(r)) - \frac{1}{\sqrt{k}}\,H^{\ell 0}(r)\,V^{\ell 0}(r)\,H^{\ell 0}(r)\,\frac{1}{\sqrt{k}}\,(e^{-i\sigma^{\ell 0}}B^{\ell 0}(r)) \tag{3.59}$$

and

$$\frac{d}{dr}\,(e^{-i\sigma^{\ell 0}}B^{\ell 0}(r)) = \frac{1}{\sqrt{k}}\,F^{\ell 0+}(r)\,V^{\ell 0}(r)\,F^{\ell 0}(r)\,\frac{1}{\sqrt{k}}\,(e^{i\sigma^{\ell 0}}A^{\ell 0}(r)) - \frac{1}{\sqrt{k}}\,F^{\ell 0}(r)\,V^{\ell 0}(r)\,H^{\ell 0+}(r)\,\frac{1}{\sqrt{k}}\,(e^{-i\sigma^{\ell 0}}B^{\ell 0}(r)) \tag{3.60}$$

For the long range potential we are considering here, the terms $F^{\ell 0}V^{\ell 0}G^{\ell 0}$, $G^{\ell 0}V^{\ell 0}F^{\ell 0}$ and $H^{\ell 0+}V^{\ell 0}H^{\ell 0+}$ oscillate rapidly outside the turning point. We thus expect them to contribute little there. Inside the turning point, we expect the contribution to the scattering of all terms to be small relative to the total contributions from outside the turning point. It seems reasonable then to neglect the oscillatory terms. Rewriting the equations as integral equations and solving by back substitution, we find the neglect of these terms to be identical to the approximations we made previously. Instead of solving by this means, we make the approximations in the differential equations, reducing them to

$$\frac{d}{dr}\,(e^{-i\sigma^{\ell 0}}A^{\ell 0}(r)) = i\,\frac{d}{dr}\,C^{\ell 0}(r)\,(e^{i\sigma^{\ell 0}}A^{\ell 0}(r)) \tag{3.61}$$

and

$$\frac{d}{dr}\,(e^{-i\sigma^{\ell 0}}B^{\ell 0}(r)) = \frac{d}{dr}\,C^{\ell 0}(r)\,(e^{i\sigma^{\ell 0}}A^{\ell 0}(r)) - i\,\frac{d}{dr}\,C^{\ell 0}(r)\,(e^{i\sigma^{\ell 0}}A^{\ell 0}(r)) \tag{3.62}$$

where

$$C^{\ell 0}(r) = \int_0^r dr'\,\frac{1}{\sqrt{k}}\,F^{\ell 0}(r')\,V^{\ell 0}(r')\,F^{\ell 0}(r')\,\frac{1}{\sqrt{k}}. \tag{3.63}$$

We note that

$$C^{\ell 0}(\infty) \equiv C^{\ell 0} \tag{3.64}$$

is just the DWBA T-matrix for Coulomb excitation.

To write the solution to the equations in a meaningful closed form, the ordering effects in r must be negligible. We must have

$$\left[\frac{d}{dr} C^{\ell_0}(r)\Big|_{r_1} , \frac{d}{dr} C^{\ell_0}(r)\Big|_{r_2} \right] = 0 \quad \forall r_1, r_2. \tag{3.65}$$

Earlier, in calculating the lowest order off-shell contribution, we avoided this assumption by restricting our attention to $\ell_0 = 0$. The matrix then degenerated to a number and we had no problem with ordering. If we were to include reorientation or states beyond the 2^+ excited state, this would not be the case even for $\ell_0 = 0$. However, when the Sommerfeld parameter, η, is large and the adiabaticity parameters, $\xi_{I+I'} \approx 1/2\ \eta(E_{I'} - E_I)/E$ are small, the elements of the commutator remain close to zero and the ordering effects are small. We will assume that they can be neglected. Neglecting ordering effects is equivalent to using the sudden and semi-classical approximations.

The solutions to the equations which satisfy the boundary conditions are then

$$A^{\ell_0}(r) = e^{-i\sigma^{\ell_0}}\ e^{-iC^{\ell_0}(r)}\ e^{iC^{\ell_0}}\ e^{i\sigma^{\ell_0}} \tag{3.66}$$

and

$$B^{\ell_0}(r) = e^{i\sigma^{\ell_0}}\ \sin C^{\ell_0}(r)\ e^{-iC^{\ell_0}}\ e^{i\sigma^{\ell_0}} \tag{3.67}$$

We thus have

$$\pi T^{\ell_0} = B^{\ell_0}(\infty) = \frac{1}{2i}\ e^{i\sigma^{\ell_0}}\ (1 - e^{-2iC^{\ell_0}})\ e^{i\sigma^{\ell_0}} \tag{3.68}$$

so that

$$S^{\ell_0} = e^{i\sigma^{\ell_0}}\ e^{-2iC^{\ell_0}}\ e^{i\sigma^{\ell_0}} \tag{3.69}$$

Using the semi-classical Coulomb correspondence between angle and total angular momentum, we find this result to be equivalent to that of Alder and Winther in the sudden limit. In particular, for the case discussed earlier, we obtain here a form which looks similar to the Adler-Winther back angle ratio to Rutherford cross section. We obtain

$$\frac{\sigma(180°)}{\sigma_R(180°)} = (\cos\sqrt{K})^2 , \quad K = \frac{16}{45}\ q^2_{0\to 2} \tag{3.70}$$

Comparing this result with the earlier expressions for the back angle cross section, we find that it agrees with the on-shell cross section through first order in K while it agrees through second order in K with the cross section containing the lowest order off-shell terms. In general, the cross section obtained including off-shell terms through order n agrees with the expression here through order n + 1. The approximate solution to the inward-outward equations contains the desired off-shell terms to all orders.

A careful analysis shows that our approximate solution can be extended to include the effects of a short range optical potential as well. For this, one replaces the Coulomb distorted waves by the distorted waves of the optical + Coulomb potential. As the optical potential is short ranged, it is unimportant over most of the range where Coulomb excitation occurs. One then replaces the distorted ingoing/outgoing waves by their Coulomb counterparts. The effects of the optical potential thus enter only through the S-matrix for the optical + Coulomb potential, $e^{i\sigma^{\ell_0}}\ \bar{S}^{\ell_0}\ e^{i\sigma^{\ell_0}}$. The total S-matrix which result is

$$S^{\ell_0} = e^{i\sigma^{\ell_0}}\ e^{-iC^{\ell_0}}\ \bar{S}_0^{\ell_0}\ e^{-iC^{\ell_0}}\ e^{i\sigma^{\ell_0}} \tag{3.71}$$

The form of this result allows a simple interpretation paralleling the approximations used to obtain it. On the approach to the scattering center, Coulomb scattering and excitations occur, leading to a factor of $e^{-iC^{\ell_0}}$

$e^{i\sigma^{\ell_0}}$ in the S-matrix. This is followed by the scattering due to the optical potential which contributes a factor $S_0^{\ell_0}$. Finally, on the outgoing phase, Coulomb excitation and scattering again occur, contributing a factor of of $e^{i\sigma^{\ell_0}}\, e^{-iC^{\ell_0}}$. Equation (3.71) has been used to calculate the sub-barrier fusion cross section of deformed nuclei

Beside yielding asymptotic quantities such as the S-matrix, the approximate solution to the inward-outward equations gives the coefficients A^{ℓ_0} and B^{ℓ_0} as functions of r. With these, we can construct the approximate wave function. We can then proceed to construct an optical potential just as we did in the on-shell approximation. Assuming the case of a rotational band built on a 0^+ ground state, we can define the contribution of Coulomb excitation to the ground state optical potential by

$$\frac{2\mu}{\hbar^2} V^{\ell_0}_{opt}(r)\, \psi^{\ell_0+}_{(\ell_0 0)(\ell_0 0)}(r) \equiv \sum_{\ell,I} V^{\ell_0}_{(\ell_0 0)(\ell I)} \psi^{\ell_0+}_{(\ell I)(\ell_0 0)}(r)$$

$$= \sum_{\ell} V^{\ell_0}_{(\ell_0 0)(\ell 2)} \psi^{\ell_0+}_{(\ell 2)(\ell_0)}(r) \qquad (3.72)$$

so that

$$V^{\ell_0}_{opt}(r) \equiv \frac{\hbar^2}{2\mu} \sum_{\ell} V^{\ell_0}_{(\ell_0 0)(\ell 2)}(r)\, \psi^{\ell_0+}_{(\ell 2)(\ell_0 0)}(r) \Big/ \psi^{\ell_0+}_{(\ell_0 0)(\ell_0 0)}. \qquad (3.73)$$

The wave functions we will use here are those obtained from the solution to the inward-outward equations. The only difference between this potential and the on-shell one is this different approximation to the wave function.

If we substitute our expressions for $A^{\ell_0}(r)$ and $B^{\ell_0}(r)$ into the ansatz for the wave function and write the result in terms of the Coulomb incoming/outgoing waves, $H^{\ell_0\pm}(r)$, we find

$$\psi^{\ell_0+}(r)\, \frac{1}{\sqrt{k}} = \frac{i}{2} \left(H^{\ell_0-}(r)\, \frac{1}{\sqrt{k}}\, e^{iC^{\ell_0}(r)}\, e^{-iC^{\ell_0}}\, e^{i\sigma^{\ell_0}} \right.$$

$$\left. - H^{\ell_0+}(r)\, \frac{1}{\sqrt{k}}\, e^{-iC^{\ell_0}(r)}\, e^{-iC^{\ell_0}}\, e^{i\sigma^{\ell_0}} \right). \qquad (3.74)$$

We can make this more transparent by defining

$$\not{H}^{\ell_0\pm}(r)\, \frac{1}{\sqrt{k}} \equiv H^{\ell_0\pm}(r)\, \frac{1}{\sqrt{k}}\, e^{\mp iC^{\ell_0}(r)}\, e^{\pm iC^{\ell_0}}\, e^{\mp i\sigma^{\ell_0}} \qquad (3.75)$$

and writing

$$\psi^{\ell_0+}(r)\, \frac{1}{\sqrt{k}} = \frac{i}{2} \left[\not{H}^{\ell_0-}(r)\, \frac{1}{\sqrt{k}} - \not{H}^{\ell_0+}(r)\, \frac{1}{\sqrt{k}}\, S^{\ell_0} \right]. \qquad (3.76)$$

The effects of a short range optical potential can be incorporated simply in the latter expressions. One needs only to substitute the distorted waves of the optical + Coulomb potential for the Coulomb waves and to use the S-matrix containing the effects of the optical potential.

We note that this wave function is regular at the origin and satisfies the incoming wave boundary condition, as desired. Because of the r dependence introduced through the matrix $C^{\ell_0}(r)$, the component of the wave function in a channel ℓI varies as a function of r. Although a reasonable result, it greatly complicates the evaluation of the optical potential. In general, only with additional approximations is it possible to proceed beyond the formal expression for the potential. A problem we have examined is that of the ground state optical potential due to Coulomb excitation of a rotational band built on a 0^+ ground state. Using additional approximations, one of which is the $\chi_{eff}(\theta)$ or $\chi(\theta)$ approximation of Alder and Winther, the potential in that case can be put in a fairly simple closed form.

Here let us consider only the simplest case of Coulomb excitation of a 2^+ state. For this case, we can write the optical potential for the 0^+ ground state as

$$V^{\ell_0}_{opt}(r) = V^{\ell_0}_{opt,o.s.}(r)\ \alpha_{\ell_0}(r) \tag{3.77}$$

where $V_{opt,o.s.}{}^{\ell_0}(r)$ is the on-shell potential obtained previously

$$V^{\ell_0}_{opt,o.s.}(r) = -\,i\,\frac{2}{5}\,\frac{E}{\eta}\ g(\xi)\ q^2\ \left(\frac{a}{r}\right)^3\ \left[\frac{3\bar{\ell}^2+1}{\bar{\ell}^2(\bar{\ell}^2+1)^2}\right.$$

$$\left. -\,\frac{\tan^{-1}\bar{\ell}}{\bar{\ell}^3} + \frac{4\bar{\ell}^2}{(\bar{\ell}^2+1)^2}\ \frac{a}{r} + \frac{2\bar{\ell}^4}{(\bar{\ell}^2+1)^2}\left(\frac{a}{r}\right)^2\right] \tag{3.78}$$

and $\alpha_{\ell_0}(r)$ is an off-shell correction factor

$$\alpha_{\ell_0}(r) = \frac{1}{e_{\ell_0}}\cdot\frac{\sin(2e_{\ell_0})\ \cos(2e_{\ell_0} f_{\ell_0}(r))}{1+\cos(2e_{\ell_0})\ \cos(2e_{\ell_0} f_{\ell_0}(r))} \tag{3.79}$$

The constant e_{ℓ_0} is given by

$$e_{\ell_0} = q\left[\frac{\chi(\xi)}{5}\left(\frac{1}{3}\ \frac{1}{(\bar{\ell}^2+1)^2} + \frac{1}{\bar{\ell}^4}\left(1-\frac{\tan^{-1}\bar{\ell}}{\bar{\ell}}\right)^2\right)\right]^{1/2} \tag{3.80}$$

with $\bar{\ell} = \ell_0/\eta$. Finally, the function $f_{\ell_0}(r)$ is defined by

$$C^{\ell_0}(r) = C^{\ell_0} f_{\ell_0}(r) \tag{3.81}$$

an approximation used in the derivation.

We note that in this case the $\chi(\theta)$ or $\chi_{eff}(\theta)$ approximation is not needed.

In this simple case, we obtain a potential which factorizes into the on-shell potential obtained for this case and an off-shell correction factor. For extremely weak coupling, this reverts to the on-shell potential since

$$\alpha_{\ell_0}(r) \xrightarrow[q\to 0]{} 1\ . \tag{3.82}$$

For e_{ℓ_0} in the range $0 < e_{\ell_0} < \pi/4$, the correction factor increases the strength of the potential at small radii and decreases it at large radii. For $e_{\ell_0} > \pi/4$, the off-shell correction factor introduces oscillations as a function of r into the potential. For $\pi/2 > e_{\ell_0} > \pi/4$, these yield the unphysical result of an optical potential which is creative rather than absorptive at large radii. We thus expect $e_{\ell_0} = \pi/4$ to mark the limit of validity of this potential. Numerical comparisons have yet to be made.

3.6 The adiabatic Polarization Potential

So far in this chapter we have concentrated our attention on the calculation of the Coulomb polarization potential that arises from the coupling of the elastic channels to low-lying inelastic channels. In cases involving strongly deformed nuclei the use of the sudden approximation which amounts to ignoring the energy losses, is found to be a very reasonable starting point in the derivation. The resulting sudden potential for e.g. the process $0^+ \to 2^+ \to 0^+$ is found to be predominantly absorptive. The on-energy shell approximation for the intermediate 2^+ Green function is quite adequate. Besides the low lying collective states, there are also giant multipole resonances that should, in principle, be taken into account. Such adiabatic polarization potentials can be calculated perturbatively as was done 30 years ago by Alder et al. [9] and the result is given in Eq. (3.1). We supply below another derivation, which has the advantage of being fully quantum mechanical. Furthermore, the same procedure that was used in deriving the sudden polarization potential, namely the Feshbach reduction method, will be adopted for the present purpose.

The general form for the nonlocal potential exactly representing the effect of Coulomb excitation on the elastic channel (ignoring reorientation) may be written, as in Eq. (3.2), for a given initial orbital angular momentum

$$U_\ell(r,r') = \frac{2\mu}{k_\lambda \hbar^2} \frac{4\pi}{(2\lambda+1)^2} e^2 B(E\lambda)\uparrow \sum_{\ell'} \langle \ell 0 \lambda 0 | \ell' 0 \rangle$$

$$\times \frac{1}{r^{\lambda+1}} \frac{1}{r'^{\lambda+1}} F_{\ell'}(k_\lambda, r_<) H_{\ell'}(k_\lambda, r_>) \qquad (3.83)$$

This expression may be written equivalently [12] in terms of regular Coulomb wave functions, $F_\ell(k,r)$

$$U_\ell(r,r') = -\frac{2\mu}{\hbar^2} \frac{8}{(2\lambda+1)^2} e^2 B(E\lambda)\uparrow \sum_{\ell'} \langle \ell 0 \lambda 0 | \ell' 0 \rangle$$

$$\times \frac{1}{r^{\lambda+1}} \frac{1}{r'^{\lambda+1}} \int_0^\infty \frac{F_{\ell'}(k,r)\, F_\ell(k,r')}{k_\lambda^2 - k^2 + i\varepsilon} \, . \qquad (3.84)$$

Now if the potential is weak in strength its lowest order effect in Born approximation is a source $\rho(r)$

$$\rho(r) = \int_0^\infty dr'\, U_\ell(r,r')\, F_\ell(k_0,r') \qquad (3.85)$$

where k_0 is the ground state momentum. The integral over r' is then the usual Coulomb wave function integral

$$I(k) = \int_0^\infty dr'\, F_{\ell'}(k,r') \frac{1}{r'^{\lambda+1}} F_\ell(k_0,r') \qquad (3.86)$$

and we note that I(k) is small if $k = k_\lambda$ and it makes its main contribution when $k = k_0$. Thus we ignore the principal part of the integral over k, factor out the denominator by setting $k = k_0$, and obtain

$$U_\ell(r,r') = -\frac{8}{(2\lambda+1)^2} Z_p^2 e^2 B(E\lambda)\uparrow \sum_{\ell'} \langle \ell 0 \lambda 0 | \ell' 0 \rangle$$

$$\times \frac{1}{r^{\lambda+1}} \frac{1}{r'^{\lambda+1}} \frac{1}{E_\lambda - E_0} \int_0^\infty dk\, F_{\ell'}(k,r)\, F_{\ell'}(k,r') \, . \qquad (3.87)$$

Asymptotically, F_ℓ becomes a sine function and so the integral over k is equal to $(\pi/2)\delta(r - r')$ [19] and we can perform the sum over ℓ' to yield

$$U(r,r') = \frac{4\pi}{(2\lambda+1)^2} Z_p^2 \frac{e^2 B(E\lambda)\uparrow}{E_\lambda - E_0} \frac{1}{r^{2\lambda+2}} \delta(r - r') \qquad (3.88)$$

which is equivalent to the local potential (Eq. (3.1)).

It is important to contrast the above real adiabatic potential, which is clearly energy- and angular momentum-independent, with its sudden counterpart e.g. Eq. (3.8), which is predominantly absorptive and has pronounced E- and ℓ-dependence. We can say loosely that, whereas the sudden Coulomb polarization potential is generated primarily from the on-energy-shell part of the intermediate channel Coulomb Green function $[-i\sigma\delta(E - H_0)]$, the adiabatic potential arises basically from the principal (off-shell) part of G which is real.

We can evaluate the strength of $V^{\lambda}_{ad.pol.}(r)$ by the use of the energy-weighted sum rule. This is accomplished by writing

$$\sum_{n\neq i} \frac{B(E\lambda;\, 0 \to n)}{E_0 - E_n} = \sum_{n\neq 0} \frac{B(E\lambda;\, 0 \to n)(E_0 - E_n)}{(E_0 - E_n)^2}$$

$$\simeq -\frac{1}{(\Delta E_\lambda)^2} \sum_n B(E\lambda;\, 0 \to n)(E_n - E_0)$$

$$\equiv -\frac{S(E\lambda)}{(\Delta E_\lambda)^2} \qquad (3.89)$$

where we have introduced the familiar notation for the energy weighted sum rule [20]

$$S(E\lambda) = \sum_n B(E\lambda;\, 0 \to n)(E_n - E_0) \qquad (3.90)$$

and denoted the excitation energy of the λ-pole giant resonance by ΔE_λ.

Bohr and Mottelson [20] derived a classical model-independent expression for $S(E\lambda)$, which we write below

$$S(E1) = 14.8\ \frac{NZ}{A}\ [e^2 fm^2 Mev]$$

$$S(E\lambda) = \frac{3\lambda(2\lambda+1)}{4\pi}\ \frac{h^2}{2m}\ \frac{Z^2}{A}\ (R)^{2\lambda-2} [e^2 fm^{2\lambda} MeV],\ \lambda \geq 2 \qquad (3.91)$$

where N is the neutron number, m is the mass of the nucleon and R is the radius of the nucleus.

After allowing for the mutual excitation of both target (T) and projectile (p), our adiabatic polarization potential, Eq. (3.88) may now be written as,

$$V^{(\lambda)}_{ad.pol.}(r) = -\frac{4\pi e^2}{(2\lambda+1)^2}\left[\frac{Z_p^2 S_T(E\lambda)}{(\Delta E_\lambda(T))^2} + \frac{Z_T^2 S_p(E\lambda)}{(\Delta E_\lambda(p))^2}\right] \cdot r^{-2\lambda-2}\ [MeV]\ . \qquad (3.92)$$

Clearly the above expression for $V^{(\lambda)}_{ad.pol.}(r)$ should be used in the discussion of heavy-ion elastic scattering at sub-barrier energies. At center-of-mass energies above the barrier the above form should be considered valid for $r > R_c$, where R_c is the radius of the charge distribution. To get a feeling about the magnitude of the effect, we give below general expressions for the isovector giant dipole ($\lambda = 1$), $T = 1$) resonance component and the isoscalar giant quadrupole resonance ($\lambda = 2$), $T = 0$) component of $V_{ad.pol.}(r)$ [21,22]

$$V^{(1)}_{ad.pol.}(r) = -\ 6.7 \times 10^{-3}\left[\frac{N_p}{Z_p A_p^{1/3}} + \frac{N_T}{Z_T A_T^{1/3}}\right] Z_p^2 Z_T^2 / r^4\ [MeV]$$

$$V^{(2)T=0}_{ad.pol.}(r) = -\ 0.0208\ (A_p^{1/3} + A_T^{1/3})\ Z_p^2 Z_T^3 / r^6\ [MeV]\ . \qquad (3.93)$$

The above expressions were obtained by inserting the expressions for $S(E\lambda)$, Eq. (3.91), into Eq. (3.92) and using for the radius parameter ($R = r_0\ A^{1/3}$ fm), the value $r_0 = 1.2$ fm. For the excitation energies $\Delta E_{\lambda=1}$ and $\Delta E_{\lambda=2}$, we have used the empirical values $80.0A^{-1/3}$ MeV and $60.0A^{-1/3}$ MeV, respectively. For nuclei with masses $A < 40$, the expression of $\Delta E_{\lambda=1}$ given above is not valid and one should instead use the following

$$\Delta E_{\lambda=1} = \frac{64.65}{A^{1/3}} - \frac{17.4}{A^{2/3}}\ \ [MeV] \qquad (3.94)$$

which follows reasonably well the systematics of the giant dipole resonance energies of light nuclei ($A < 40$).

Finally, one may easily add the contribution of the isovector giant quadrupole resonance to $V^{(2)}_{ad.pol.}(r)$ by recognizing that the excitation energy of the ($\lambda = 2$, $T = 1$) resonance is almost twice that of the isoscalar resonance and thus one obtains

$$V^{(2)T=1}_{ad.pol.}(r) = +\frac{1}{4}\ V^{(2)T=0}_{ad.pol.}(r)\ . \qquad (3.95)$$

Therefore the added contributions of the $\lambda = 2$, $T = 0$ and $\lambda = 2$, $T = 1$ resonances become

$$V^{(2)}_{ad.pol.}(r) = -\frac{5}{4}\ (0.0208)(A_p^{1/3} + A_p^{1/3})\ Z_p^2 Z_T^2 / r^6\ [MeV]\ . \qquad (3.96)$$

There has been some recent experimental discussion concerning the isoscalar giant octupole resonance [23]. The excitation energy seems to be roughly $150\ A^{-1/3}$ MeV. For the purpose of completeness, we give below the

polarization potential arising from the coupling to the giant 3^- resonance. It is

$$V^{(3)}_{ad.pol.}(r) = - 3.56 \times 10^{-3}(A_T + A_p)\, Z_p^2 Z_T^2 / r^8 \ [\text{MeV}] \ . \qquad (3.97)$$

Potentials of higher multipolarities, may also be easily evaluated from our general expression Eq. (3.92). However, these are of a lesser importance, as the strength of the coupling goes down with λ.

The giant multipole polarization potentials for $\lambda = 1$, 2 and 3 have been calculated for the systems $^{16}O + ^{208}Pb$ and $^{208}Pb + ^{208}Pb$ at $E_{CM} = 78$ MeV and 567 MeV, corresponding approximately to their respective Coulomb barrier heights. The results are shown in Figure 3.6. For comparison, we also show in Figure 3.6 the ion-ion nuclear interaction constructed from the Christensen-Winther [24] empirical formula,

$$V_n(r) = - 50 \frac{R_1 R_2}{R_1 + R_2} \exp\left[- \frac{r - R_1 - R_2}{a_v} \right] ,$$

with $R_i = 1.233\, A_i^{1/3} - 0978\, A_i^{-1/3}$ [fm] and $a_v = 0.63$ fm.

It is clear from the figure that $V^{(\lambda)}(r)$ becomes more important than $V_n(r)$ at distances $r > 17$ fm in these cases. This leads to the conclusion that any unambiguous "observation" of the physical effects generated by $V^{(\lambda)}(r)$ in the elastic scattering of heavy ions is possible only with energies that correspond to distances of closest approach larger than 17 fm in these case. This is accomplished at sub-barrier energies, as was recently done by Lynch et al. [25], who have presented a clear evidence of the rather small deviations from the pure Rutherford scattering of closed-shell heavy-ion systems, arising from the adiabatic polarization due to the virtual giant resonance excitation,

as well as other effects such as relativistic correction, atomic screening and vacuum polarization. We will not discuss atomic screening or vacuum polarization further here, but we will discuss the relativistic correction to Rutherford scattering since it takes the form of a smooth polarization potential.

3.7 Relativistic Potential

We consider Coulomb elastic scattering of a spin zero projectile on a spin zero target. A classical Hamiltonian may be written down which contains relativistic effects to first order in $1/MC^2$. The Darwin Hamiltonian [26] takes the following form in the center of mass system

$$H = \frac{p^2(m_1 + m_2)}{2m_1 m_2} + \frac{Z_1 Z_2 e^2}{r} - \frac{p^4}{8C^2}\left(\frac{1}{m_1^3} + \frac{1}{m_2^3} \right)$$

$$+ \frac{Z_1 Z_2 e^2}{2m_1 m_2 C^2}\left(\frac{p^2 + p_r^2}{r} \right) . \qquad (3.98)$$

The first two terms on the right hand side are the usual nonrelativistic forms. The third term arises from the momentum correction of special relativity. The fourth term comes from the magnetic interaction arising from the motion of a finite mass target.

To evaluate the effect of these last two terms we begin by rewriting the radial momentum p_r

$$p_r^2 = p^2 - \frac{L^2}{r^2} \qquad (3.99)$$

where L is the orbital angular momentum of the scattering system. Furthermore, only in these correction terms we make use of the zeroth order expression for p^2

$$p^2 = \frac{2m_1m_2}{(m_1 + m_2)}\left(E - \frac{Z_1Z_2e^2}{r}\right) \tag{3.100}$$

where E is the asymptotic center of mass kinetic energy.

If one makes these substitutions and collects terms the Hamiltonian becomes

$$H = \frac{p^2(m_1 + m_2)}{2m_1m_2} - \frac{(m_1^2 + m_2^2 - m_1m_2)}{2(m_1 + m_2)m_1m_2c^2}E^2$$
$$+ \frac{Z_1Z_2e^2}{r}\left(1 + \frac{(m_1^2 + m_2^2 + m_1m_2)E}{(m_1 + m_2)m_1m_2c^2}\right)$$
$$- \frac{(m_1^2 + m_2^2 + 3m_1m_2)}{2(m_1 + m_2)m_1m_2c^2}\left(\frac{Z_1Z_2e^2}{r}\right)^2 \tag{3.101}$$
$$- \frac{Z_1Z_2e^2}{2m_1m_2c^2}\frac{L^2}{r^3} \quad .$$

The polarization potential from relativity is thus the last two terms (in $1/r^2$ and L^2/r^3). We will ignore the relativistic effects in the slight change of constants in the other terms which give a slight angle-independent change in the overall cross section equivalent to a slight change in the beam energy.

4. Calculation of the Cross-Section

4.1 The Cross-Section Formula

Within the spirit of the preceeding sections, namely the obtaining of closed expressions for the polarization potentials, it seems natural to seek also closed expressions for the differential cross section that contain the effect of the polarization potential. To lay the grounds for such derivation, we note first that we are discussing low-energy heavy ion scattering. Therefore the elastic scattering differential cross section is Coulomb dominated, and the polarization potentials enter as small deviations from the Rutherford cross section.

Let us start with the partial wave expansion of the scattering amplitude

$$f(\theta) = \frac{1}{2ik}\sum_{\ell=0}^{\infty}(2\ell+1)(S_\ell^n e^{2i\sigma_\ell} - 1)\,P_\ell(\cos\theta), \tag{4.1}$$

where $S_\ell^n \equiv |S_\ell^n| e^{2i\delta_\ell^n}$ is the nuclear partial wave S-function and σ_ℓ the Rutherford spase shift.

We now use the asymptotic form of the Legendre polynomial and consider only the near-side part which behaves as $e^{-i\ell\theta}$. Because of the dominance of the Coulomb repulsion, it is expected that the far-side component, $e^{i\ell\theta}$ would contribute very little to $f(\theta)$.

Consequently, after replacing the partial sum by an integral, we have

$$f(\theta) = \frac{1}{\sqrt{2\pi\sin\theta}}\, e^{i\pi/4}\int_0^{\infty}\lambda^{1/2}d\lambda\, \exp[2i(\delta^n(\lambda)+\sigma(\lambda)) - i\lambda\theta]\,\left|S^n(\lambda)\right| \tag{4.2}$$

where $\lambda \equiv \ell + 1/2$

Owing to the small value of $\delta^n(\lambda)$ (which represents the phase shift arising from the polarization potentials), we evaluate Eq. (4.2) using a single stationary phase point, λ_0, to obtain

$$f(\theta) = \frac{\sqrt{\lambda_0}}{\sqrt{\sin\theta}\ 2\pi k}\left[\frac{2\pi}{\frac{d\theta}{d\lambda}_{\lambda_0}}\right]^{1/2} \exp[2i(\delta^n(\lambda_0)+\sigma(\lambda_0)) - i\lambda_0\theta]\ \left|S^n(\lambda_0)\right| \qquad (4.3)$$

In the above $\theta(\lambda_0)$ represents the classical deflection function,

$$\theta(\lambda_0) = 2\,\frac{d}{d\lambda}(\delta^n+\sigma)\Big|_{\lambda_0} \qquad (4.4)$$

With the above form for $f(\theta)$, the cross section comes out to be

$$\frac{d\sigma}{d\Omega} = \left|f(\theta)\right|^2 = \frac{\lambda_0}{k\sin\theta}\ \frac{1}{\frac{d\theta}{d\lambda}\Big|_{\lambda_0}}\ \left|S^n(\lambda_0)\right|^2 \qquad (4.5)$$

Eq. (4.5) is just the classical expression for the cross section multiplied by a damping factor $\left|S^n(\lambda_0)\right|^2$, which arises from absorption.

Since the deflection function $\theta(\lambda_0)$ deviates slightly from the Rutherford one, we can write Eq. (4.5) as

$$\frac{d\sigma}{d\Omega} = \frac{d\sigma_{Ruth}}{d\Omega}\left[1 + \frac{1}{2}\Delta\theta\ \tan\frac{\theta}{2} + \frac{3}{2}\Delta\theta\ \cot\frac{\theta}{2} - \frac{d}{d\theta}\Delta\theta\right]\ \left|S^n(\lambda_R(\theta))\right|^2, \qquad (4.6)$$

where $\Delta\theta$ is the deviation in θ, $\Delta\theta \equiv \theta - \theta_{Ruth}$,

$$\theta_{Ruth} = 2\tan^{-1}\frac{\eta}{\lambda_R}\ , \text{ and}$$

$$\frac{d\sigma_{Ruth}}{d\Omega} = \frac{a^2}{4\sin^4\frac{\theta}{2}}\ . \qquad (4.7)$$

η is the usual Sommerfeld parameter and half the distance of closest approach. The angular deviation, $\Delta\theta$, can be easily related to the underlying real component of the polarization potential, through

$$\Delta\theta = 2\frac{d}{d\lambda}\delta\Big]_{\lambda_0}$$

$$= 2\frac{d}{d\lambda}\left[\sqrt{\frac{2\mu}{\hbar^2}}\int_{r_{t.}(\ell)}^{\infty}\frac{(V(r)/2)}{\sqrt{\frac{2\mu}{h^2}\left(E-V_c(r) - \frac{\hbar^2\ell(\ell+1)}{2\mu r^2}\right)}}\,dr\right] \qquad (4.8)$$

Owing to the existence of the classical trajectory relation

$$\frac{1}{r} = \frac{1}{a}\,\frac{\cos\theta_0}{\sin^2_\theta}\,(\cos\theta - \cos\theta_0), \qquad (4.9)$$

we can re-write Eq. (4.8) as (see Ref. [30]

$$\Delta\theta = -\frac{1}{E}\frac{\partial}{\partial b}\left[\frac{1}{b}\int_0^{\phi_0} r^2 V(r)\,d\phi\right] \qquad (4.10)$$

where $\phi_0 = \tan b/a$, and b is the impact parameter (see Figure 4.1)

To first order in the potential, the damping factor $\left|S^n(\lambda_0)\right|^2$ is given by

$$\left|S^n(\lambda_0)\right|^2 = \exp\left[-2\int_{r_t^c(\ell)}^{\infty}\frac{\frac{2\mu}{\hbar^2}W(r)\,dr}{\sqrt{\frac{2\mu}{\hbar^2}\left(E-V_c(r) - \frac{\hbar^2\ell(\ell+1)}{2\mu r^2}\right)}}\right]$$

$$= \exp\left[-\frac{4}{\hbar}\frac{\mu}{\hbar}\frac{1}{\lambda_0(\theta)}\int_0^{\phi_0(\theta)} r^2\ W(r)\ d\phi\right] \qquad (4.11)$$

$$= \exp\left[-\frac{4\mu}{\hbar^2}\frac{\tan\theta/2}{\eta}\int_0^{\frac{\pi-\theta}{2}} r^2\ W(r)\ d\phi\right] \qquad (4.12)$$

Another form can be derived for $\Delta\theta$ and $\left|S^n(\lambda_0)\right|^2$ namely by

$$\Delta\theta = -2\frac{\partial}{\partial\lambda}\left[\frac{1}{\hbar}\int_0^\infty V(r(t))dt\right] \tag{4.13}$$

$$\left|S^n(\lambda_0)\right|^2 = \exp\left[-\frac{2}{\hbar}\int_0^\infty W(r(t))dt\right] \tag{4.14}$$

As we shall see later, the forms (4.11) and (4.12) are convenient for cases involving long range polarization potentials, whereas (4.13) and (4.14) are more adequate for short range potentials (e.g. due to particle transfer).

4.2 Applications

a) The Coulomb polarization potential ("sudden potentials")

As was already discussed, the Coulomb polarization potential associated with coupling to low-lying collective states is predominantly absorptive. Therefore the cross section becomes, after ignoring the small real component of the polarization potential, in Eq. (4.6)

$$\frac{d\sigma}{d\Omega} = \frac{d\sigma_{Ruth}}{d\Omega}\exp\left[-\frac{4\mu}{\hbar^2}\frac{\tan\theta/2}{\eta}\int_0^{\frac{\pi-\theta}{2}} r^2\, W_\ell(r)d\phi\right] \tag{4.15}$$

The potential W(r) is given by Eq. (3.35) namely

$$W_\ell(r) = \frac{\hbar\omega a_\ell}{r^3} + \frac{\hbar\omega b_\ell}{r^4} + \frac{\hbar\omega c_\ell}{r^5} \tag{4.16}$$

Carrying out the ϕ integration, one then obtains

$$\frac{\sigma}{\sigma_{Ruth}} = \exp\left[-\left(\hbar\omega a_{\lambda_0(\theta)}I_3(\theta) + \hbar\omega b_{\lambda_0(\theta)}I_4(\theta) + \hbar\omega c_{\lambda_0(\theta)}I_5(\theta)\right)\right], \tag{4.17}$$

where the angle functions $I_\ell(\theta)$, are given by

$$I_3(\theta) = \tan^2\frac{\theta}{2}\left[1-\left(\frac{\pi-\theta}{2}\right)\tan\frac{\theta}{2}\right]\frac{2\eta}{Ea^3} \tag{4.18}$$

$$I_4(\theta) = 2\tan^4\frac{\theta}{2}\left[\left(\cot^2\frac{\theta}{2}+3\right)\left(\frac{\pi-\theta}{2}\right)\tan\frac{\theta}{2} - 3\right]\frac{2\eta}{Ea^4} \tag{4.19}$$

$$I_5(\theta) = 2\tan^6\frac{\theta}{2}\left[\frac{4}{3}\cot^2\frac{\theta}{2}+5\right) - \left(3\cot^2\frac{\theta}{2}+5\right)\left(\frac{\pi-\theta}{2}\right)\tan\frac{\theta}{2}\Big]\frac{2\eta}{Ea^5} \tag{4.20}$$

and the angle-dependent coefficients $a_{\lambda_0(\theta)}$, $b_{\lambda_0(\theta)}$ and $c_{\lambda_0(\theta)}$ are given e.g. in Eqs. (3.35) and (3.38).

Such a formula for $\sigma_{e\ell}/\sigma_R$ was used in Refs [4] and [7] to calculate Coulomb damping in the elastic channel. In Ref. [4] the orbit integrals were evaluated in a slightly different way from (4.18) to (4.20) above, but a continuation was made to above the barrier. However, below the barrier the results agree almost identically with the expression here with the a_ℓ, b_ℓ and c_ℓ chosen to include only $0^+\text{-}2^+$ coupling.

Application of Eq. (4.17) - (4.20) can be seen using imaginary potential (3.39) (coupling only to the 2^+ state but including reorientation) which yields

$$\frac{\sigma_{e\ell}}{\sigma_R}(\theta) = \exp\left[-\frac{16}{45}q^2_{0\to2}g_{02}(\varepsilon_{02})\left\{1+\frac{4}{49}q^2_{2\to2}f(\theta)\right\}^{-1}f(\theta)\right] \tag{4.21}$$

where

$$f_1(\theta) = \left[\left(1-\left(\frac{\pi-\theta}{2}\right)\tan\frac{\theta}{2}\right)^2\tan^4\frac{\theta}{2} + \frac{1}{3}\sin^4\frac{\theta}{2}\right] \tag{4.22}$$

and $f(\theta)$ is the universal function of angle[4] (3.11) or more properly (3.14).

Further discussion of cross section applications is given in Ref. [7]. We should only note here the connection between such applications involving the imaginary polarization potentials and the formulation for directly calculating such elastic scattering cross sections semiclassically by Alder and Winther[12]. For example the expression Eq. (3.14) is just the semiclassical

angular distribution for excitation of the 2^+ state and the use of it in e.g. Eq. (4.21) just expresses the removal of that 2^+ flux from the elastic channel. These cross section calculations are not a replacement for the semiclassical theory but rather to clarify the nature of the absorptive potential.

Finally, we give below the elastic scattering cross section evaluated at $\vartheta = \pi$ from potential Eq. (3.40) (included in this calculation are the couplings to the 2^+ and 4^+ states as well as the reorientation of the 2^+ state)

$$\frac{\sigma_{el}(\pi)}{\sigma_R(\pi)} = \exp\left[-\frac{16}{45}q^2_{0\to2}g_{0\to2}(\xi_{0\to2})\right.$$
$$\left.\times\frac{1 + 0.065q^2_{2\to4}g_{2\to4}(\xi_{2\to4})}{0.036q^2_{2\to2}+\left[1 + 0.065q^2_{2\to4}g_{2\to4}(\xi_{2\to4})\right]^2}\right]. \qquad (4.23)$$

While this expression gives one a reasonable qualitative account of a sub barrier imaginary polarization potential and the mechanism of several couplings, it is in the next section that we will see the more quantitatively useful cross section expressions derived from real polarization potentials.

b) The adiabatic Coulomb polarization and relativistic potentials.

Here we have an attractive real potential, so we will assume $\left|S^n(\lambda_R(\theta))\right|^2$ of Eq. (4.6) is unity and work out $\Delta\theta$ for each V_0/r^n real potential. The $\Delta\theta$ results for $1/r^4$, $1/r^6$, and $1/r^8$ potentials (corresponding to virtual dipole, quadrupole, and octupole excitation, Section 3.6) are given in Appendix C. If we write

$$V^\lambda(r) = \frac{V_0^{(\lambda)}}{r^{2\lambda+2}} \qquad (4.24)$$

and then make use of the Appendix C results in Eq. (4.6) we obtain the closed forms

$$\frac{d\sigma^{(1)}}{d\Omega} = \frac{d\sigma_{Ruth}}{d\Omega}\left\{1 - \frac{V_0^{(1)}}{2Ea^4}\frac{\cos^3\phi_0}{\sin^7\phi_0}\left[\frac{3}{2}(1 + 16\cos^2\phi_0\right.\right.$$
$$\left.\left. + 8\cos^4\phi_0) - \frac{1}{2}(29 + 46\cos^2\phi_0)\cos\phi_0\sin\phi_0\right]\right\} \qquad (4.25)$$

$$\frac{d\sigma^{(2)}}{d\Omega} = \frac{d\theta_{Ruth}}{d\Omega}\left\{1 - \frac{V_0^{(2)}}{8Ea^6}\frac{\cos^6\phi_0}{\sin^{10}\phi_0}\left[-\frac{3}{2}\tan\phi_0 - \frac{9}{2}???\phi_0\right).\right.$$
$$\cdot(-315\phi_0 + 420\phi_0\sin^2\theta_0 - 120\phi_0\sin^4\phi_0$$
$$- 315\cos\phi_0\sin\phi_0 - 210\cos\phi_0\sin^3\phi.$$
$$+ 8\cos\phi_0\sin^5\phi_0) + \frac{1}{2}(840\phi_0\sin\phi_0\cos\phi_0$$
$$- 480\phi_0\sin^3\phi_0\cos\phi_0 - 840\sin^2\phi_0$$
$$\left.+ 960\sin^4\phi_0 - 48\sin^6\phi_0)\right]\right\} \qquad (4.26)$$

and

$$\frac{d\sigma^{(3)}}{d\Omega} = \frac{d\sigma_{Ruth}}{d\Omega}\left\{1 - \frac{V_0^{(3)}}{80Ea^8}\frac{\cos^8\phi_0}{\sin^{14}\phi_0}\left[-\frac{5}{2}\tan\phi_0 - \frac{13}{2}\cot\phi_0\right]\right.$$
$$\cdot\left[-15015\phi_0 + 27720\phi_0\sin^2\phi_0 - 15120\phi_0\sin^4\phi_0\right.$$
$$+ 2240\phi_0\sin^6_0 + 15015\cos\phi_0\sin\phi_0 - 17710\cos\phi_0\sin^3\phi_0$$
$$+ 4648\cos\phi_0\sin^5\phi_0 - 80\cos\phi_0\sin^7\phi_0)$$
$$+ \frac{1}{2}(55440\phi_0\cos\phi_0\sin\phi_0 - 60480\phi_0\cos\phi_0\sin^3\phi_0$$
$$+ 13440\phi_0\cos\phi_0\sin^5\phi_0 - 55440\sin^2\phi_0$$
$$\left.\left.+ 78960\sin^4\phi_0 - 26208\sin^6\phi_0 + 640\sin^8\phi_0)\right]\right\} \qquad (4.27)$$

We write the percentage deviation

$$\Delta\sigma^{(\lambda)} \equiv \left[\frac{d\sigma^{(\lambda)}}{d\Omega} - \frac{d\sigma_{Ruth}}{d\Omega}\right] / \frac{d\sigma_{Ruth}}{d\Omega}$$

in the following form

$$\Delta\sigma^{(1)} = -\frac{V_0^{(1)}}{2Ea^4} g^{(1)}(\theta)$$

$$\Delta\sigma^{(2)} = \frac{V_0^{(2)}}{8Ea^6} g^{(2)}(\theta)$$

$$\Delta\sigma^{(3)} = -\frac{V_0^{(3)}}{80Ea^8} g^{(3)}(\theta) \qquad (4.28)$$

The three universal functions $g^{(1)}(\theta)$, $g^{(2)}(\theta)$ and $g^{(3)}(\theta)$ are shown in Fig. (4.2). As one clearly sees, all universal functions attain their maximum value at $\theta = 180°$. Further they have zero contribution at $\theta=0$. This implies that measurement of these effects should be made in the backward hemisphere. We should mention that Eq. (4.25) for $\lambda=1$, has been previously obtained by Baur et al. [31]

A simple measure of $\Delta\sigma^{(\lambda)}$ may be obtained by setting $\theta=180°$

$$\Delta\sigma^{(1)}(\theta=\pi) = \frac{3.66E^3}{(Z_1Z_2e^2)^4} V_0^{(1)}$$

$$\Delta\sigma^{(2)}(\theta=\pi) = \frac{4.43E^5}{(Z_1Z_2e^2)^6} V_0^{(2)}$$

$$\Delta\sigma^{(3)}(\theta=\pi) = \frac{5.09E^7}{(Z_1Z_2e^2)^8} V_0^{(3)} \qquad (4.29)$$

Note that $V_0^{(\lambda)}$ are intrinsically negative.

Since the numerical factors appearing in the expressions above vary very slowly with λ, one may, to get an order of magnitude estimate of $\Delta\sigma^{(\lambda)}$, write a general expression valid for any λ

$$\Delta\sigma^{(\lambda)}(\theta=\pi) = \frac{E^{2\lambda+1}}{(Z_1Z_2e^2)^{2\lambda+2}} V_0^{(\lambda)} \qquad (4.30)$$

The calculation of the deviation $\Delta\sigma^{(R)}$ due to relativistic effects is straightforward and follows the same lines as the ones used to evaluate $\Delta\sigma^{(\lambda)}$ above. As we have seen in Section 3.7 there are two "polarization" terms arising from special relativity (Eq. (3.101)), namely

$$V_1^{(R)} = -\frac{M_1^2 + M_2^2 + 3M_1M_2}{2(M_1+M_2)M_1M_2C^2}\left(\frac{Z_1Z_2e^2}{r}\right)^2 \qquad (4.31)$$

$$V_2^{(R)} = -\frac{Z_1Z_2e^2}{2M_1M_2C^2}\frac{L^2}{r^3} \qquad (4.32)$$

The corresponding changes in the classical deflection function, Eqs. (4.9), (4.10) may be easily evaluated

$$\Delta\theta_1^{(R)} = \frac{M_1^2 + M_2^2 + 3M_1M_2}{2(M_1+M_2)M_1M_2C^2}\frac{(Z_1Z_2e^2)^2}{Ea^2}\cot^2\phi_0 \cdot[-\phi_0 + \sin\phi_0\cos\phi_0] \qquad (4.33)$$

$$\Delta\theta_2^{(R)} = \frac{Z_1Z_2e^2}{2M_1M_2C^2}\frac{2M_1M_2}{(M_1+M_2)a}\cot^2\phi_0[-\phi_0 + \sin\phi_0\cos\phi_0] \qquad (4.34)$$

Summing Eqs. (4.33) and (4.34), we obtain the total change in the deflection function due to relativistic effects

$$\Delta\theta^{(R)} = \frac{2E}{\mu c^2}\cot^2\phi_0\left[-\phi_0 + \frac{1}{2}\sin 2\phi_0\right] \tag{4.35}$$

where $\mu = \frac{m_1 m_2}{m_1+m_2}$, is the reduced mass.

The effect on the Rutherford cross section then obtains from Eq. (4.6)

$$\frac{d\sigma^{(R)}}{d\Omega} = \frac{d\sigma_{Ruth}}{d\Omega}\left\{1 + \frac{2E}{\mu c^2}\tan^2\frac{\theta}{2}\right.$$

$$\left.\cdot\left[\frac{1}{2}\cot\theta(\sin\theta + \theta - \pi) - \cos^2\frac{\theta}{2}\right]\right\} \tag{4.36}$$

The corresponding universal angle-function $g^{(R)}(\theta)$ defined through

$$\Delta\sigma^{(R)} = -\frac{2E}{\mu c^2}\, g^{(R)}(\theta) \tag{4.37}$$

is shown in Fig. 4.3

Note that in Eq. (4.36) there is no dependence on Z_1Z_2 in the relativistic correction term; a $1/a^2$ has cancelled the numerator of the potential. At 180° the angle dependent coefficient of $2E_{cm}/\mu\, c^2$ is $-2/3$, and it remains negative going to $-1/2$ at 90° and to $-\pi\theta/8$ at small angles. For an infinite mass target μ is equal to the projectile mass, and $2\, E_{cm}/\mu\, c^2$ is equal to v_∞^2/c^2. As we stated in Section 3.7, for a finite mass target relativistic magnetic effects enter in. Their lowest order effect in combination with the lowest order relativistic scalar potential term is to cause the mass, μ, in Eq. (4.36) to be equal to the reduced mass of the system. For the case of spin 1/2 electron scattering a similar relativistic correction has been derived to lowest order in $Z_1Z_2e^2/hc$ (which is inappropriate here), but it only includes the $\cos^2\theta/2$ term in the square brackets [32].

We present in Table 4.1 the results obtained from Eq. (4.29) for several heavy-ion systems with E taken to be equal to the height of the Coulomb barrier at 1.44 $(A_p^{1/3} + A_T^{1/3})$ fm. The strengths $V_0^{(\lambda)}$ are calculated from Eqs. (3.93) - (3.97). The effect on the cross section is as

largeas 2% for the summed effect of dipole, quadrupole and octopole excitations with two heavy nuclei and about 0.6% for ^{16}O on a heavy nucleus. Though the octopole excitation is quite small, the quadrupole one is not negligible, a little less than half that of the dipole. The relativistic effect is largest for uranium on uranium (.8%) but not much less for any of the other cases.

Since the experiments of Lynch et al. [25] were done at very low energies, the dipole effect (which goes ad E^3) is relatively more important than the quadropole effect (which goes as E^5) when compared to our calculation of 78 MeV ^{16}O on ^{208}Pb. The highest energy measured was 55.7 MeV which corresponds to a distance of closest approach, $2.0(A_p^{1/3}+A_T^{1/3})$fm. At this energy we calculate a quadrupole contribution of $\Delta\sigma^{(2)} = -.03\%$ at 150°, to be added to the dipole contribution of $-.2\%$ obtained by these authors with a $V_0^{(1)} = -2.24\times10^3$ (MeV fm), slightly larger in magnitude than our $V_0^{(1)}$ value. Our formula for $\Delta\sigma^{(R)}$ agrees with the angular curve for 50 MeV $^{16}O + ^{208}Pb$ calculated numerically by Lynch et al [25] and we also agree with their energy dependent calculation of the relativistic effect.

Before ending this section, we give below the contribution to the sub-barrier cross-section arising from the short range nuclear optical potential. Clearly, the kind of analysis done by Lynch et al., involving spherical nuclei, one has to consider, aside from the giant resonance polarization, relativistic correction, vacuum polarization etc., the small contribution of the nuclear potential. From our Eq. 4.12 for $\Delta\theta(\ell)$, we have

$$\Delta\theta_N(\ell) = 2\frac{\partial}{\partial\ell}\left[-\frac{1}{\hbar}\int_0^\infty V_N(r(t))\, dt\right] \tag{4.38}$$

where r(t) describes the Coulomb trajectory. Using an exponential form for V_N, which is the real part of the ion-ion optical potential

$$V_N(r) = -V_0 e^{-(r-R_v)/a_v}, \tag{4.39}$$

are have, after expanding r(t) to second order in t, $r(t) = r(0) + \frac{1}{2}\ddot{r}(0)t^2$,

$$\Delta\theta_N(\ell) \approx \sqrt{\frac{2a_r}{r(0)}}\,\frac{\sqrt{\pi}}{2}\,\frac{V_0}{\hbar}\,e^{-(r(0)-R_v)/a_v}\;\cdot\frac{1}{ka_r}\,\frac{\ell}{\sqrt{\eta^2+\ell^2}} \qquad (4.40)$$

Straightforward calculation, given for the cross section ratio to Rutherford (Eq. 4.6)

$$\frac{\sigma}{\sigma_{Ruth}}(\theta) = \Big\{1 - \frac{1}{\hbar}\,\frac{-V_0\; e^{-(r(0)-R_v)/a_v}}{ka_r}\,\frac{1+\frac{3}{2}\hat{\ell}^2}{(1+\ell^2)^{1/2}}$$

$$- \frac{V_0\; e^{-(r(0)-R_v)/a_v}}{k^2a^2}\,\frac{\hat{\ell}^2}{2}\;\tau_r(\theta)\Big]$$

$$\cdot\ \exp\ -\frac{2\tau_I(\theta)}{\hbar}\,W_0\exp\big[-(r(0)-R_W)/a_W\big]\ , \qquad (4.41)$$

where $\tau_{r_I}(\theta)$, correspond to the classical, angle dependent collision time

$$\tau_{\frac{r}{I}}(\theta) = \frac{\hbar}{E}\sqrt{2\pi\eta ka_{\frac{r}{I}}}\;\frac{1}{2}\Big[(1+\hat{\ell}^2)^{-1/4} + (1+\hat{\ell}^2)^{1/4}\Big] \qquad (4.42)$$

and $\ell \equiv \hat{\ell}/\eta$

Eq. (4.41), has been used previously by Landrone and Wolter [33], and it was found to reproduce very well the more exact optical model calculation. One sees clearly from Eq. (4.41) that the cross section is more sensitive to the imaginary part than the real part of the interaction, for large values of ka_r.

It is important to mention that our formula, Eq. (4.41), is also applicable to any short-ranged nuclear polarization potentials, e.g. transfer, of the type discussed in Section 6.

Finally, we stress, that when applied to a particular situation, one has to add up all the $\Delta\theta$'s arising from the different real (refractive) polarization potentials, and use the resulting total angular deviation to construct the cross section, according to Eq. (4.6). Of course the absorptive components of the polarization potentials enter additively in the exponent of $|S^{\mathfrak{N}}(\lambda_0)|^2$ (Eq. (4.10) and (4.6)).

4.3 Comparison with Coupled Channels and Trivially Equivalent Local Potentials

A number of comparisons have been made between calculations using polarization potentials and the exact coupled channels calculations which they purport to represent. Figure 4.4 shows the results of the sub-Coulomb 70 MeV ^{20}Ne scattering on Sm isotopes [27] along with calculations using the BKGP potential in the closed formula Eq. (3.9) (dashed line) and coupled channels calculations (solid line). Terms for both Sm and ^{20}Ne were included. While the qualitative agreement is good, at backward angles discrepancies occur especially for ^{148}Sm and ^{150}Sm. These discrepancies may be at least partially attributed to the larger energy loss factors ξ, which are only described approximately by the angle independent factor $g_2(\xi)$. At angles farther forward and especially for cases with a very low-lying 2^+ state (small ξ) we expect the potential and thus the cross section formula to have greater validity.

Investigation has also been made of the validity of the multiple Coulomb polarization potential of Section 3.4 by comparison with coupled channels performed by the code CHORK [28]. Table 1 shows 180° calculation results for 48 MeV ^{16}O on ^{152}Sm performed with an artificially large value for the couplings $q_{I-I'}$ to probe the limits of potential validity.

The quatitative effect both of including reorientation of the 2^+ state and of including coupling to the 4^+ state is seen to be a reduction in the total absorption. This comes about because the lowest order imaginary contribution to the potential is from four step processes from both the reorientation and the 4^+ coupling. Since each step contributes a phase factor -1, there is an overall change in sign from the two step (negative imaginary potential) to the four step (positive imaginary potential) processes. The most obvious discrepancy between the optical model calculations and the coupled channels calculations is in the

basic $0+2^+$ coupling to which the higher orders are added. The optical model ratio to Rutherford cross section is 0.421 at back angles compared to 0.373 for the coupled channels.

Table 4.3 investigates the breakdown of the optical potential representation in a series of calculations in which the coupling strength is increased for the 48 MeV $^{16}O + ^{152}Sm$ two channel case. In addition to the coupled channels and optical model calculations, we also present cross sections calculated with the JWKB evaluation of the optical model cross section, Eq. (3.9), the on-shell summation formula for the cross section, Eq. (3.53), and the summation formula including lowest order off-shell effects, Eq. (3.51). It is clear that as the coupling strength is increased, the optical potential representation of the coupling effects loses its validity. At K = 2.24 the optical model cross section is an order of magnitude larger than the coupled channels cross section. However, our lowest order off-shell summation formula is remarkably accurate when compared to the coupled channels cross sections throughout the range of coupling constants taken. The success of the JWKB formula is limited to being a good evaluation of the optical potential cross section.

Since the polarization potentials have shown some success in representing coupled channels, it would be interesting to see how a trivially equivalent local potential would compare to the analytical form. Figure 4.5 shows calculations of Franey and Ellis [29] for the 72 MeV $^{16}O + ^{151}Sm$ pure Coulomb case without reorientation. The dotted line is the BKGP potential. At lower partial waves the general trend agrees, although there is some oscillation corresponding to maxima and minima in the scattering wave functions. At higher partial waves the correspondence between the trivially equivalent local potential generated from coupled channels and the BKGP potential is impressive.

The adiabatic case has also been considered. Figure 4.6 shows the ratio to Rutherford cross section for 78 MeV ^{16}O on ^{208}Pb calculated only considering the isoscaler quadrupole giant resonance in ^{208}Pb. The coupled channels calculation, the optical model calculation with $1/r^6$ potential and the classical formula Eq. (4.28) all agree to within about a percent of the deviation from Rutherford scattering at all angles. This not only assures us that the classical scattering theory provides a very accurate cross section for the $1/r^6$ potential, but that the adiabatic polarization potential truly and accurately represents the effects of channel coupling when used to provide a cross section calculation.

Figure 4.7 shows the trivially equivalent local potential calculated for three initial orbital angular momenta in our test case compared with the analytical $1/r^6$ potential. In the crucial turning point region the correspondence is good with oscillations or "have" such as seen in the sudden case [4, 29] appearing at larger radii.

5. The Volume Heavy Ion Optical Potential

It is appropriate to discuss the volume heavy ion optical potential before discussing the nuclear polarization potential because the volume potential is an ingredient in the construction of the nuclear polarization potential. We follow a simplified proximity potential approach [34] because it emphasizes the geometrical aspects of the volume heavy ion potential and clarifies the relationship between the folding model [35,36] and the proximity [37,38] or global [24] type potentials.

If one considers a simple two channel problem with nuclear quadrupole coupling then the coupled equations may be written

$$(E_0 - T + U_v^0(r))\chi_0(r) = U_v^2(r)\chi_2(r) \tag{5.1a}$$

$$(E_2 - T + U_v^0(r))\chi_2(r) = U_v^2(r)\chi_0(r) \tag{5.1b}$$

with reorientation ignored for simplicity. $U_v^0(r)$ and $U_v^2(r)$ are the L=0 and 2 angular momentum projections of a deformed volume optical potential $V(r,\theta)$

$$U_v^0(r) = \frac{1}{4\pi}\int d\Omega V(r,\theta) \tag{5.2}$$

$$U_v^2(r) = \int d\Omega Y_{L0}(\Omega)V(r,\theta). \tag{5.3}$$

If we write equation (2.1B) in an integral equation form we have

$$\chi_2(r) = \int G_2(r,r')U_v^2(r')\chi_0(r')dr' \tag{5.4}$$

which in the usual way may be substituted into Eq. (5.1a) to yield

$$(E_0 - T + U_v^0(r))\chi_0(r) = \int dr'V(r,r')\chi_0(r') \tag{5.5}$$

with

$$V(r,r') = U_v^2(r)G_2(r,r')U_v^2(r'). \tag{5.6}$$

The non-local polarization potential V(r,r') from which we will construct a local equivalent, clearly depends directly on the L=2 components of the volume potential and indirectly on the L=0 component through the distorted Green function $G_2(r,r')$.

The preceeding example is but an illustration of how the volume potential is bound up in any consideration of a polarization potential above the Coulomb barrier. The usual practice in fitting data is to paramaterize this potential with a complex Woods-Saxon form. This proceedure is often adequate in practice because the quasi-elastic scattering is only sensitive to the tail of the potential with strong absorption damping out contributions from the radius at which the two nuclei touch and smaller.

Attempts at calculating the volume real potential have concentrated on two approaches, the folding model and the proximity potential. As we will show below, the proximity potential can be geometrically related to the folding model in that a proximity formulation can be shown to be an accurate approximation to the folding model for all heavy ion reactions.

A comprehensive review of the folding model for heavy-ion scattering has been given by Satchler and Love [36]. They consider in detail the double-folded potential of the form (Fig. 5.1)

$$U_F(\vec{R}) = \int d\vec{r}_1 \int d\vec{r}_2 \rho_1(\vec{r}_1)\rho_2(\vec{r}_2)V(r_{12} = |\vec{R} + \vec{r}_2 - \vec{r}_1|) \tag{5.7}$$

where V is the nucleon-nucleon effective interaction with its various central spin-orbit, and tensor terms. Love and Satchler utilized a G-matrix constructed from the Reid potential and were able to produce a real folded potential which fit a number of heavy ion scattering cases with an average normalization increase in the potential of 11%.

Another way to write the folded potential is

$$U_F(\vec{R}) = \int d\vec{r} U_p(\vec{R}-\vec{r})\rho_T(\vec{r}) \tag{5.8}$$

where

$$U_p(\vec{R}-\vec{r}) = \int d\vec{r}_p \rho p(\vec{r}_p)V(|\vec{R}-\vec{r}_1-\vec{r}_p|) \tag{5.9}$$

If U_p is simply taken as a phenomenological nucleon-nucleus potential instead of this integral of a two body nucleon-nucleon interaction over the nucleus

density, then we have the single folding model in Eq. (5.8). Although the potential of Eq. (5.9) gives a moderately successful representation of nucleon-nucleus scattering, the single folding nucleus-nucleus potential U_p invariably overestimates the strength of the real potential required by heavy ion scattering data by a factor of about two. The seeming discrepancy implied can be resolved by consideration of the effect of the density dependence from both nuclei in the double folded model and the details of the surface shape of the potential U_p [36].

For an analysis of global systematics of nucleus-nucleus scattering the proximity potential is the natural approach. Since we are interested in a volume potential to be used in a Schroedinger equation for one or at most several low lying states, then the proximity form of the folding model is appropriate rather than the proximity form of an interaction potential in which the two nuclei dynamically readjust into highly excited states. Such a situation might be better described by the Thomas-Fermi approach for example as developed by Brink and Stancu [38]. A pertinent disadvantage of the Thomas-Fermi approach is that it breaks down in the low density regime, which is just theregime of interest for constructing polarization potentials which represent the effects of surface interactions.

$$V(\vec{r}') = V_0\delta(\vec{r}') \tag{5.10}$$

The folded potential then becomes

$$U_F(\vec{R}) = F_0 \int d\vec{r}_1\rho_2(\vec{R}-\vec{r}_1)\rho_1(\vec{r}_1) \tag{5.11}$$

Of course this integral may be evaluated exactly on a computer. To obtain its proximity form we follow the approach of Brink and Stancu and make use of the spherical symmetry to rewrite Eq. (5.11) as a two dimensional integral over r_T and r_p (Fig. 5.2).

$$U(R) = \frac{2\pi V_0}{R} \int r_T\, dr_T r_p dr_p \rho(r_p - R_p)\rho(r_T - R_T) \tag{5.12}$$

with the limits of integration

$$r_T + r_p > R > |r_R - r_p|$$

From this form Brink and Stancu obtain a two term proximity potential

$$U_{p2}(R) = 2\pi \frac{R_T R_p}{(R_T+R_p+S)} \left[\varepsilon_0(S) + \frac{R_T R_p}{2R_T R_p}\varepsilon_1(S)\right] \tag{5.13}$$

where ε_0 and ε_1 are one dimension functions of the distance S between the nuclear surfaces along the line between the centers:

$$\varepsilon_n(S) = \int_S^\infty t^n e(t)dt \tag{5.14}$$

and, in our particular folding-potential case

$$e(t) = V_0\int_{-\infty}^{\infty} \rho_p(\mu)\rho_T(t-\mu)du \tag{5.15}$$

This two-term proximity potential contains the next correction for finite curvature, in comparison to the more approximate one-term proximity potential of Blocki et al. [37],

$$U_{p1}(R) = 2\pi \frac{R_T R_p}{R_T+R_p}\varepsilon_0(S) \tag{5.16}$$

This one term form becomes the same as the global potential of Christensen and Winther [24] when one takes an empirical form for

$$\varepsilon_0(S) = \frac{50}{2\pi} \exp\left(\frac{S}{.63}\right) \tag{5.17}$$

To make a more detailed geometrical analysis of $\varepsilon_0(S)$ we assume that both the projectile and target densities have the same Fermi function form (with the same diffuseness)

$$\rho_p(r_p) = \frac{\rho_p^0}{1 + \exp[(r_T - R_T)/a]} \tag{5.18a}$$

$$\rho_T(r_T) = \frac{\rho_T^0}{1 + \exp[(r_p - R_p)/a]} \tag{5.18b}$$

Then the integral in Eq. (5.15) is equal to

$$e(t) = \rho_p^0 \rho_T^0 \frac{t}{\exp(t/a) - 1} \tag{5.19}$$

Brink [34] suggested this form for the one-term proximity version of the folding potential Eq. (5.16), which becomes

$$U_{p1}(R) = 2\pi V_0 \rho_p^0 \rho_T^0 \frac{R_T R_p}{R_T + R_p} \int_{R-R_T-R_p}^{\infty} \frac{t\,dt}{\exp[t(a) - 1]} \tag{5.20}$$

Baltz and Bayman [34] have adapted Eq. (5.19) also for the two-term proximity potential, Eq. (3.13), and obtain

$$U_{p1}(R) = 2\pi V_0 \rho_p^0 \rho_T^0 \frac{R_T R_p}{R} \left[\int_{R-R_1 R_p}^{\infty} \frac{t\,dt}{\exp[t(a) - 1]} + \frac{R_T + R_p}{2R_T R_p} \int_{R-R_T-R_p}^{\infty} \frac{t^2 dt}{\exp[t(a) - 1]} \right] \tag{5.21}$$

Figure 5.3 shows a global comparison of the one- and two-term proximity potentials generated by Eqs. (5.20) and (5.21) with exact results obtained by numerical folding on a computer. Five representative cases were taken, spanning the region of heavy-ion reactions: $^{16}O + {}^{16}O$, $^{16}O + {}^{58}Ni$, $^{16}O + {}^{208}Pb$, $^{58}Ni + {}^{208}Pb$, and $^{208}Pb + {}^{208}Pb$. The plotted results have a clear interpretation: The proximity potential in its two-term form is in excellent agreement with the folding model for all heavy-ion reactions, not only in shape, but in absolute magnitude. Furthermore, with a slightly increased normalization, the one-term proximity potential is also essentially geometrically identical to the folding model.

6. The Nuclear Polarization Potential

One of the first treatments of the effect of inelastic scattering on the elastic channel in terms of an optical potential component was made by Glendenning, Hendrie, and Jarvis [40], who considered the case of 50 MeV α-scattering on Samarium isotopes. While Coulomb excitation is non-negligible in this case, the dominant coupling is nuclear with the L = 2 component of the deformed optical potential of ^{154}Sm providing a strong coupling between the ground state and first excited 2^+ state. Thus the optical potential parameters required to fit the elastic scattering were somewhat different depending on whether a full coupled channels or simple optical model was utilized.

For the spherical ^{148}Sm, on the other hand, the back coupling effect on the elastic channel from coupled channels calculations was small enough that the elastic cross section was insignificantly different from a simple optical model calculation. Furthermore the optical parameters used for the coupled channels calculations were (apart from the $A^{1/3}$ — dependence) identical in the deformed and spherical Sm isotopes. Glendenning, Hendrie, and Jarvis identified the difference between the coupled channels optical potential and the simple one channel optical potential for ^{154}Sm as the polarization potential component of the Feshbach formula Eq. (2.1). Of course this potential difference is empirical, with no ℓ-dependence as the computed polarization potential would in general have.

Further investigation of this optical potential was subsequently made by Baltz, Glendenning, Kauffmann, and Pruess [4]. These authors calculated the local equivalent of the L-dependent non-local optical potential representation of the coupling to the first 2^+ state in ^{154}Sm. Reorientation and the coupling to higher states was ignored, with the non-local potential explicitly constructed as in Eq. (2.6). The local equivalent was then constructed by iteration, i.e.,

$$(E_l - H)f_l^0 = 0,$$

$$U_l^0(r) = \frac{1}{f_l^0(r)} \int dr' U_l(r,r') f_l^0(r'),$$

$$(E_l - H - U_l^0(r)) f_l^1(r) = 0,$$

$$U_l^1(r) = \frac{1}{f_l^1(r)} \int dr' U_l(r,r') f_l^1(r'),$$

$$(E_l - H - U_l^{N-1}(r)) f_l^n(r) = 0,$$

$$U_l^n(r) = \frac{1}{f_l^n(r)} \int dr' U_l(r,r') f_l^n(r').$$

The real part of the calculated optical potential is exhibited in Fig. 6.1 as a function of orbital angular momentum ℓ. Clearly it is highly ℓ-dependent, repulsive in the low partial waves, increasing in magnitude to the surface, changing sign and becoming attractive, and then decreasing in magnitude for high partial waves. The empirical optical model component from the original analysis is also shown in the figure to be ℓ-independent and repulsive. The data is clearly sensitive to exclusion of flux from the interior in low partial waves; at high partial waves the angular momentum barrier decreases the sensitivity to such a potential.

The imaginary part of the optical potential component for this case is shown in Fig. 6.2. It is ℓ-dependent, but absorptive for all partial waves. The empirical imaginary potential component is of small magnitude, but relatively diffuse in its small absorption outside the surface.

A heavy ion case was also investigated by these authors. 60 MeV ^{16}O scattering on ^{40}Ca with excitation of the 3^- state in the target was treated

with no reorientation in the coupled channels, thus making the optical model formulation exactly equivalent to the coupled channels. In Figs. 6.3 and 6.4 are shown the real and imaginary parts of the ℓ-dependent local equivalent potential component which exactly represents the coupling of the 3^- state upon the elastic scattering. The general pattern is similar to the α-Sm case: The real potential component is repulsive for low partial waves and the imaginary potential component is dominantly absorptive with an ℓ-dependence of strength peaking in the surface partial waves. The interpretation of the real potential is less clear. It has been suggested that the complex potential as a whole be considered as approximated by one radial function times a pole in ℓ. [48]

Similar calculations of a polarization potential component were later performed by Franey and Ellis [29]. The case considered, 68 MeV ^{13}C scattering on ^{40}Ca with excitation of the 3^- target state is similar to the case just discussed, and it is not surprising that the results for the computed potential components are similar as is seen in Fig. 6.5. It is interesting from a technical standpoint that Franey and Ellis used the general procedure described in Equation (2.12) to obtain the potential rather than explicit construction of the non local potential such as was followed in the ^{16}O case.

We have discussed what a polarization potential component would look like for one strongly coupled inelastic channel. Of course in the general heavy ion scattering case there are many channels both inelastic and particle transfer contributing to the elastic optical potential. Frahn and Hussein [42] have worked out general expressions for such direct reaction polarization potential contributions in terms of the closed S-matrix formalism. The result is a complex, ℓ-dependent, potential sum of components arising from various dynamical origins.

Broglia, Pollarolo, and Winther [41] have considered the same problem in a semiclassical context with the assumption that the important contributions

should be only absorptive. The basic idea used in constructing their absorptive potential is that its integral over the semiclassical path should be proportional to the flux lost into the coupled channels considered. Since such a procedure does not give a potential as a function of radius, but only a constraint on its integrated value over a path, there is the ambiguity of a large class of phase shift equivalent potentials. Broglia et al. attempt to remove this ambiguity by requiring the absorptive polarization potential to be angular momentum independent. The resulting potential due to the nuclear interaction then has a long range component due to single-particle transfer and a short range part due to inelastic scattering. While this approach has some intuitive attraction, it misses one of the aspects seen above in our examples, namely the real repulsive potential in the low partial waves. It would be interesting to investigate just how universal this potential type is, and whether such a potential arises from transfer also, but one needs a more quantum mechanical formulation such as that of Frahn and Hussein if one is not to exclude the real polarization potential a priori.

Polarization Potentials and the DWBA

Our emphasis in this report is the representation of the effect of channel coupling as a potential in the elastic channel. A further interesting application is their use in constructing scattering solutions for the distorted waves of the various channels in DWBA calculations. For example let us consider the amplitude for inelastic scattering to the 3^- state in ^{40}Ca induced by the 60 MeV ^{16}O beam considered above. If all excited states are coupled only to the elastic state, then the wave function for any of them can be written in the form

$$\chi^{3-} = G^{(+)}_{3-} V_{3-0} \chi^{0+}$$

from coupled equations of the form Eq. (5.4). Taking a partial wave we find the asymptotic form

$$\chi_l^{3-}(r\to\infty 0 = h_l^{3-}(r\to\infty) \sum_r C_r \int_0^\infty f_l^{3-}(r')V(r')\chi_r^{0-}(r')dr'. \qquad (6.2)$$

Since the coefficient of the outgoing wave function is the scattering amplitude we have the coupled-channels equivalent for the inelastic scattering transition amplitude in the form of DWBA. All 0^+-3^- coupling effects through the ground state wave function $\chi_{0+}(r')$, and the excited state wave function $f_{3-}(r')$ is just an optical model wave function without the effect of the strong coupling to the 0^+ ground state.

As Ascuitto et al. [43] have pointed out for the $^{16}O + ^{40}Ca$ case, it is most crucial in fitting the angular distribution of the 3^- and 5^- cross sections with a DWBA type cross section that the effects of the specific 3^- coupling not be included in the final channel wave functions. (This is clear in our eq. (6.2).) In this particular case the strong ℓ-dependence of the calculated potentials is of less importance in obtaining a DWBA type cross section similar to that generated by coupled channels calculations.

Since the DWBA can be thought of as an approximation to coupled channels, it is not very helpful to say that it may be used in conjunction with a bare final state optical potential determined only by a coupled channels fit to the initial channel. Kubo and Hodgson [44] attempted to remedy this difficulty by calculating the nuclear polarization potential in the Love, Terasawa, and Satchler approximation and then subtracting it from the optical model fitted potential to obtain the bare potential.

Tanimura et al. [45] pointed out that in the more general case where excited channels are coupled not only to the elastic channel but to each other there will be a channel dependent polarization potential to be used in the non-elastic channels as well. These potentials as well as the coupling interactions for first and second-order DWBA formulations of the exact coupled channels problem are determined by the truncation of the channel space.

7. Conclusions

In this report we have reviewed a number of aspects of the polarization potential representation of heavy ion elastic scattering. What should have become evident, especially in the treatment of the Coulomb polarization potential, is the constant interplay between classical and quantum mechanical aspects of heavy ion potentials. The adiabatic real potential was originally derived semi-classically, but we presented the derivation in quantum mechanical framework. The BKGP imaginary potential was originally derived in a quantum mechanical framework, but those who came after and extended the idea often worked using the concepts of the semiclassical scattering theory.

Treatment of the potentials in closed form scattering theories followed a method which may be called semi-classical for the imaginary potential and classical for the real potential. In general both these methods are accurate evaluations of the cross sections due to long range imaginary or real polarization potentials.

The accuracy of the potentials themselves as a representation of coupled channels is in general greatest when the effect of the coupling is perturbative. Thus the adiabatic polarization potential is an excellent and accurate representation of the virtual Coulomb excitation of giant dipole, quadrupole and octupole excitations. And since we know that the classical scattering theory is a good evaluation of the long range real potentials we have accurate closed forms for the effect of the giant multipoles as well as an accurate evaluation of the classics relativistic Rutherford cross section for spin zero particles.

For the case of the Coulomb polarization potential arising from multiple Coulomb excitation the accuracy is limited by off-shell effects and the nonperturbative nature of the reaction. These effects are interrelated. When

the coupling is weak enough that only the effect of the first 2^+ state enters in, then the off-shell effects of high couplings vanish. Energy loss can also provide a limitation of this potential. The whole treatment is intimately related to the semiclassical theory of Coulomb and does not intend to replace it. Nevertheless, looking at multiple Coulomb excitation in a potential represetation has allowed us to see how multi-step contributions come to the Feshbach potential Eq. (2.1) in a specific case.

Appendix A The Total Reaction Cross Section

In this appendix, we supply a derivation of Eq. (2.5) for the total reaction cross section. Consider the optical model Schrodinger equation

$$\frac{-\hbar^2}{2\mu}\nabla^2\psi^{(+)} + (V - iW)\psi^{(+)} = E\psi^{(+)}, \tag{A.1}$$

Where we take $W > 0$ to describe absorption. From (A.1) one can immediately derive the equation for flux conservation,

$$-\hbar \int \vec{\nabla}\cdot\vec{J}\, d^3r = 2 \langle\psi^{(+)}|W|\psi^{(\pm)}\rangle \tag{A.2}$$

where $\vec{J}$ in the probability current

$$\vec{J} = \frac{\hbar}{2\mu i}\left[\psi^*\vec{\nabla}\psi - (\vec{\nabla}\psi^*)\psi\right] \tag{A.3}$$

Applying Gauss' theorem to the LHS of (A.2), we have then

$$-\int \vec{J}\cdot d\vec{A} = \frac{2}{\hbar}\langle\psi^{(+)}|W|\psi^{(+)}\rangle, \tag{A.4}$$

where the integral is over any surface surrounding the interaction, in a region where the potential has vanished. Eq. (A.4) simply says that the net radial flux is not zero because of absorption. The total reaction cross section is defined as the net inward radial flux given by the LHS of (A.4) devided by the incident flux $|\psi^{(+)}|^2 v$, where v is the asymptotic relative velocity.

$$\sigma_R = \frac{-\int \vec{J}\cdot d\vec{A}}{|\psi^{(+)}|^2 v} = \frac{2}{\hbar v}\frac{\langle\psi^{(+)}|W|\psi^{(+)}\rangle}{|\psi^{(+)}|^2} \tag{A.5}$$

If we choose the normalization of $\psi^{(+)}$ to be $|\psi^{(+)}|^2 = 1$ we obtain our expression for σ_R Eq. (2.5)

$$\sigma_R = \frac{2}{\hbar v}\langle\psi^{(+)}|W|\psi^{(+)}\rangle = \frac{k}{E}\langle\psi^{(+)}|W|\psi^{(+)}\rangle \tag{A.6}$$

We leave it to the reader to convince himself that Eq. (A.4) can be written in the more familiar optical theorem form,

$$\frac{4\pi}{k}\,\mathrm{Im}\, f(0) - \int |f(\theta)|^2 d\Omega = \frac{2}{\hbar v}\langle\psi^{(+)}|W|\psi^{(+)}\rangle, \tag{A.7}$$

where the first term is the total cross section and the second the total elastic cross section. Clearly (A.6) is consistent with (A.7).

Appendix B Large ℓ 3-j and 6-j Coefficients

In this appendix are given the approximate, large ℓ limit, values of the 3-j and 6-j symbols needed in the calculation. Throughout we shall use the definitions and convention of Edmonds. [30]

a) 3-j symbols

$$\begin{pmatrix} \ell & \ell & 2 \\ 0 & 0 & 0 \end{pmatrix} = (-)^{\ell+1}\left[\frac{\ell(\ell+1)}{(2\ell+3)(2\ell+1)(2\ell-1)}\right]^{1/2}$$

$$\simeq \frac{(-)^{\ell+1}}{\sqrt{8\ell}} \qquad \text{(B.1)}$$

$$\begin{pmatrix} \ell & \ell+2 & 2 \\ 0 & 0 & 0 \end{pmatrix} = (-)^{\ell}\left[\frac{3}{2}\frac{(\ell+2)(\ell+1)}{(2\ell+5)(2\ell+3)(2\ell+1)}\right]^{1/2}$$

$$\simeq (-)^{\ell}\sqrt{\frac{3}{16\ell}} \qquad \text{(B.2)}$$

b) 6-j symbols

In the following $\ell \gg I$, $\ell \gg m$.

$$\begin{Bmatrix} \ell & \ell+M & I \\ 2 & I-2 & \ell+m-2 \end{Bmatrix}$$

$$= \left[\frac{1}{2\ell}\frac{(m+I-3)(m+I-2)(m+I-1)(m+I)}{(2I-3)(2I-2)(2I-1)(2I)(2I+1)}\right]^{1/2} \qquad \text{(B-3)}$$

$$\begin{Bmatrix} \ell & \ell+m & I \\ 2 & I-2 & \ell+m \end{Bmatrix}$$

$$= \left[\frac{3}{\ell}\frac{(m+I-1)(m+I)(I-m-1)(I-m)}{(2I-3)(2I-2)(2I-1)(2I+1)(2I)}\right]^{1/2} \qquad \text{(B.4)}$$

$$\begin{Bmatrix} \ell & \ell+m & I \\ 2 & I-2 & \ell+m+2 \end{Bmatrix}$$

$$= \left[\frac{1}{2\ell}\frac{(I-m-3)(I-m-2)(I-m-1)(I-m)}{(2I-3)(2I-2)(2I-1)(2I)(2I+1)}\right]^{1/2} \qquad \text{(B.5)}$$

$$\begin{Bmatrix} \ell & \ell+m & I \\ 2 & I & \ell+m+2 \end{Bmatrix}$$

$$= \left[\frac{3}{\ell}\frac{(m+I-1)(m+I)(I-m+1)(I-m+2)}{(2I-1)(2I)(2I+1)(2I+2)(2I+3)}\right]^{1/2} \qquad \text{(B.6)}$$

$$\begin{Bmatrix} \ell & \ell+m & I \\ 2 & I & \ell+m \end{Bmatrix}$$

$$= \frac{(3m^2 - I(I+1)}{[\ell I(2I-1)(2I+1)(2I+2)(2I+3)]^{1/2}} \qquad \text{(B.7)}$$

Appendix C Angular Deviation for Virtual Dipole, Quadrupole, and Octupole Excitation

We give in this appendix the expressions for $\Delta\theta^{(1)}$, $\Delta\theta^{(2)}$ and $\Delta\theta^{(3)}$, calculated using Equations (4.10) and (4.24)

$$\Delta\theta^{(1)} = -\frac{V_0^{(1)}}{2Ea^4}\frac{\cos^4\phi_0}{\sin^6\phi_0}\left[-15\phi_0 + 12\phi_0\sin^2\phi_0 + 15\sin\phi_0\cos\phi_0 - 2\cos\phi_0\sin^3\phi_0\right] \quad (C.1)$$

$$\Delta\theta^{(2)} = -\frac{V_0^{(2)}}{8Ea^6}\frac{\cos^6\phi_0}{\sin^{10}\phi_0}\left[-315\phi_0 + 420\phi_0\sin^2\phi_0 - 120\theta_0\sin^4\phi_0 + 315\cos\phi_0\sin\phi_0 - 210\cos\phi_0\sin^3\phi_0 + \cos\phi_0\sin^5\phi_0\right] \quad (C.2)$$

$$\Delta\theta^{(3)} = -\frac{V_0^{(3)}}{80Ea^8}\frac{\cos^8\phi_0}{\sin^{14}\phi_0}\left[-15015\phi_0 + 27720\phi_0\sin^2\phi_0 - 15120\phi_0\sin^4\phi_0 + 2240\phi_0\sin^6\phi_0 + 15015\sin\phi_0\cos\phi_0 - 17710\cos\phi_0\sin^3\phi_0 + 4648\cos\phi_0\sin^5\phi_0 - 80\cos\phi_0\sin^7\phi_0\right] \quad (C.3)$$

As shown in figure (C.1) the three angular deviations have similar behavior, all peaking at an intermediate angle. Further they attain zero value at $\phi_0 = 0$ and $\pi/2$ which correspond to $\theta=0$ and π, respectively.

References

[1] H. Feshbach, Ann. Phys. (N.Y.) 19, (1962) 287.

[2] C. Mahaux, Microscopic Optical Potentials, Proceedings of the Hamburg Topical Workshop on Nuclear Physics, Springer-Verlag (Berlin, 1979) p. 1.

[3] W.G. Love, T.Terasawa and G.R. Satchler, Phys. Rev. Lett. 39, 6 (1977); Nucl. Phys. A291 (1977) 183.

[4] A.J. Baltz, S.K. Kauffman, N.K. Glendenning, and K. Pruess, Phys. Rev. Lett. 40 (1978) 20; A.J. Baltz, N.K. Glendenning, S.K. Kauffmann and K. Pruess, Nucl. Phys. A327 (1979) 221.

[5] M.S. Hussein, Phys. Lett. B88 (1979) 31.

[6] R. Donangelo, L.F. Canto and M.S. Hussein, Nucl. Phys. A320 (1979) 422; Phys. Rev. C19 (1979) 1801.

[7] B.V. Carlson, M.S. Hussein and A.J. Baltz, Phys. Lett. B98 (1981) 409; Ann. Phys. (N.Y.) 138 (1982) 215.

[8] P. Pechukas, Phys. Rev. 181 (1969) 166.

[9] K. Alder, A. Bohr, T. Huus, B. Mottelson and A. Winther, Rev. Mod. Phys. 28 (1956) 1432.

[10] C.E. Thorn, M.J. LeVine, J.J. Kolata, C. Flaum, P.D. Bond and J.C. Sens, Phys. Rev. Lett. 38 (1977) 384.

[11] D.J. Weber, M.A. Franey, D. Dehnhard, J.L. Artz, V. Shkolnik and N.M. Hintz, Bull. Am. Phys. Soc. 21, 1006 (1976).

[12] K. Alder and A. Winther, Electromagnetic Excitations, North-Holland, Amsterdam, 1975.

[13] R.A. Broglia and A. Winther, Heavy Ion Reactions, W.A. Benjamin (1982).

[14] R. Frobrich, R. Lipperheide and H. Fiedeldey, Phys. Rev. Lett. 43 (1979) 1147.

[15] L.D. Tolsma, Phys. Rev. C20 (L(&() 592.

[16] M. Rhoades-Brown, M.H. Macfarlane and S.C. Pieper, Phys. Rev. C21 (1980) 2417; 2436.

[17] A.J. Baltz, Phys. Rev. C25 (1982) 240.

[18] M. Ichimura, M. Igaroski, S. Landowne, C.H. Dasso, B.S. Nilsson, R.A. Broglia and A. Winther, Phys. Lett. 67B (1977) 129.

[19] L.I. Schiff, Quantum Mechanics, Second Edition, McGraw-Hill, New York 1955.

[20] A. Bohr and B.R. Mottelson, Nucl. Structure, Vol. II, Benjamin, N.Y. 1975.

[21] J. Rasmussen, P. Moller, M. Guidry and R. Neese, Nucl. Phys. A341 (1980); M.S. Hussein, Proceedings of the 1st Brazilian Symposium on Photo-nuclear Reactions, Sao Paulo (1982). To appear.

[22] A.J. Baltz and M.S. Hussein, Phys. Lett. 132B (1983) 274.

[23] R. Bonin, N,. Alamanos, B. Berthier, G. Bruge, J. L. Esurdie, H. Faraggi, D. Legrand, J.C. Lugol, W. Mittig, L. Papinean, J. Arvieux, L. Farvacque, M. Levine, D.K. Scott, A.I. Yavin and M. Buenerd, MSU Annual Report (1982) 50.

[24] P.R. Christensen and A. Winther, Phys. Lett. 65B (1976) 19.

[25] W.G. Lynch, M.B. Tsang, H.C. Bhang, J.G. Cramer and R.J. Puigh, Phys. Rev. Lett. 48 (1982) 979.

[26] J.D. Jackson, Classical Electrodynamics, Second Edition, J. Wiley, New York, 1975, p. 616.

[27] P. Doll, M. Bini, D.L. Hendrie, S.K. Kauffmann, J. Mahoney, A. Menchaca-Rocha, D.K. Scott, T.J.M. Symons, K. van Bibber, Y.P. Viyogi, H. Wieman and A.J. Baltz, Phys. Lett. 76B (1978) 566.

[28] CHORK, version of coupled-channels code CHUCK by P.D. Kung as modified by L. Rickertson, unpublished.

[29] M.A. Franey and P.J. Ellis, Phys. Rev. 23C (1981) 787.

[30] L.D. Landau and E.M. Lifshitz, Mechanics, London, 1960.

[31] G. Baur, F. Rosel and D. Trautman, Nucl. Phys. A288 (1977) 113.

[32] N.J. Mott and H.S.W. Massey, The Theory of Atomic Collisions, Third Edition, Oxford, 1965.

[33] S. Landowne and H. Wolter, Nucl. Phys. A351 (1981) 171; see also A. Trabor, D. Trautmann and F. Rosel, Nucl. Phys. A291 (1977) 221.

[34] A.J. Baltz and B.F. Bayman, Phys. Rev. C26 (1982) 1969.

[35] P.J. Moffa, C.B. Dover and J.P. Vary, Phys. Rev. C16 (1977) 1857.

[36] G.R. Satchler and W.G. Love, Phys. Reports 55C (1979) 183.

[37] J. Blocki, J. Randrup, W.J. Swiatecki and C.F. Tsang, Ann. Phys. (N.Y.) 105 (1977) 427.

[38] D.M. Brink and Fl. Stancu, Nucl. Phys. A299 (1978) 321.

[39] D.M. Brink, J. Phys. C37 (1976) 5.

[40] R.A. Broglia, G. Pollarolo, and A. Winther, Nucl. Phys. A361 (1981) 307; N.K. Glendenning, D.L. Hendrie and O.N. Jarvis, Phys. Lett. 26B (1968) 131.

[41] G. Pollarolo, R.A. Broglia and A. Winther, Nucl. Phys. A406 (1983) 369.

[42] W.E. Frahn and M.S. Hussein, Phys. Lett. 90B (1980) 358.

[43] R.J. Ascuitto, J.F. Peterson and E.A. Seglie, Phys. Rev. Lett. 41 (1978) 1159.

[44] K.-I. Kubo and P.E. Hodgson, Phys. Lett. 100B (1981) 453.

[45] O. Tanimura, R. Wolf, R. Kaps and U. Mosel, Phys. Lett. 132B (1983) 249.

[46] A. Edmonds, Angular Momentum in Quantum Mechanics, 2nd Ed. Princeton, 1960.

[47] I.Y. Lee and J.K. Saladin, Phys. Rev. C9 (1974) 2406.

[48] R.C. Fuller, private communication.

Figure Captions

3.1 Cross sections calculated with the LTS and BKGP ℓ-dependent potentials compared with a calculation without long range absorption. Woods-Saxon optical model parameters are from ref [3].

3.2 Illustrative calculations of the effects of E2 Coulomb excitation on the elastic cross sections for very heavy systems using the LTS potential. Dashed curves are for nuclear optical potentials alone [3].

3.3 (a) Universal function of angle $f(\theta)$. (b) Ratio of $f(\bar{\theta})$ for the LTS potential to $f(\theta)$ for BKGP Potential. (c) Elastic scattering cross section for $^{16}O + ^{162}Dy$ at ^{48}MeV calculated from Eq. (3.9) incorporating $f(\theta)$ and $f(\bar{\theta})$. Data are from Lee and Saladin [47].

3.4 The coefficients a_ℓ, b_ℓ and c_ℓ plotted as functions of $\ell[-(\ell+\bar{l}/2)/\eta]$ for several values of the quadrupole coupling parameter q. A factor η/E was taken out of the coefficients in order to present the results in as general a form as possible.

3.5 The coefficients, a_ℓ, b_ℓ and c_ℓ plotted as functions of the quadrupole coupling parameter q for several values of $\bar{\ell}[=(\ell+1/2)/\eta]$.

3.6 The giant multipole polarization potentials for λ = 1, 2 and 3 for the systems (a) $^{16}O + ^{208}Pb$ and (b) $^{208}Pb + ^{208}Pb$ at E_{cm} = 78.0 MeV and 567.0 MeV respectively. Also shown is the Christensen-Winther [24] potential.

4.1 Variables for a classical Coulomb scattering trajectory.

4.2 The universal functions $g^{(1)}(\theta)$, $g^{(2)}(\theta)$ and $g^{(3)}(\theta)$, Eq. (4.25), plotted versus the center of mass angle.

4.3 The universal function $g^{(R)}(\theta)$ associated with the relativistic effects, Eq. (4.36), plotted versus the center of mass angle.

4.4 Angular distributions from elastic scattering of ^{20}Ne on samarium nuclei. Dashed curves show calculations using Eq. (3.9) with a term for the ^{20}Ne 2^+ excitation added in. Solid curves show coupled channel calculations with both 2^+ states and reorientation included. The lower solid curve for ^{152}Sm shows the calculation without reorientation--a significant effect for this isotope.

4.5 Imaginary trivially equivalent local potential for 72 MeV $^{16}O + ^{152}Sm$ taken as a pure Coulomb case (without reorientation). The arrows mark values of r where $|\phi_\ell(r)|$ has maxima.

4.6 Cross sections as ratio to Rutherford for 78 MeV (cm) $^{16}O + ^{208}$ Pb with excitation of the giant isoscaler quadrupole resonance in ^{208}Pb. Optical model and coupled channels calculations were performed with the code CHORK [28].

4.7 Comparison of the trivially equivalent potential computed with the code CHORK [28] for orbital angular momenta 0, 40, 80 with the analytical form. Parameters are the same as for Figure 3.6.

5.1 Coordinates and volume element for the folding potential.

5.2 Coordinates for a two-dimensional integral in the folding model.

5.3 Comparison of proximity and folding model calculations of the ion-ion potential. Both V_0 and p_0 are normalized to unity.

6.1 Real potential component for 50 MeV $\alpha + ^{154}Sm$ scattering.

6.2 Imaginary potential component for 50 MeV $\alpha + ^{154}Sm$ scattering.

6.3 Real potential component for 60 MeV $^{16}O + ^{40}Ca$ scattering.

6.4 Imaginary potential component for 60 MeV $^{16}O + ^{40}Ca$ scattering.

6.5 Imaginary (a) and real (b) potential component for 68 MeV $^{13}L + ^{40}Ca$ scattering. The dashed curve is the bare potential.

C.1 The angular deviation, $\Delta\theta^{\lambda=1}$, $\Delta\theta^{\lambda=2}$ and $\Delta\theta^{\lambda=3}$, plotted versus the center of mass angles.

Table 4.1 - Adiabatic polarization potentials due to giant dipole, quadrupole and ocutpole excitations are tabulated. Percentage reduction in 180° cross sections are also shown for each contribution as well as for the relativistic effects. Reductions are angular, relative only to the $(\sin \theta/2)^{-4}$ Rutherford distribution.

System	$E_{c.m.}$ (MeV)	$V_0^{(1)}$ (MeV fm^4)	$V_0^{(2)}$ (MeV fm^8)	$V_0^{(3)}$	$V_0^{(R)}$ (%)	$\Delta\sigma^{(1)}$ (%)	$\Delta\sigma^{(2)}$ (%)	$\Delta\sigma^{(3)}$ (%)	$\Delta\sigma^{(R)}$ (%)
$^{40}Ar + ^{160}Gd$	130	6.24×10^3	3.05×10^5	9.45×10^5	8.73×10^{-3}	0.66	0.24	5.26×10^{-3}	0.582
$^{40}Ar + ^{148}Sm$	128	5.71×10^3	2.81×10^5	8.34×10^5	8.74×10^{-3}	0.66	0.24	5.37×10^{-3}	0.583
$^{16}O + ^{148}Sm$	64	1.08×10^3	4.99×10^5	1.44×10^5	9.52×10^{-3}	0.40	0.176	4.76×10^{-3}	0.635
$^{16}O + ^{208}Pb$	78	1.89×10^3	9.45×10^4	3.43×10^5	1.13×10^{-2}	0.42	0.168	4.84×10^{-3}	0.753
$^{208}Pb + ^{208}Pb$	567	1.57×10^5	1.39×10^7	6.70×10^7	1.17×10^{-2}	1.192	0.44	8.32×10^{-3}	0.780
$^{238}U + ^{238}U$	683	2.45×10^5	2.30×10^7	1.21×10^8	1.23×10^{-2}	1.30	0.46	8.77×10^{-3}	0.820

Table 4.2 Elastic ratio to Rutherford cross sections calculated at 180° for 48 MeV ^{16}O on ^{152}Sm with q_{002} = 1.572 and rotational values for q_{202} and q_{2+4}.

	Coupled channels	Optical model
q_{0+2} only	0.373	0.421
q_{0+2}, q_{2+2} only	0.396	0.445
q_{0+2}, q_{2+2}, q_{2+4}	0.418	0.487

Table 4.3 Elastic ratio to Rutherford cross sections calculated at 180° for 48 MeV ^{16}O on ^{152}Sm with only 0+2 coupling and various values for the strength.

$\sigma^{2+}_{(1)}/\sigma R$	0.88	1.76	2.24	3.52
Coupled channels	0.3726	0.0747	0.0121	0.0662
Optical model	0.4214	0.1776	0.1108	0.0317
JWKB	0.4147	0.1720	0.1066	0.0296
On-shell series	0.4087	0.1518	0.0797	0.0041
On-shell plus lowest off-shell	0.3552	0.0703	0.0122	0.0521

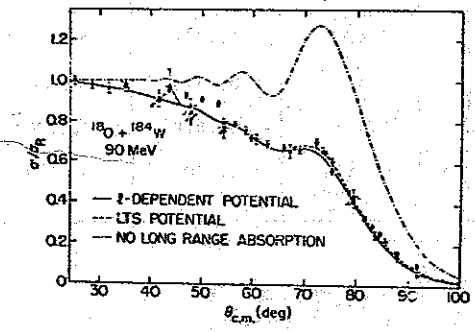
$^{18}O + ^{184}W$
90 MeV
— ℓ-DEPENDENT POTENTIAL
--- LTS POTENTIAL
— NO LONG RANGE ABSORPTION
σ/σ_R
$\theta_{c.m.}$ (deg)

Fig 3.1

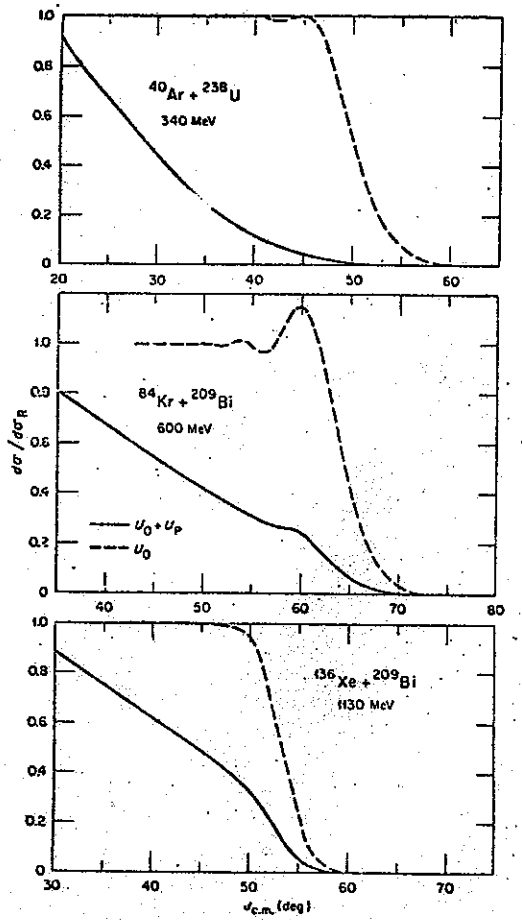
$^{40}Ar + ^{238}U$
340 MeV
$^{84}Kr + ^{209}Bi$
600 MeV
$U_0 + U_P$
U_0
$^{136}Xe + ^{209}Bi$
1130 MeV
$d\sigma / d\sigma_R$
$\theta_{c.m.}$ (deg)

Fig 3.2

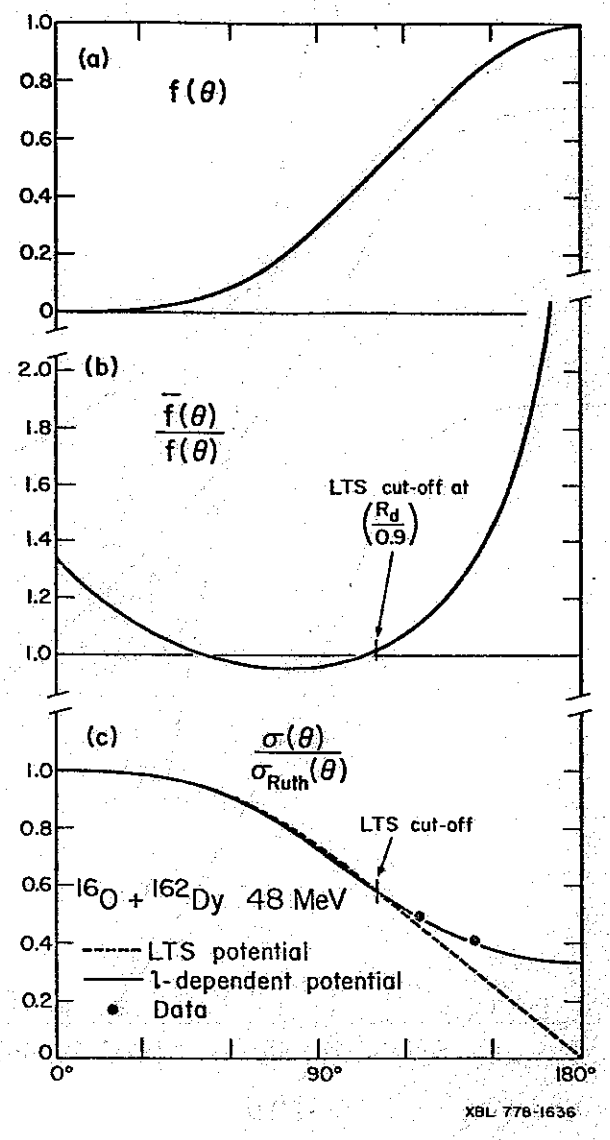
(a)
f(θ)
(b)
f̄(θ)/f(θ)
LTS cut-off at (R_d/0.9)
(c)
σ(θ)/σ_Ruth(θ)
LTS cut-off
16O + 162Dy 48 MeV
LTS potential
l-dependent potential
Data
0°
90°
180°
XBL 778-1636

Fig 3.3

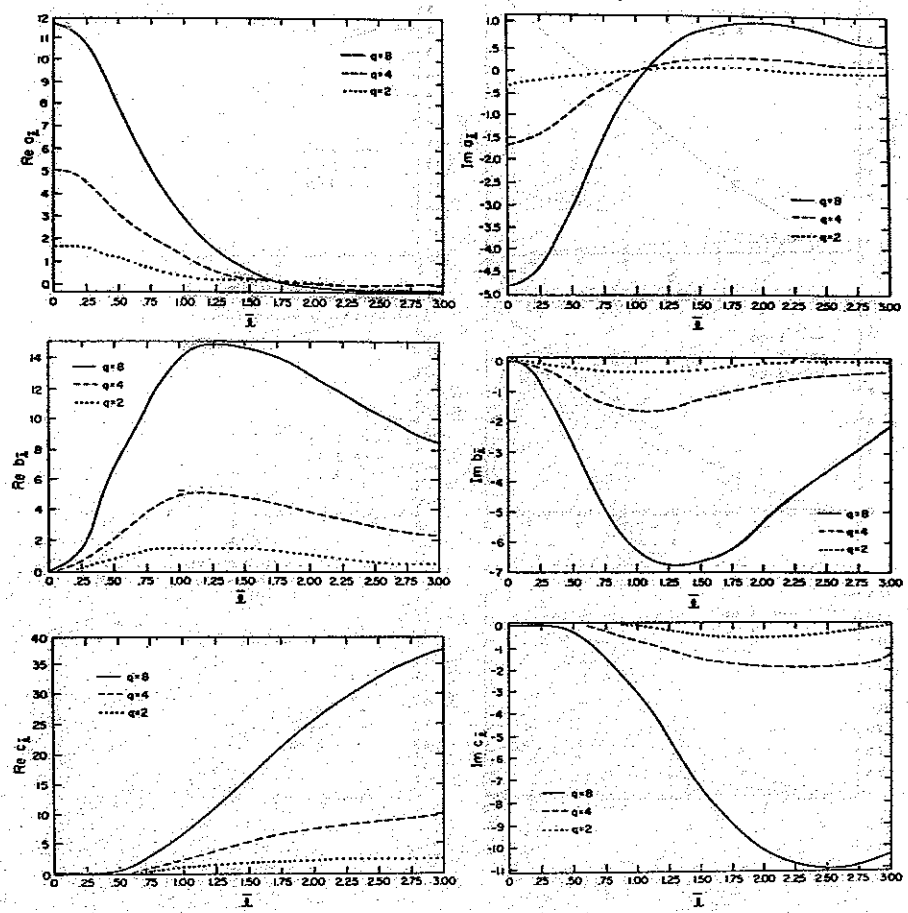
Re q_l
Im q_l
Re b_l
Im b_l
Re c_l
Im c_l
q=8
q=4
q=2
l̄

Fig 3.4

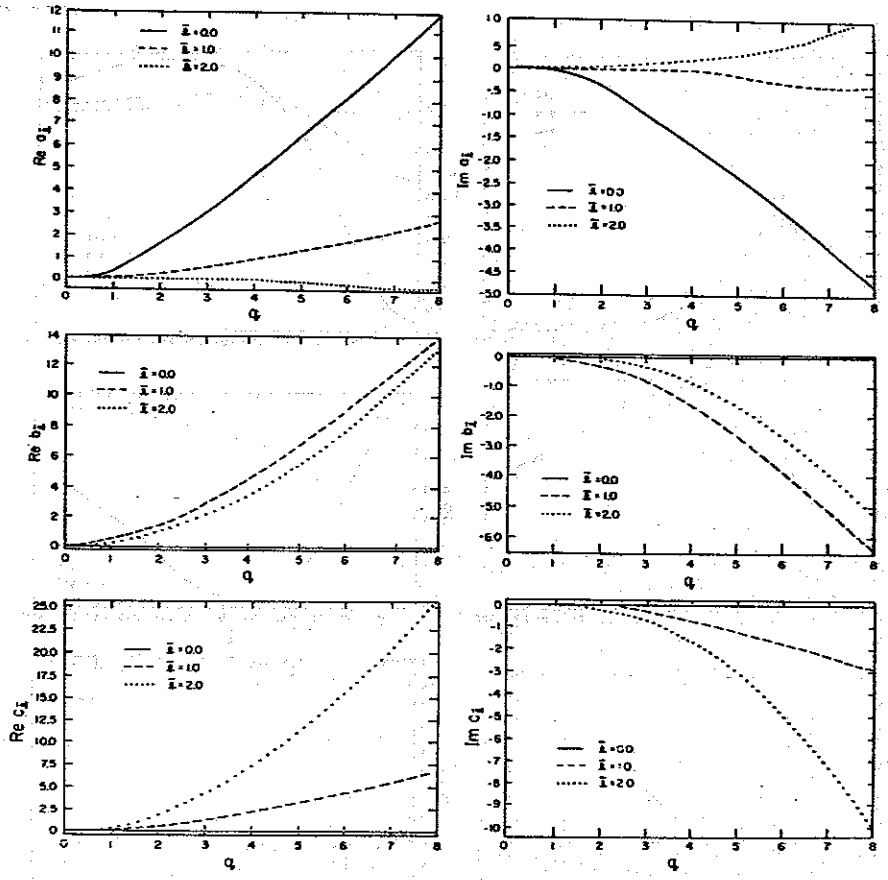

Fig 3.5

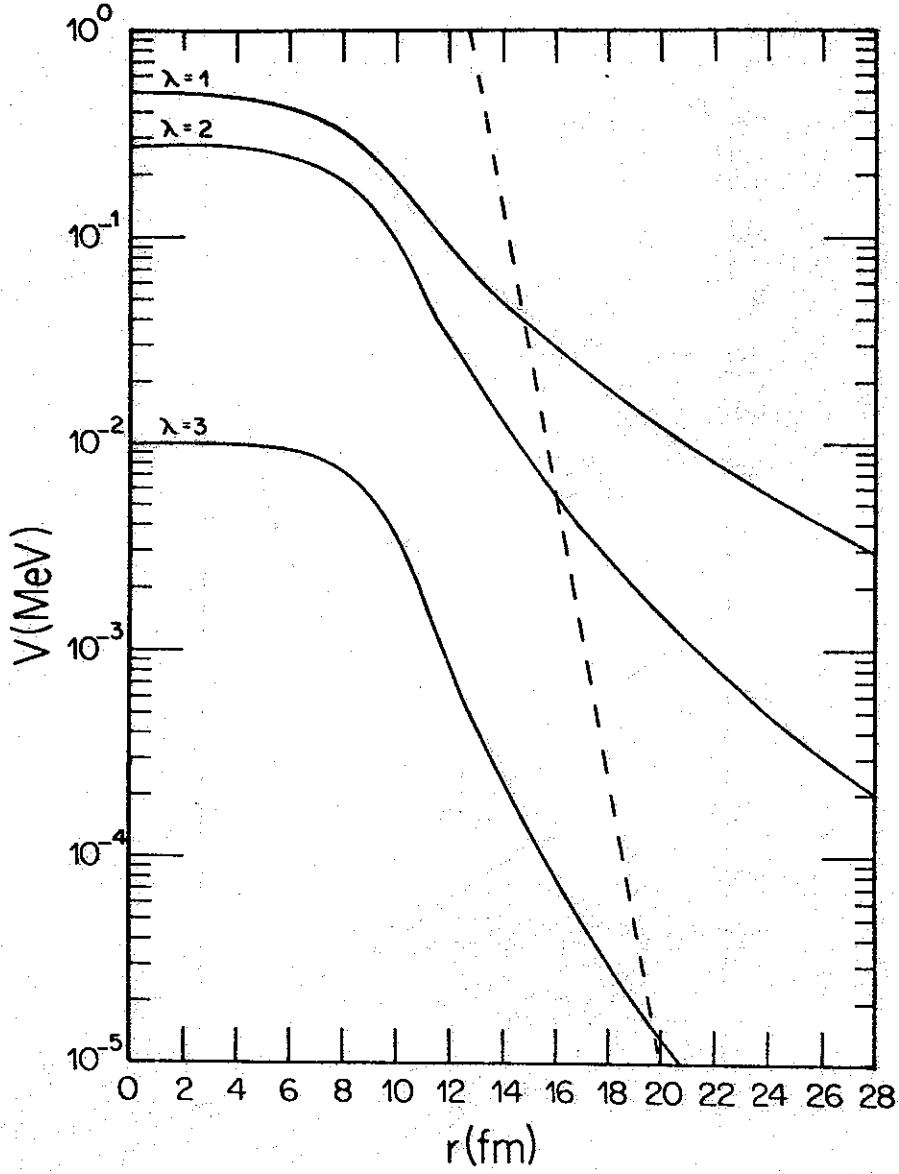

Fig 3.6 a

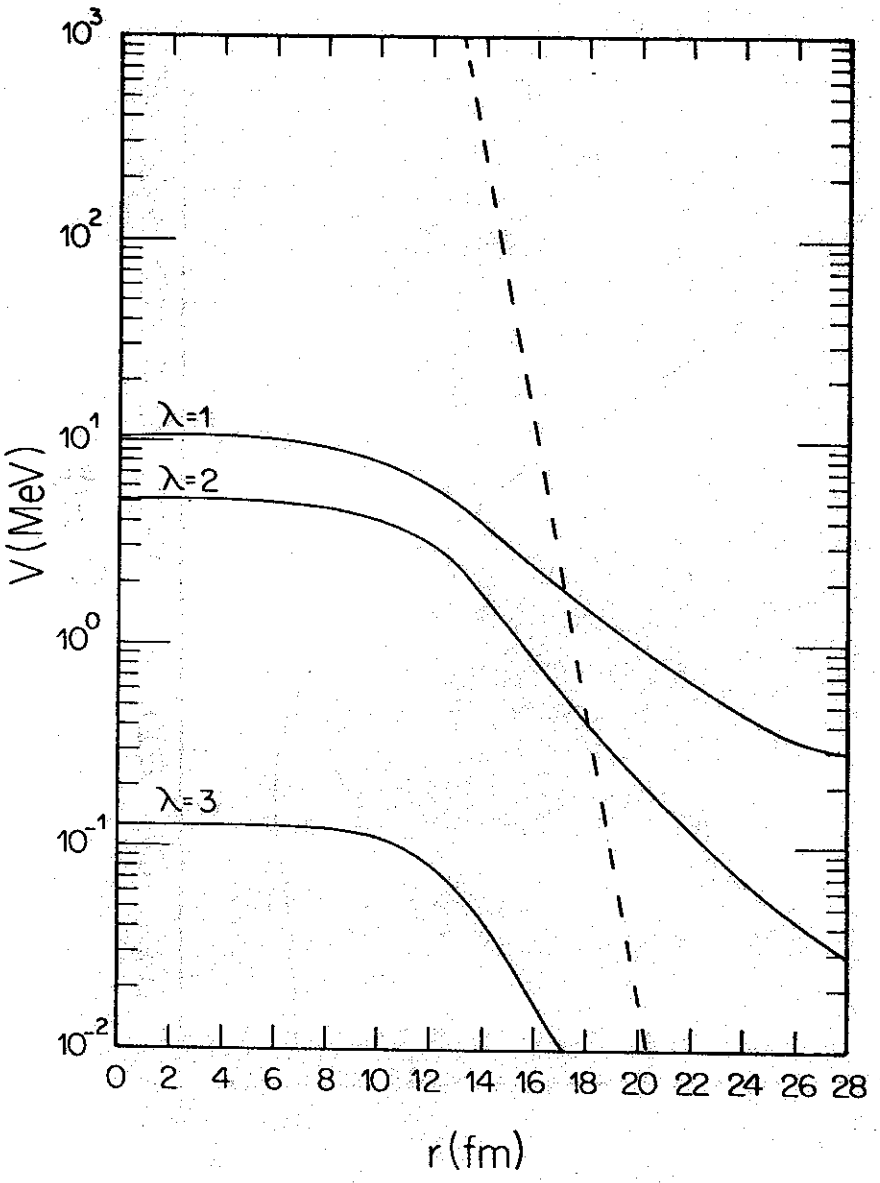

Fig 3 6 b

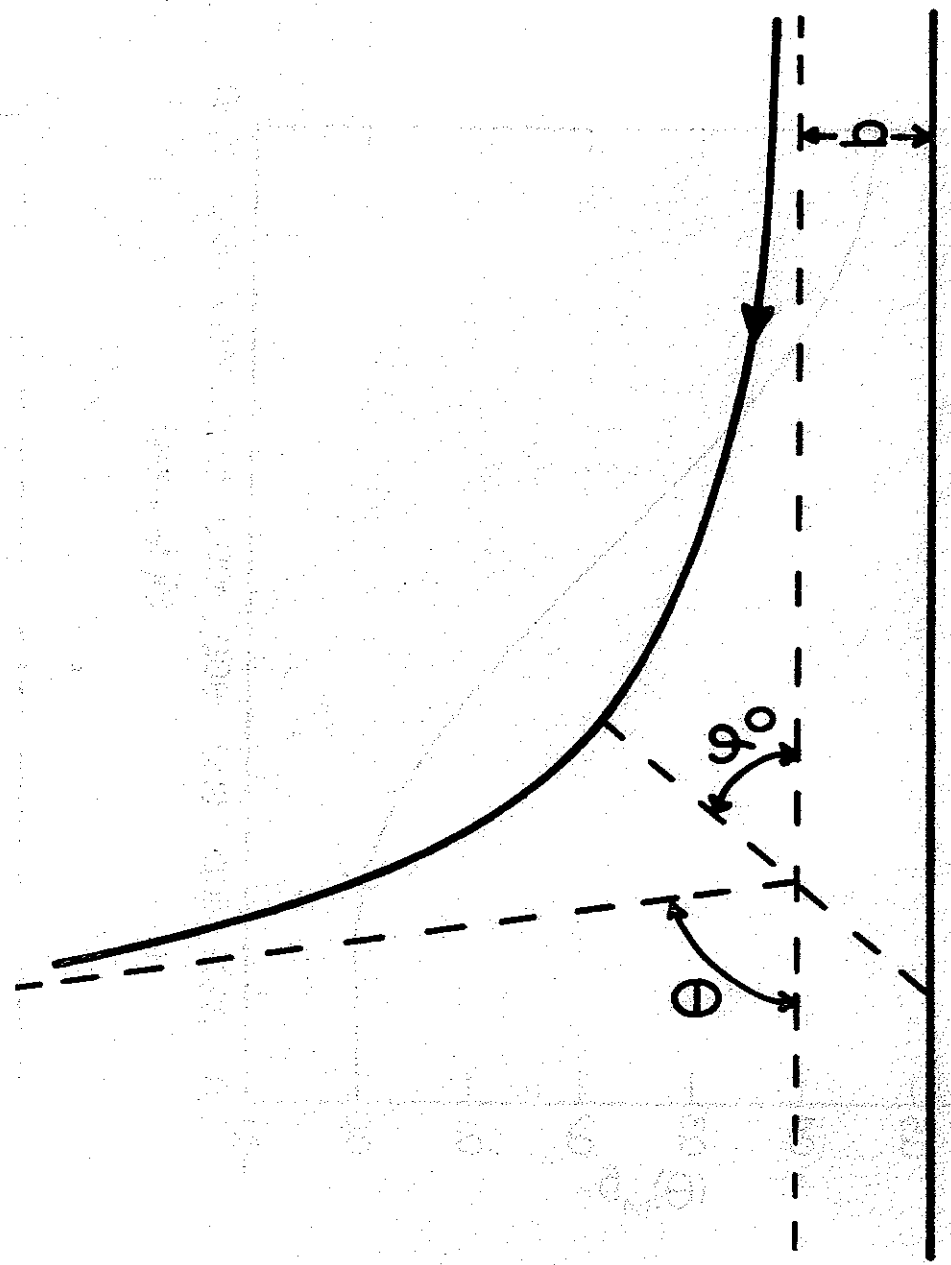

Fig. 4.1

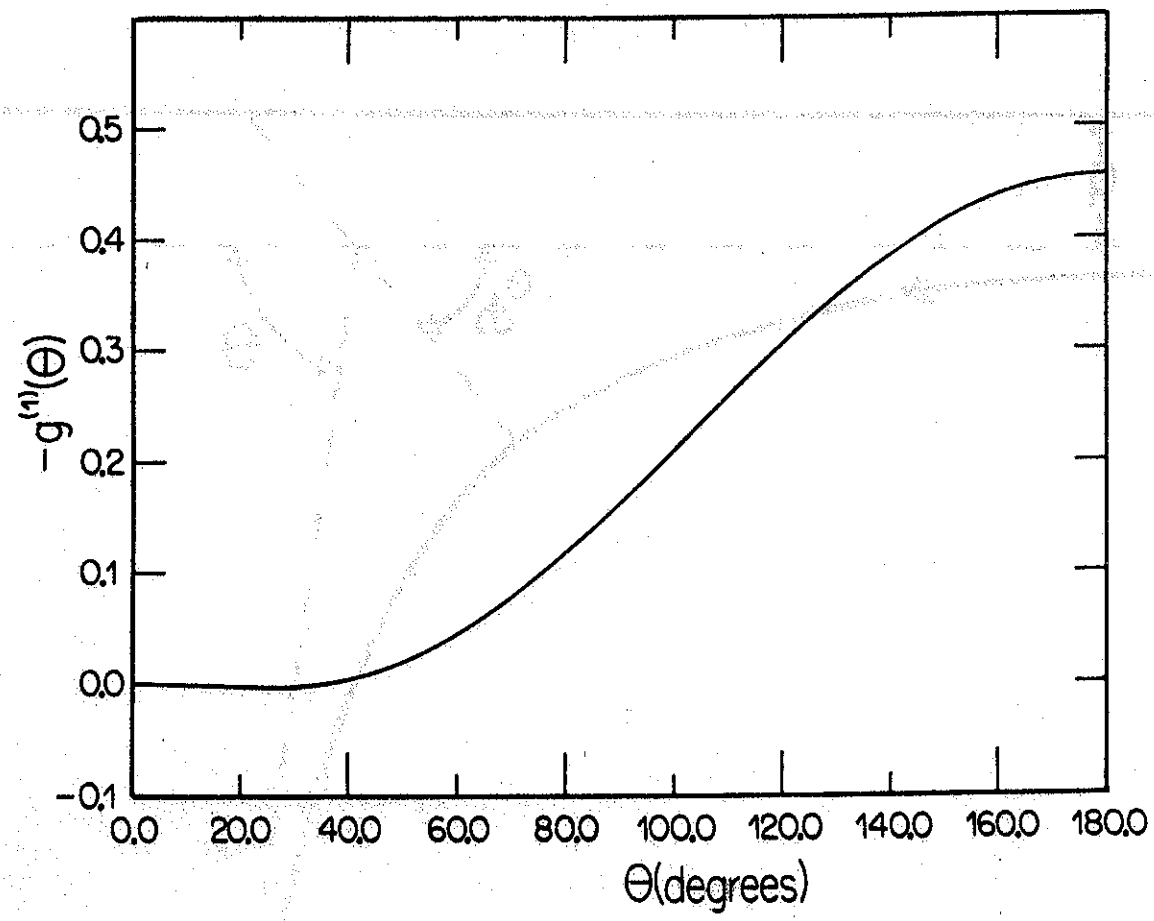

Fig 4.1 a

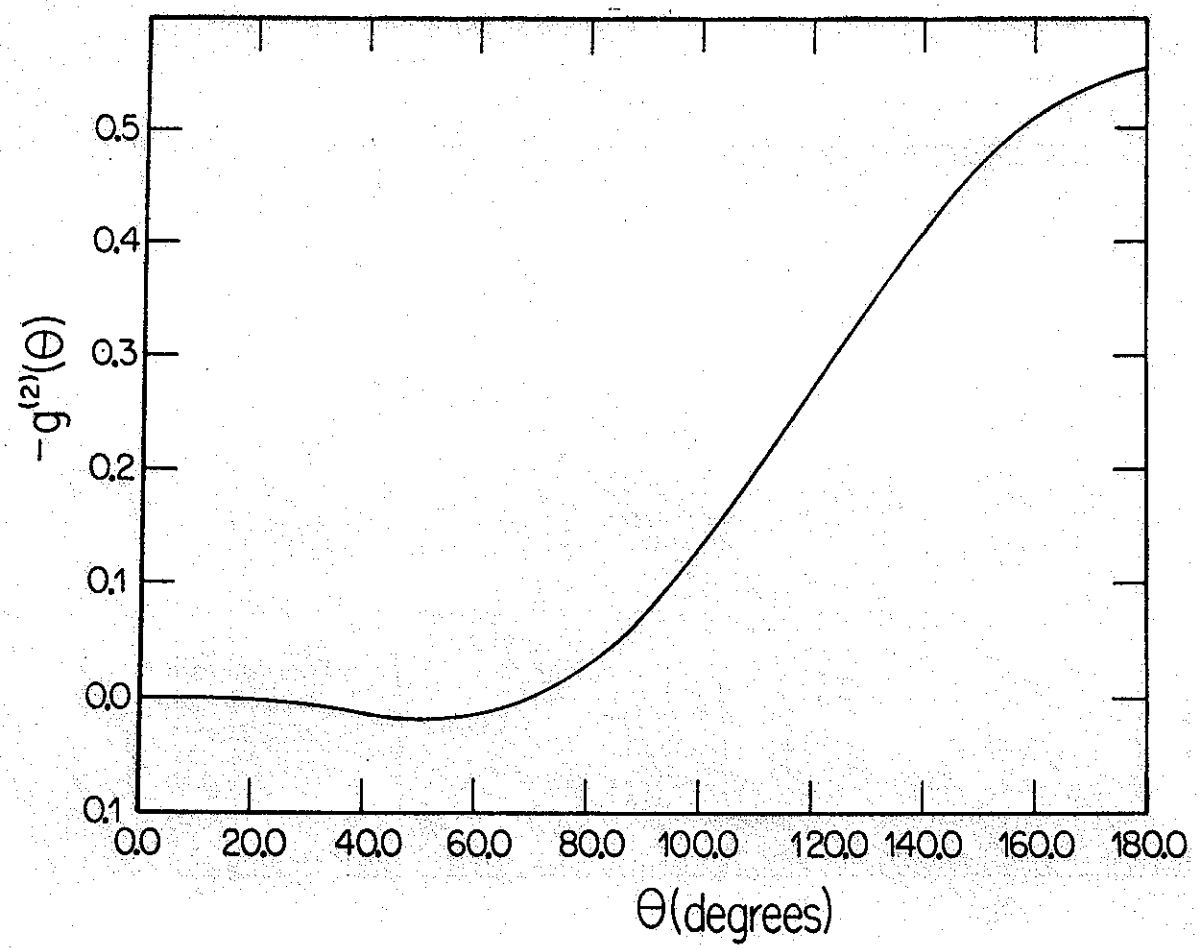

Fig 4.1 b

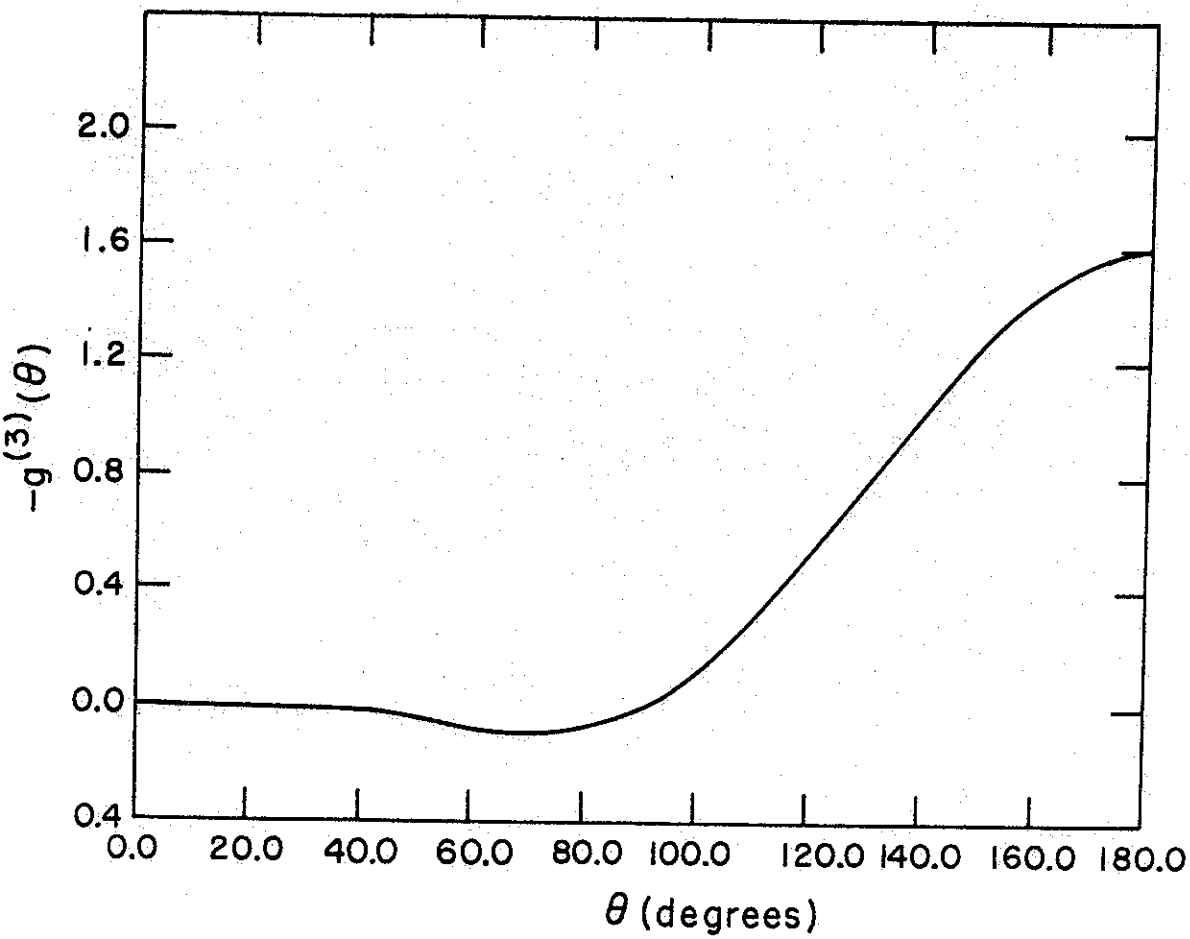

Fig 4.1c

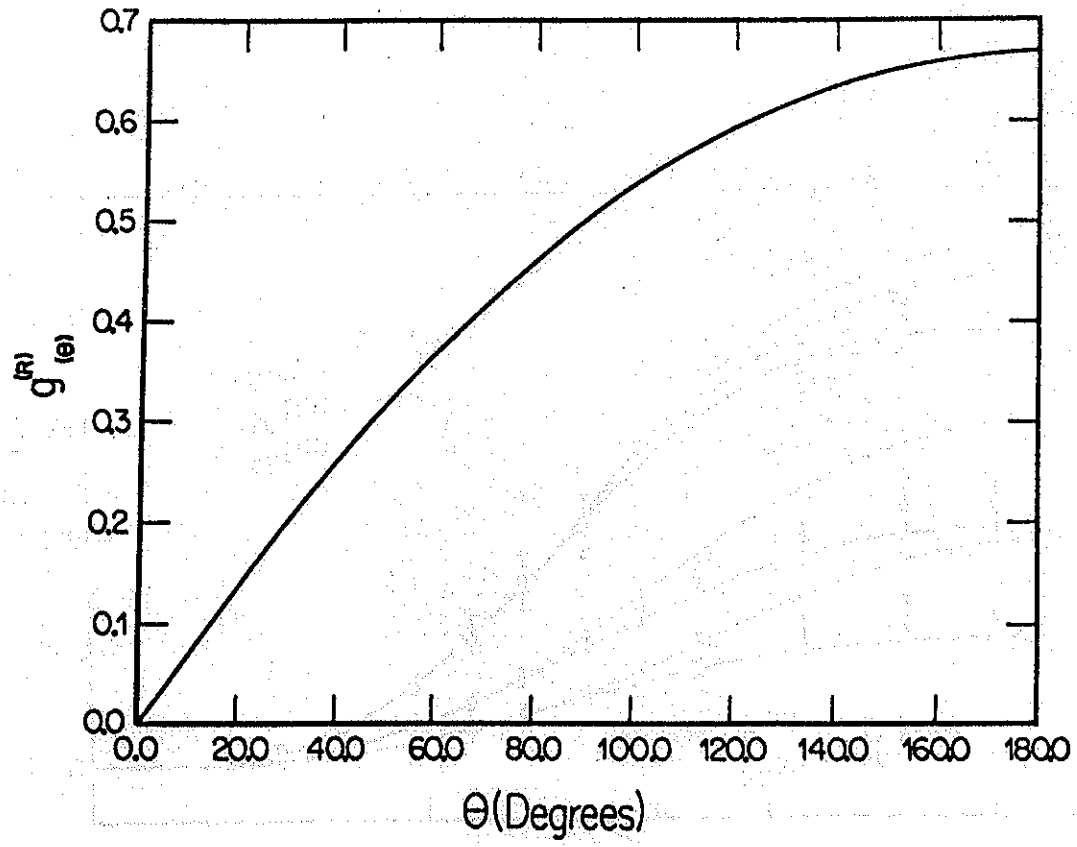

Fig 4.3

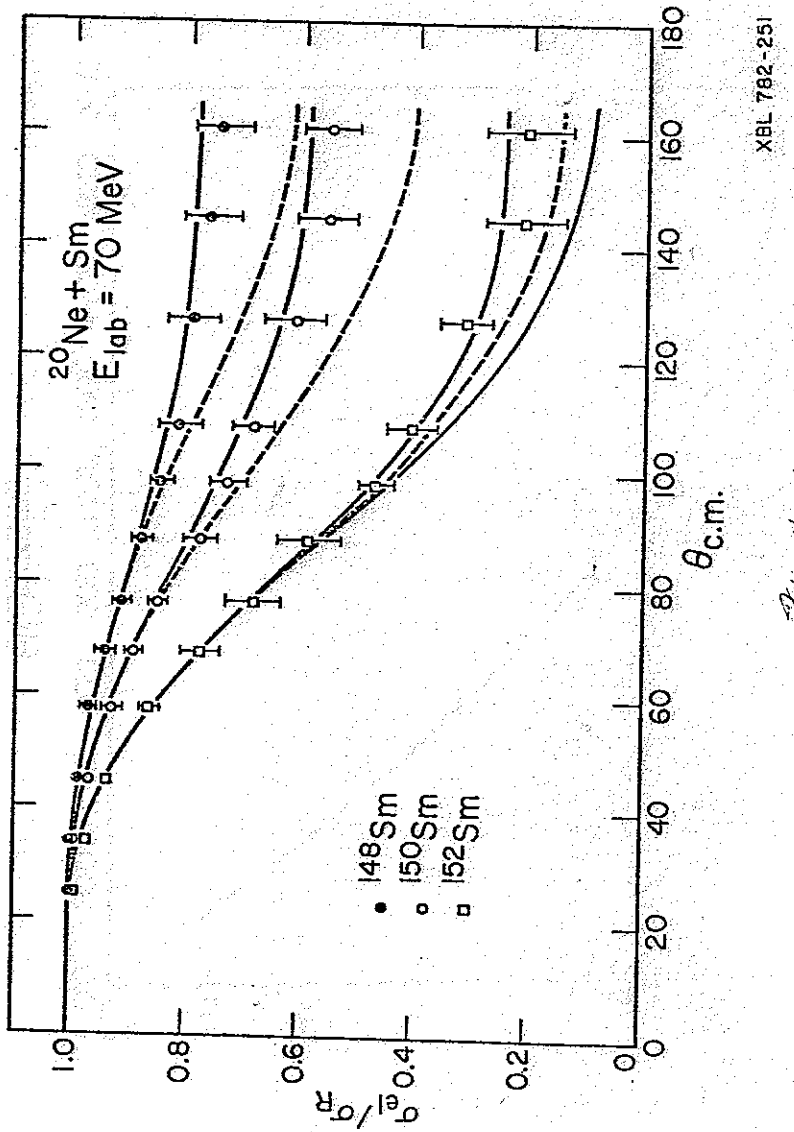
^{20}Ne + Sm
E_{lab} = 70 MeV
^{148}Sm
^{150}Sm
^{152}Sm
σ_{el}/σ_R
$\theta_{c.m.}$
XBL 782-251

Fig. 4.4

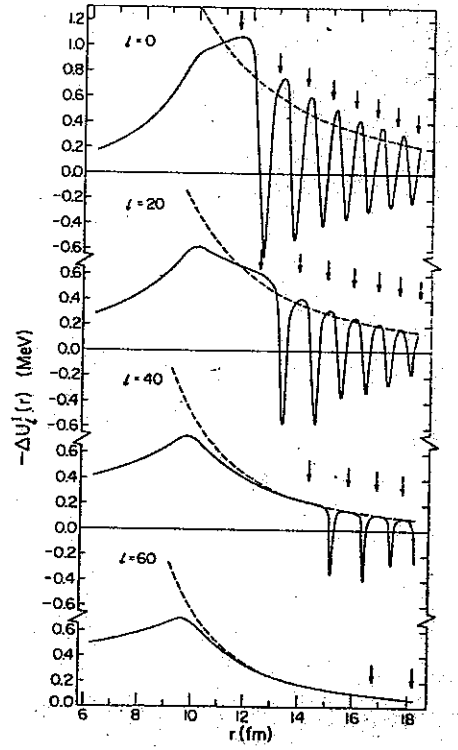
ℓ = 0
ℓ = 20
ℓ = 40
ℓ = 60
$-\Delta U_\ell^I(r)$ (MeV)
r (fm)

Fig 4.5

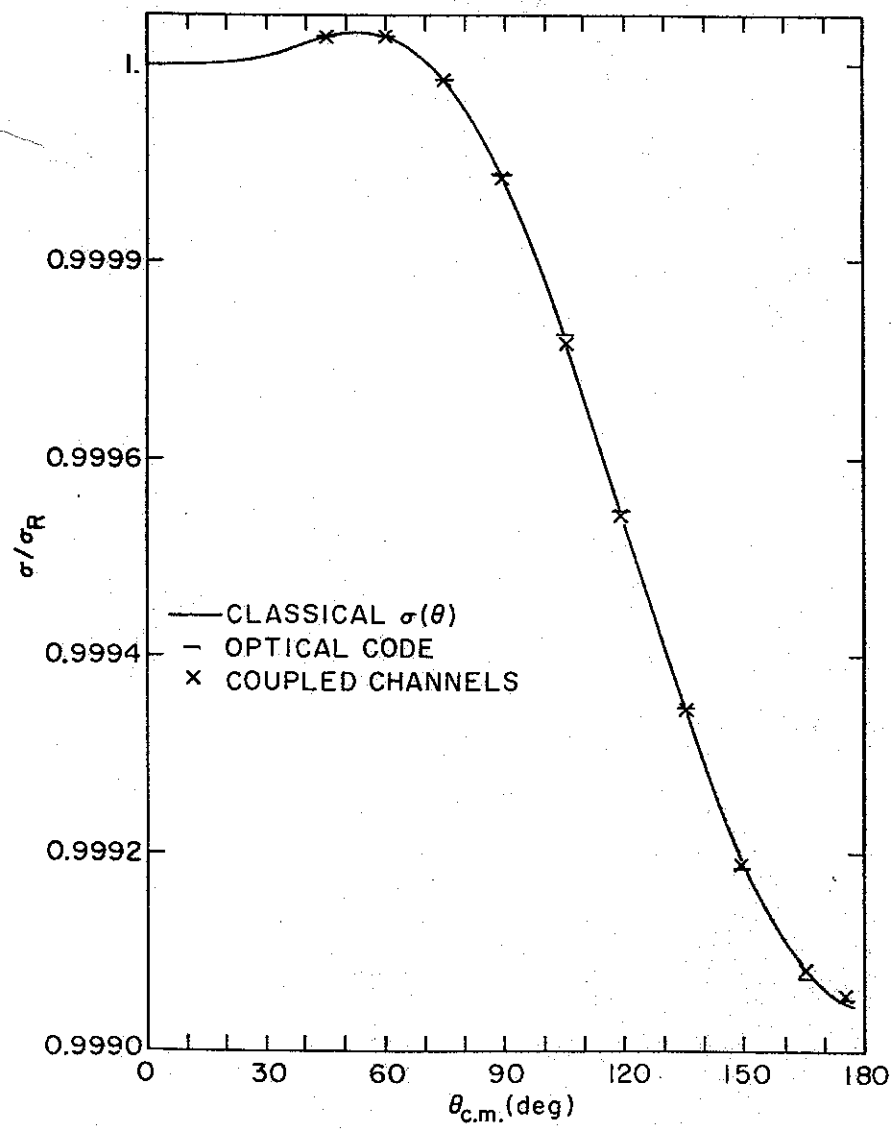
1.
0.9999
0.9996
0.9994
0.9992
0.9990
σ/σR
0
30
60
90
120
150
180
θc.m.(deg)
CLASSICAL σ(θ)
OPTICAL CODE
COUPLED CHANNELS

Fig 4.6

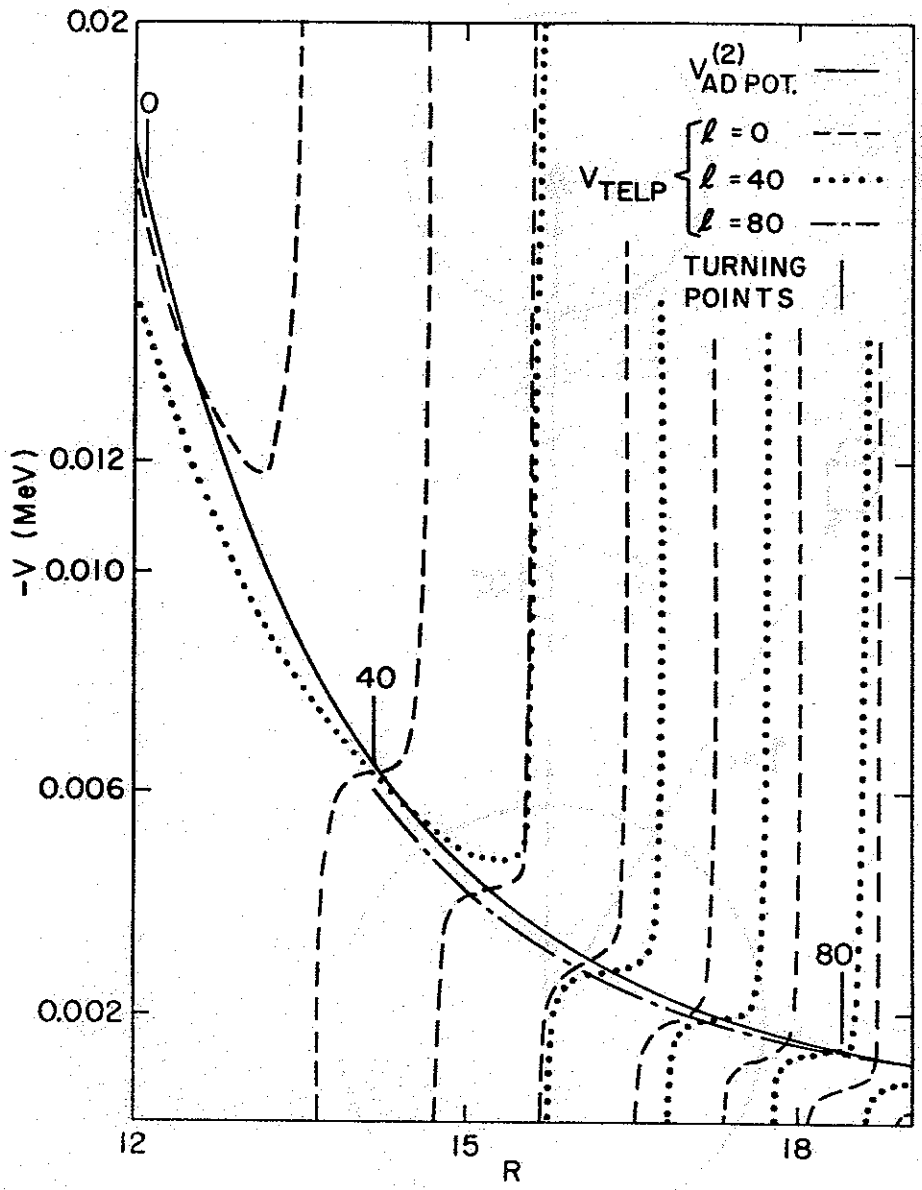
0.02
0.012
0.010
0.006
0.002
-V (MeV)
12
15
18
R
0
40
80
V(2) AD POT.
VTELP
ℓ = 0
ℓ = 40
ℓ = 80
TURNING POINTS

Fig 4.7

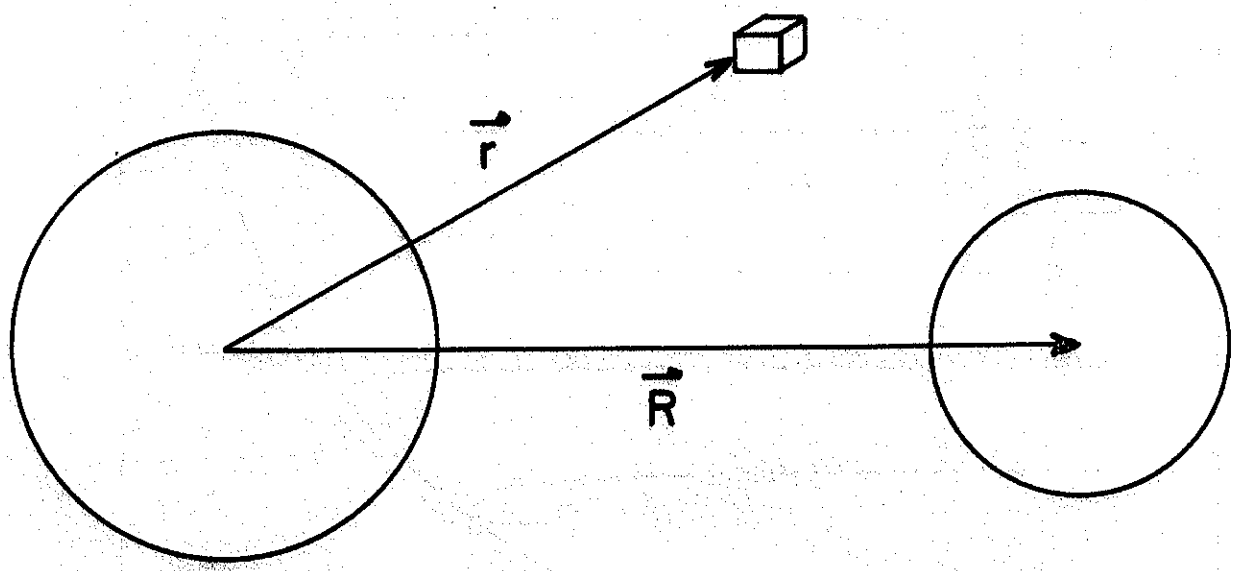

Fig 5.1

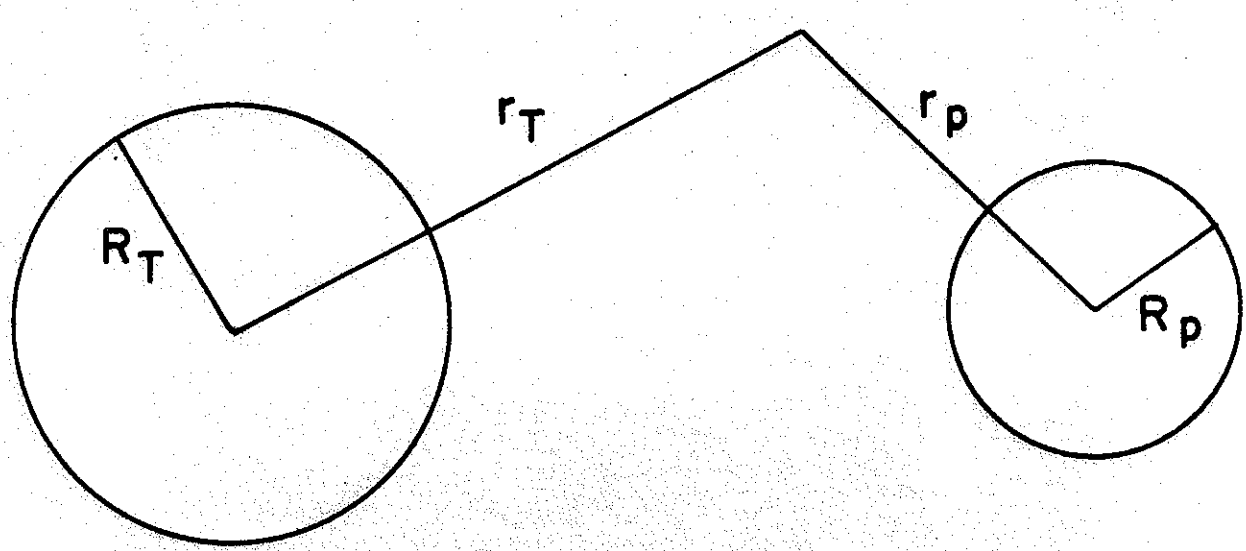

Fig 5.2

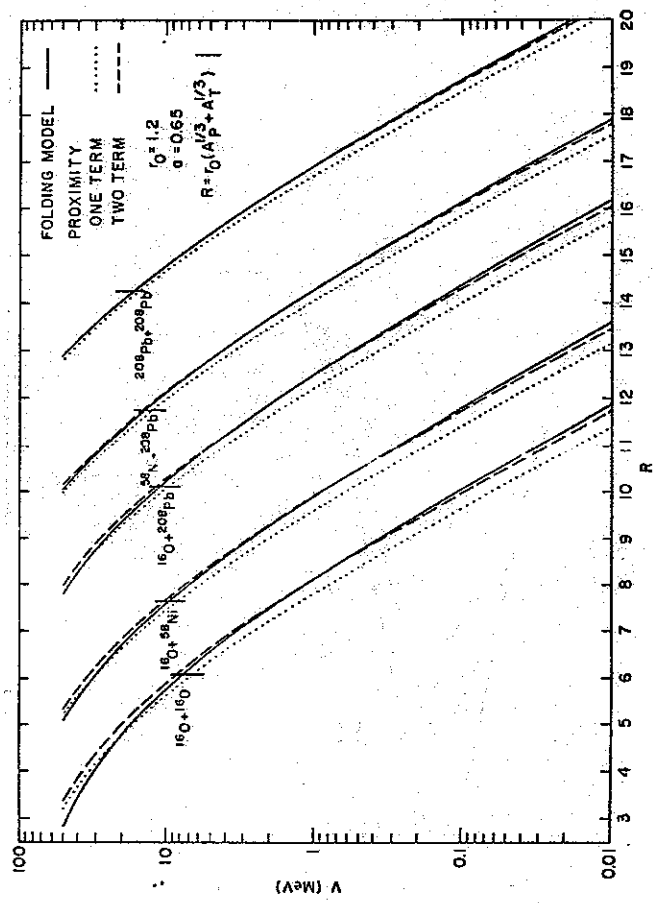
FOLDING MODEL
PROXIMITY
ONE TERM
TWO TERM
$r_0 = 1.2$
$a = 0.65$
$R = r_0(A_P^{1/3} + A_T^{1/3})$
$^{208}Pb + ^{208}Pb$
$^{58}Ni + ^{208}Pb$
$^{16}O + ^{208}Pb$
$^{16}O + ^{58}Ni$
$^{16}O + ^{16}O$
V (MeV)
R

Fig 5.3

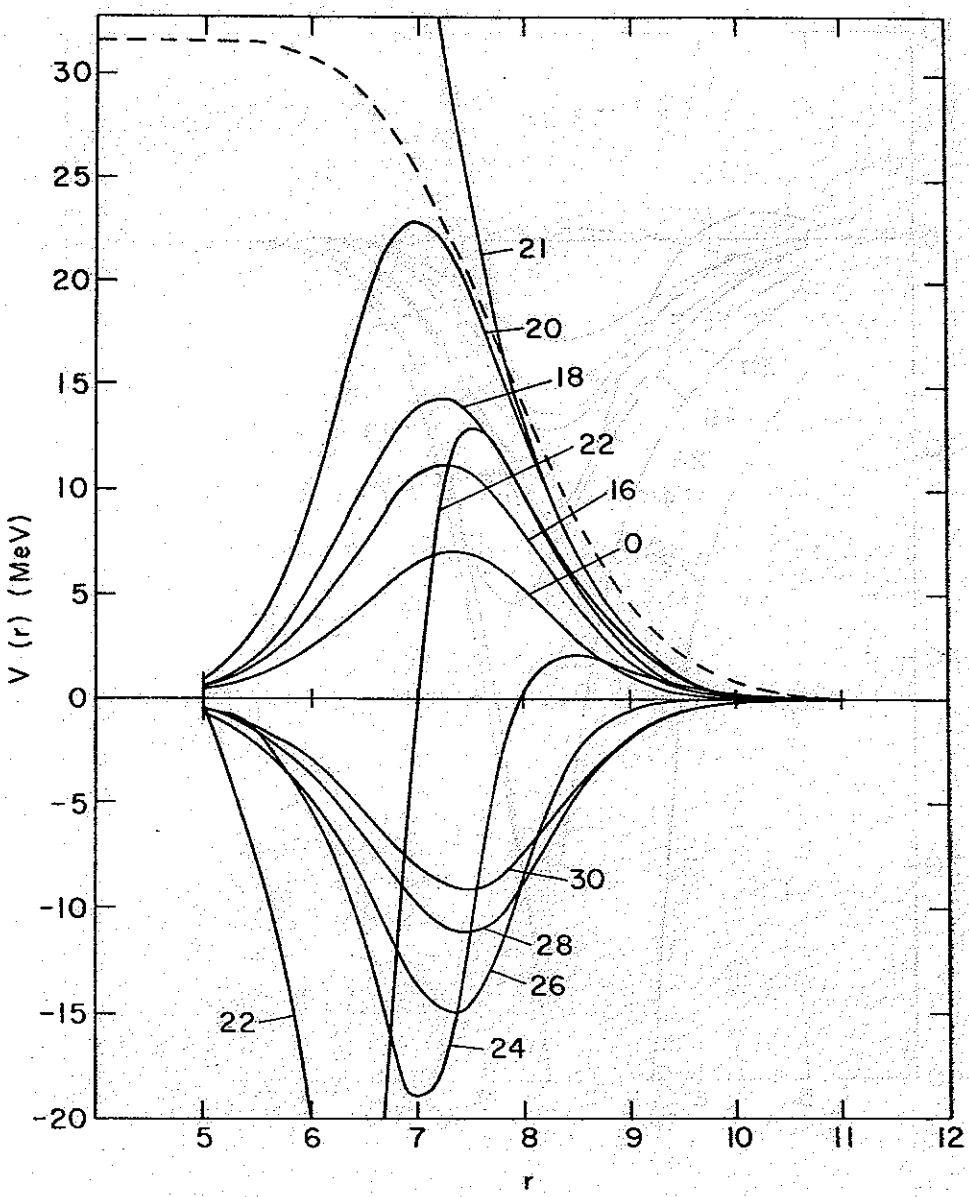
V (r) (MeV)
r
21
20
18
22
16
0
30
28
26
24
22

Fig 6.1

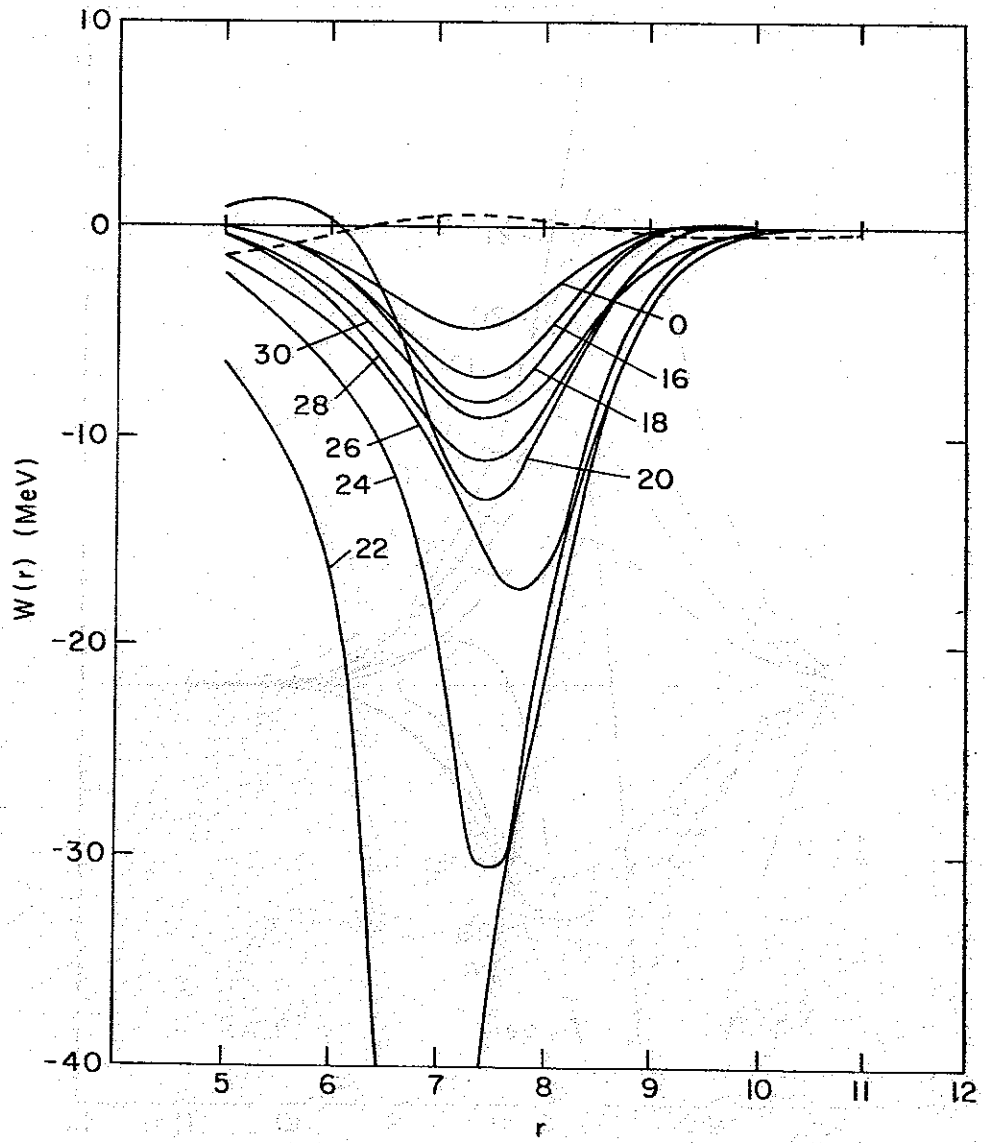
10
0
-10
-20
-30
-40
W(r) (MeV)
5
6
7
8
9
10
11
12
r
0
16
18
20
22
24
26
28
30

Fig 6.2

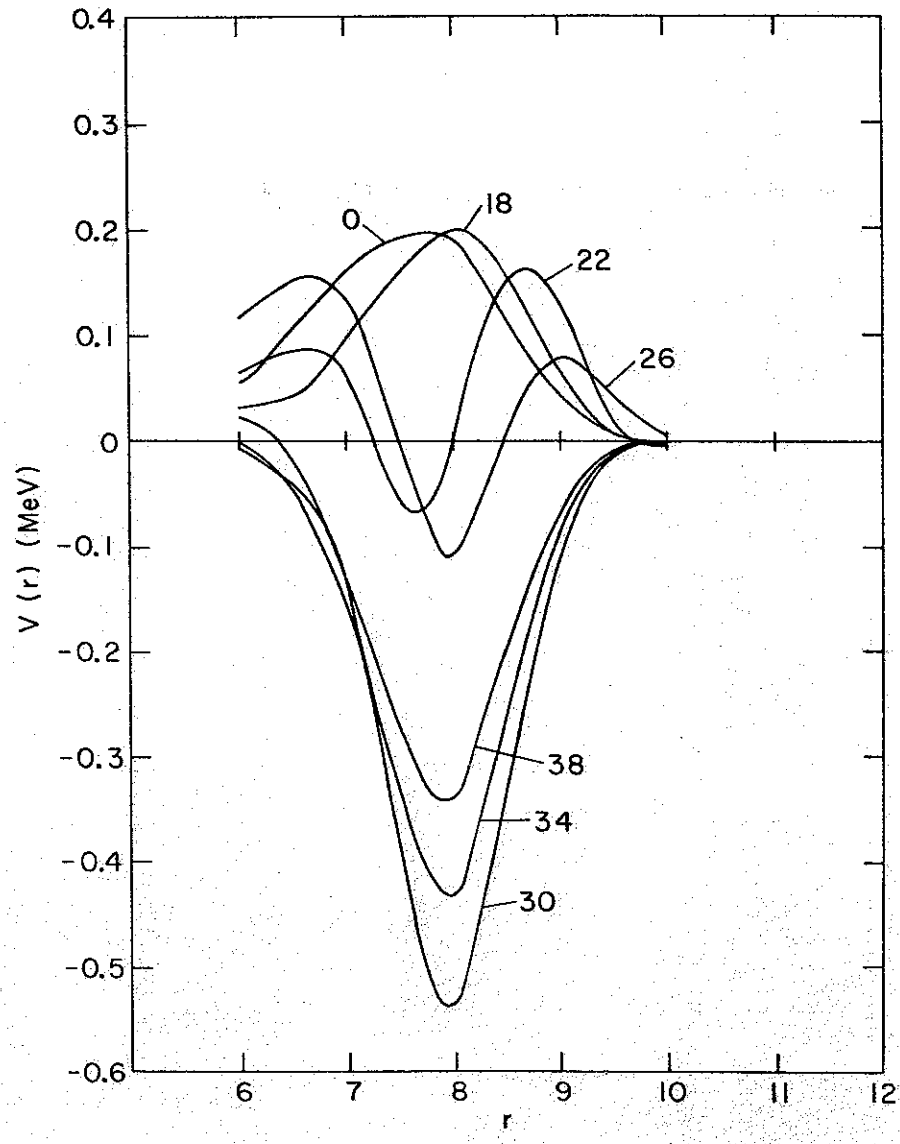
0.4
0.3
0.2
0.1
0
-0.1
-0.2
-0.3
-0.4
-0.5
-0.6
V (r) (MeV)
6
7
8
9
10
11
12
r
0
18
22
26
38
34
30

Fig 6.3

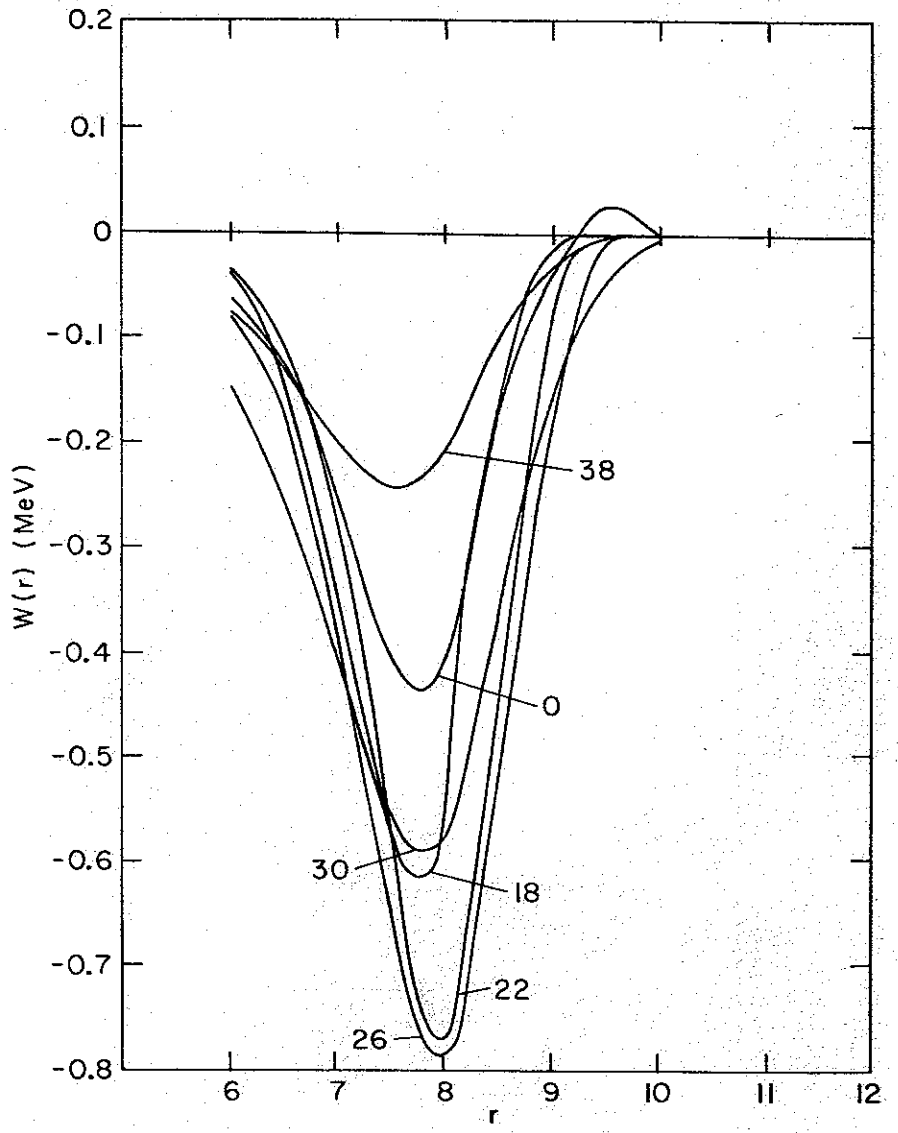
0.2
0.1
0
-0.1
-0.2
-0.3
-0.4
-0.5
-0.6
-0.7
-0.8
W(r) (MeV)
6
7
8
9
10
11
12
r
38
0
30
18
22
26

Fig 6.4

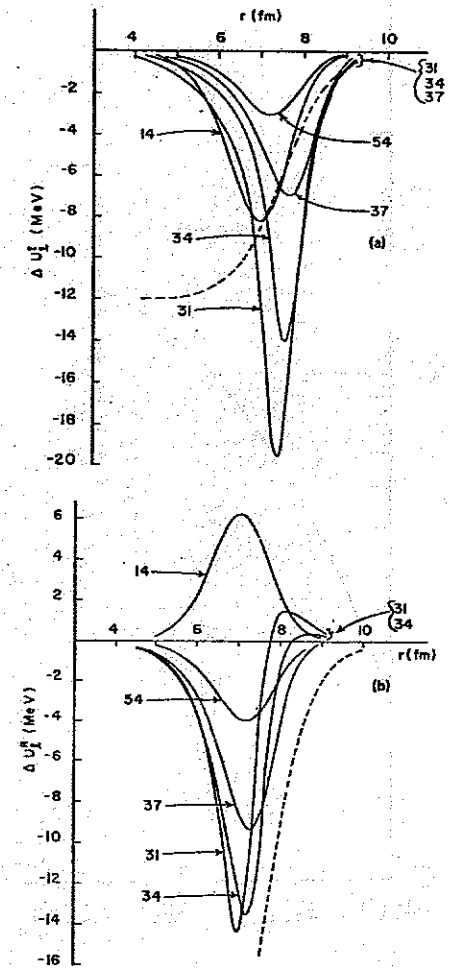
r (fm)
4
6
8
10
31
34
37
14
54
37
34
31
(a)
Δ U$_l^I$ (MeV)
-2
-4
-6
-8
-10
-12
-14
-16
-18
-20
6
4
2
14
31
34
4
6
8
10
r(fm)
(b)
54
37
31
34
Δ U$_l^R$ (MeV)
-2
-4
-6
-8
-10
-12
-14
-16

Fig 6.5

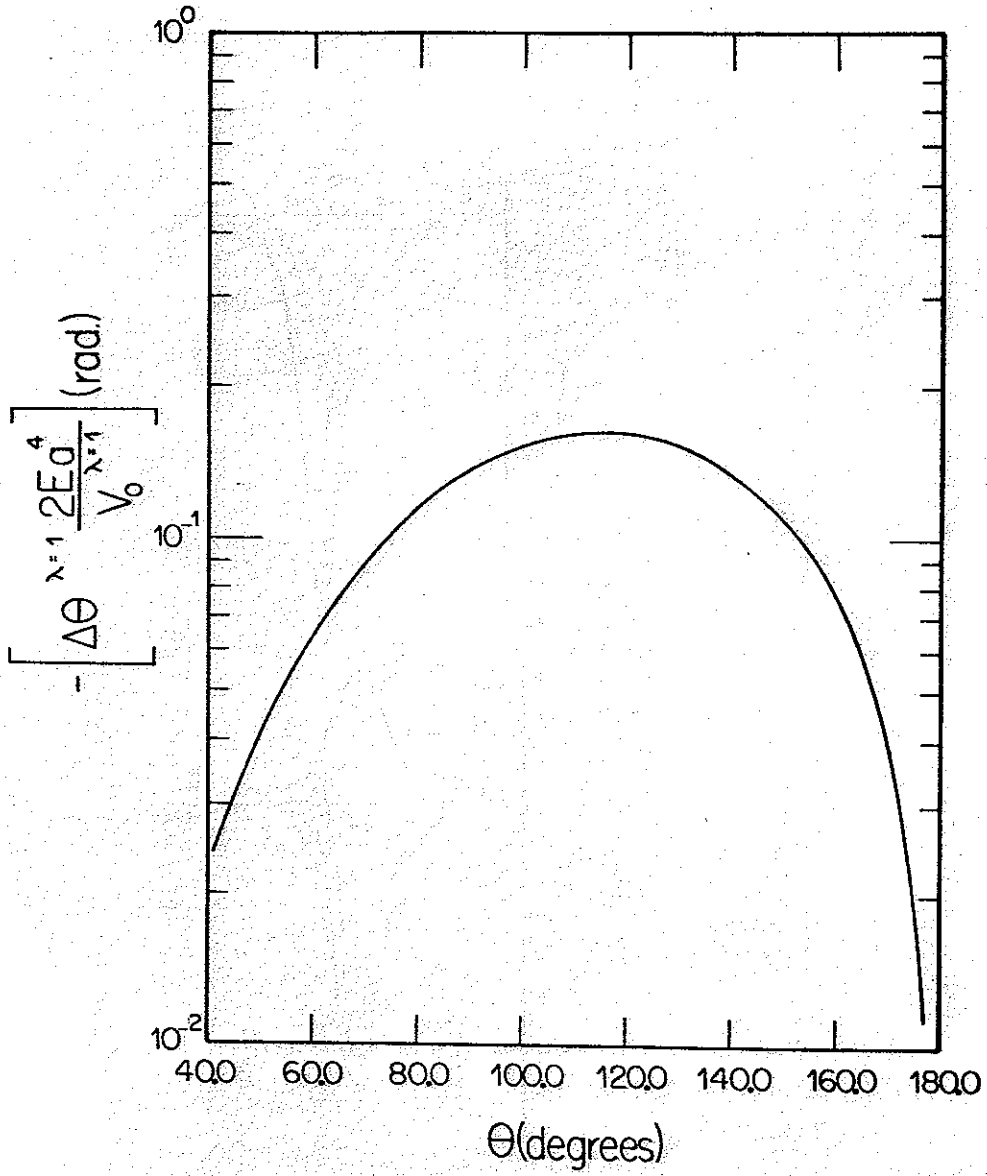

Fig C.1 a

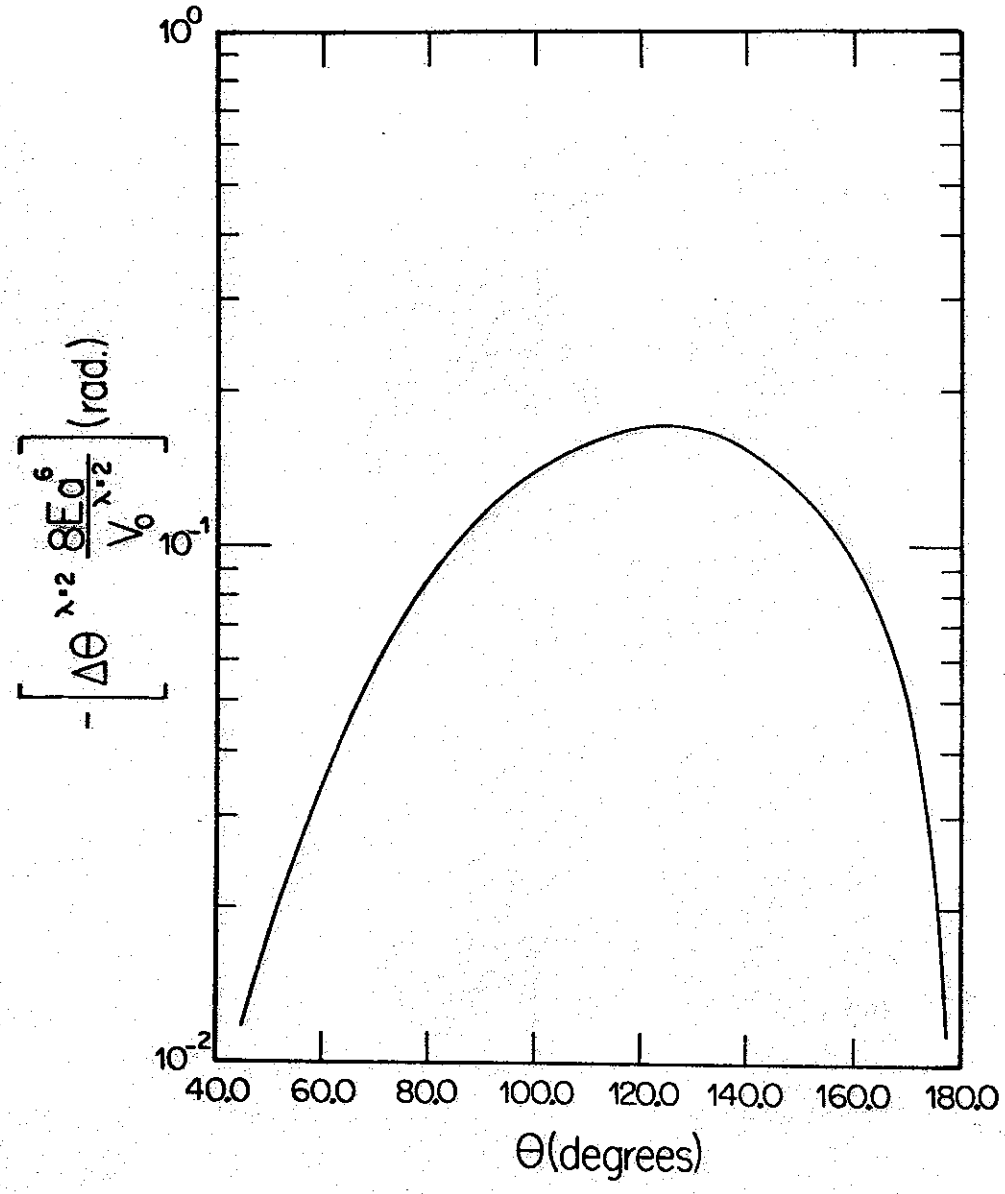

Fig C.1 b

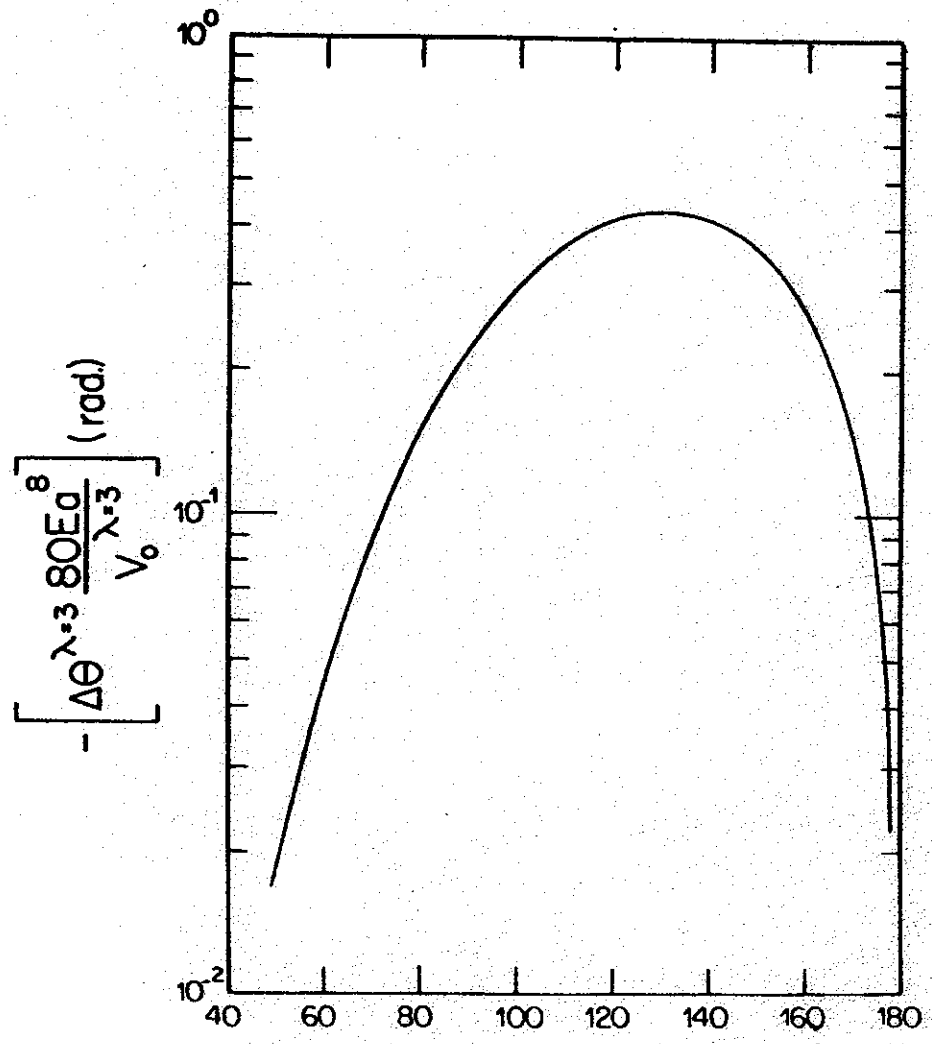
10^0
10^{-1}
10^{-2}
40
60
80
100
120
140
160
180
$-\left[\Delta\theta^{\lambda=3}\,\frac{80Ea}{V_o}^{8}\right]$ (rad.)

Fig C.1 c